# DEVELOPMENT OF A MULTICOMPONENT FILM DIFFUSION CONTROLLED MIXED BED ION EXCHANGE COLUMN MODEL APPLICABLE TO VARIABLE INFLUENT SYSTEMS

By

DENNIS FRANK HUSSEY

Bachelor of Science
Oklahoma State University
Stillwater, Oklahoma
1994

Master of Science
Oklahoma State University
Stillwater, Oklahoma
1997

Submitted to the Faculty of the
Graduate College of the
Oklahoma State University
in partial fulfillment of
the requirements for
the Degree of
DOCTOR OF PHILOSOPHY
May, 2000

DEVELOPMENT OF A MULTICOMPONENT FILM DIFFUSION CONTROLLED MIXED BED ION EXCHANGE COLUMN MODEL APPLICABLE TO VARIABLE INFLUENT SYSTEMS

Thesis Approved:

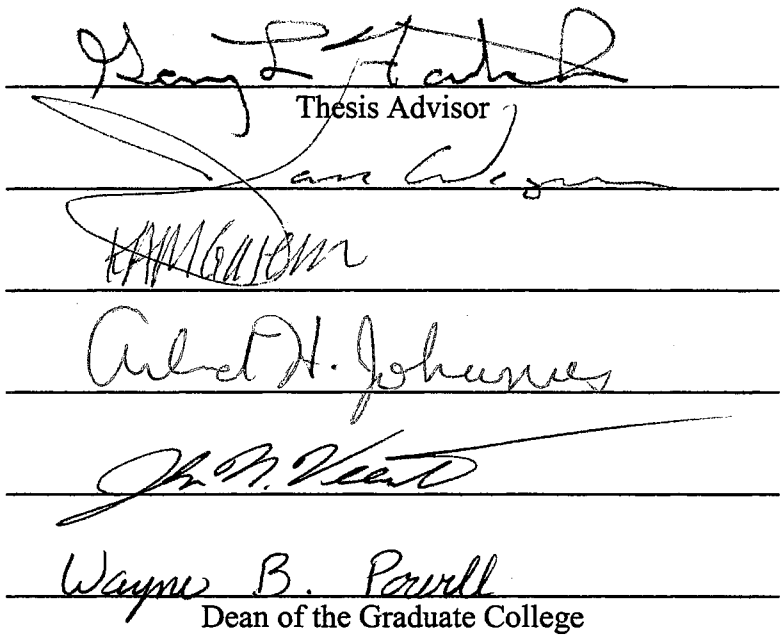

Thesis Advisor

Dean of the Graduate College

# PREFACE

This work is directed towards the applications of ion exchange processes in the nuclear and semiconductor industries. Optimization of mixed bed ion exchange columns cycle times require a better understanding of multicomponent ion exchange dynamics. To meet this objective, this work proposes a generalized, multicomponent mixed bed ion exchange column simulator. Emphasis has been placed on industrial water chemistries, bed configurations, and variable influent conditions.

Many people have contributed to the development of this model. I wish to express my deepest appreciation to my major advisor Dr. Gary L. Foutch. I have learned much from his guidance, patience, creativity and flexibility throughout my master's and doctorate programs. In addition to his technical competence; his character, honor and integrity have served as a model worthy of emulation. I look forward to more opportunities to work with him. I am also grateful to Dr. Jan Wagner, Dr. Khaled Gasem, Dr. Arland Johannes and Dr. John Veenstra for their helpful suggestions and insights while serving on my advisory committee.

Particular thanks goes to Dr. Yunquan Liu for his suggestions and previous work with the mixed bed model. I also acknowledge Jaehyun Lee for his assistance with the external material balance. Particular thanks goes to my assistants Steve Jenks, Adam Roberts and Blake Masters in helping evaluate the model and apply it to industrial problems.

Special gratitude is extended to our industrial sponsors; most notably Dave Morgan of Pennsylvania Power and Light, Barry Widman of Knoll's Atomic Power Laboratory and Chris Bates of British Energy. Their financial support and enthusiasm for applying the model to their particular scenarios was invaluable for troubleshooting and evaluation. I would also like to thank Dr. Michael Patterson of the Intel Corporation for providing me the opportunity to gain industrial experience in the ultrapure water field; his comments and insights have always been lucid and practical.

Special gratitude and appreciation are expressed to my parents Dale and Sandra Marlin, and to my brother's family, Sean, Renee, Alexandra and Brannon Hussey, for their encouragement and support throughout the years of this study.

Financial assistance from the School of Chemical Engineering, the members of the Ultrapure Water Consortium, and the Electrical Power Research Institute is greatly appreciated.

The assistance and advice of the faculty and staff of the School of Chemical Engineering is also gratefully appreciated.

TABLE OF CONTENTS

LIST OF FIGURES

LIST OF TABLES

# CHAPTER I

## INTRODUCTION

The study of water and its application to science and engineering is almost immeasurable; water is used or studied in virtually every biological and physical science. Libraries of research have been dedicated to the definition, application, and modeling of water systems; and considerable effort from numerous researchers has been devoted solely to water purification. This work proposes a generalized, variable system, mixed-bed ion exchange column model applicable at ultrapure water concentrations.

The advancement of many technologies can arguably be linked with the advancement of water handling and purification. When one considers the range of water applications throughout history, from water wheels providing rotational energy for milling grain, its use as a working fluid in steam engines and electrical power plants, or its application in the semiconductor industry as a rinse chemical; it can be shown that technological advancements have prompted the needs for pure water beyond the needs of potable water supplies.

The properties of water make it very suitable as a working fluid for steam cycles. It is often present in abundance, and it is a liquid at ambient temperatures and pressures. Water vaporizes with considerable latent heat at pressures and temperatures that are

manageable with modern materials of construction. The combination of these properties in a heat-power steam cycle allows the relatively safe generation of enormous quantities of electrical power.

The chemical properties of water are also very diverse; the self-dissociation of the water molecule into hydronium and hydroxyl ions creates an ionic environment that makes it a flexible non-polar solvent with almost infinite chemical applications. The solvent properties are a curse for some industries; the ionic environment facilitates the corrosion of metals and other materials, especially in the presence of ionic contaminants.

Industry has driven the water purification requirements to such levels that the water produced may be labeled a specialty chemical known as 'ultrapure water.' The applications of ultrapure water will soon be discussed, but first the formal definition of ultrapure water is presented.

## Ultrapure water

Ultrapure water is typically defined as water with dissolved impurity concentrations less than 1 part per billion (ppb, or μg/L), although this definition is relaxed for dissolved oxygen and nitrogen. Another definition of ultrapure water is water with conductivity less than 0.1 μS/cm.

Numerous contaminants may be found in water, and they may be natural or anthropogenic in origin. Luckily, a most contaminants may be removed with relatively few unit operations. For this work it serves to separate the contaminants into five categories based on their common solution properties:

1. Weak and strong electrolytes

2. Organic chemicals
3. Particulate material
4. Biological contaminants
5. Dissolved gases

There are several removal methods for each contaminant type. Table I-1 below summarizes the unit operations for the removal of each type of water contaminant. The table is not meant to be inclusive; instead it illustrates the various technologies used for contaminant removal and in which conditions they are most applicable.

Note the removal of one contaminant type may lead to the generation of another. For example, consider the oxidation of organic compounds using ozone as the oxidizing agent. The organic compound removed by oxidizing the hydrocarbon with ozone to produce carbon dioxide and water as follows.

$$C_xH_y + \left(\frac{2x}{3} + \frac{y}{6}\right)O_3 \overset{v}{\Rightarrow} xCO_2 + \frac{y}{2}H_2O \qquad (I.1)$$

The excess carbon dioxide must be removed from the remaining water by either degasification or ion exchange, or more likely a combination of the two.

Ion exchange resins cause similar problems. Although ion exchange efficiently removes ionic contaminants, they act as a substrate for biological contaminants and shed particles, requiring sterilization and filtration following the final mixed bed polish vessel in semiconductor applications.

Table I-1 Unit operations required for contaminant removal in ultrapure water manufacture

| *Contaminant type* | *Unit operation for removal* | *Advantages* | *Disadvantages* |
|---|---|---|---|
| Ionic contaminants | Reverse Osmosis | No chemicals<br><br>Useful for high ionic concentration waters | Limited removal efficiency<br><br>Brine product stream |
| | Ion Exchange | Highest removal efficiency<br><br>Relatively economical | Regeneration chemicals and systems required<br><br>Generates particles and bacteria |
| | Electrodeionization | No regeneration chemical required<br><br>High removal efficiency | Technology in development<br><br>Fouling potential |
| Organic chemicals | Activated carbon | Useful for high contaminant concentrations | Finite capacity requires regeneration or replacement |
| | Ozonation/UV oxidation | Effective at part per billion (ppb) concentrations | Ineffective in turbid waters |
| Particulates | Multimedia filtration | Useful for large diameter particles | Small particle diameter particles pass through |
| | Cartridge filter | Useful for filtering small particle diameters | May be clogged if challenged |
| Bacterial contaminants | Ozonation | Economical and effective sterilization technique | Bacterial remains are particulate matter |
| | UV Sterilization | Sterilizes without oxygen | Only effective in non-turbid waters |
| | Cartridge filtration | Removes bacteria physically | Sterilization must precede filter or a culture may develop |
| Dissolved gases | Forced draft degasification | Removes excess carbon dioxide | Dissolved oxygen and carbon dioxide remains |
| | Vacuum degasification | Removes almost all dissolved gases | Capital costs |
| | Membrane contactors | Requires less space, lower capital costs | Fouling potential |

## Ion exchange

Ion exchange units are currently the most effective method for removing the ionic contaminants of large volumes of ultrapure water. Ion exchange units are usually operated as fixed beds, most often in axial flow, but also occasionally in radial flow. Ion exchange units that contain only cation or anion resin are termed mono-beds or homogeneous beds (colloquially, in a facility they are often referred to as 'cation beds' or 'anion beds'). Ion exchange units that contain both cation and anion resin are called mixed beds.

Ion exchange is a stoichiometric reaction; ionic equivalents in the solution phase are replaced by ionic equivalents from the resin phase. Ion exchange resin beads are typically composed of a polymer matrix of polystyrene crosslinked with divinyl benzene (see Figure I-1).

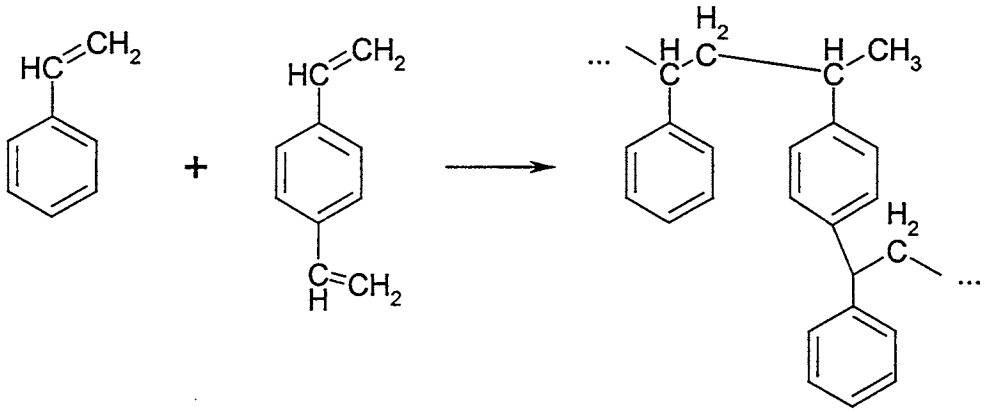

Figure I-1 Copolymerization of styrene and divinyl benzene

Several types of functional groups have been added to the polymer matrix in ion exchangers. A resin is classified as a cation or anion exchange resin depending upon the

species that is exchanged. A cation exchange resin exchanges positively charged species, while an anion resin exchanges negatively charged species.

Ion exchange behavior is determined by the resin chemical composition and the functional groups. There are four basic types of ion exchange resins; strong acid cation, strong base anion, weak acid cation and weak base anion. The type of resin is determined by the functional group attached to the resin matrix. Strong acid cation resins typically have sulfonic groups, while weak acid cation resins have carboxylic acid groups. Strong base anion exchangers are usually made of quaternary ammonium groups, and weak base anion exchangers have either primary, secondary or tertiary amine groups, or a mixture of these groups.

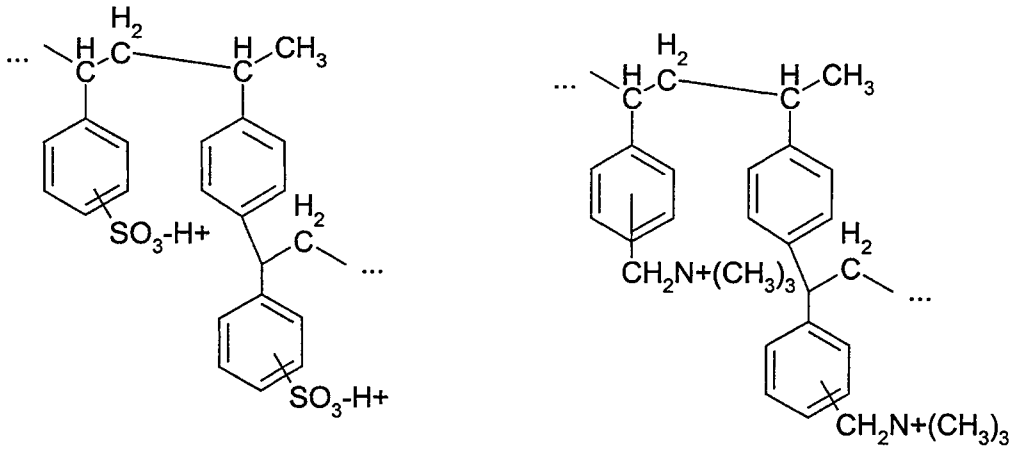


Cation resin

Anion resin

Figure I-2 Cation and anion resin with sulfonic and quaternary ammonium functional groups

Strong base anion exchangers are classified into two types: Type I anion resins having a $N^{+}(CH_3)_3$ functional group as the exchange site, or Type II anion resins with a -$N^{+}(CH_3)_2(CH_2CH_2OH)$ group as the active site. Type II resins are easier to regenerate,

but they are less chemically stable than Type I resins. Type I resins are employed most often by semiconductor and nuclear applications.

## Mixed-bed ion exchange

Kunin and McGarvey (1951) developed the concept of mixed bed ion exchange (MBIE). The process is a convenient and economical method for deionization of water to ultrapure water concentrations. As the name implies, a mixed bed is the addition of cation and anion resins in the same vessel. Combining the resins in the same vessel puts the resins in intimate contact, and allows the reactants and products of both cation and anion exchange to interact. This is illustrated by the parallel chemical reaction scheme below for a completely dissociated arbitrary alkali metal cation $M^+$ and an arbitrary halide anion, $X^-$.

$$M^+ + R-H^+ \Leftrightarrow R-M^+ + H^+ \qquad \text{(cation exchange)} \qquad \text{(I.2)}$$

$$X^- + R-OH^- \Leftrightarrow R-X^- + OH^- \qquad \text{(anion exchange)} \qquad \text{(I.3)}$$

$$H^+ + OH^- \Leftrightarrow H_2O \qquad \text{(water neutralization)} \qquad \text{(I.4)}$$

Notice water neutralization reactants consist of the hydrogen and hydroxyl ion products from the cation and anion exchange reactions. Water neutralization acts as a nearly infinite product sink for hydrogen and hydroxyl ions, and the reaction equilibrium of Equations (I.2) and (I.3) will shift to the right according to LeChatlier's principle. Through experimental evidence and calculation, it can be shown that equilibrium ionic contaminant concentrations are often below one part per trillion for many species. Figure I-1 demonstrates the removal of sodium chloride using a mixed bed system.

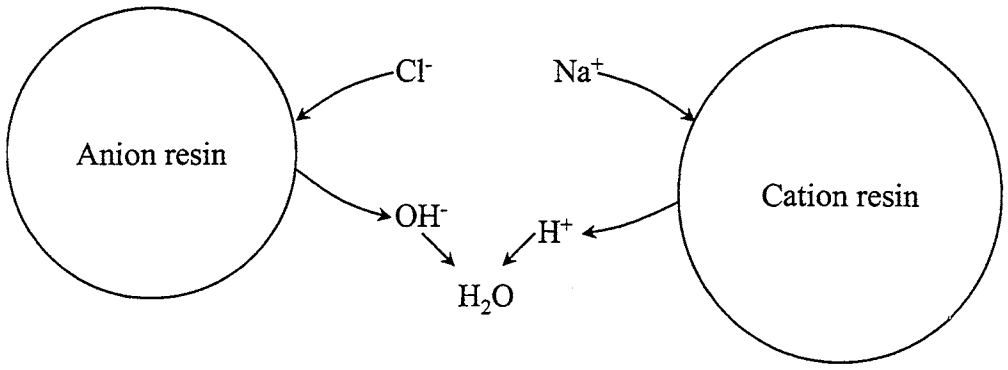


Figure I-3 Removal of sodium chloride from water using mixed bed ion exchange

As will be discussed in Chapter 2, bulk neutralization also aids the kinetics of the exchange reaction. The consumption of hydrogen and hydroxide in the bulk solution increases the concentration gradient from the surface of the resin across the stagnant film into the bulk solution. For the cation case, the increased hydrogen concentration driving force increases the hydrogen flux. In order to maintain electroneutrality and continuity, the sum of the equivalent fluxes must be zero, or

$$\sum_{i=1}^{m} z_i J_i = 0 \qquad \text{(I.5)}$$

where $J_i$ is flux, defined as the mass flow rate per unit area of an arbitrary cation into the resin, and $z_i$ is the charge of the ionic species. The sign convention for the flux is negative for ions entering the resin and positive for ions leaving the resin.

Inspection of the equation shows for non-zero values of $J_i$, the sum of positive fluxes must equal the sum of negative fluxes. So if the hydrogen or hydroxyl ion flux is increased (leaving the resin), it increases the fluxes of the ions entering the resin (the contaminants being removed from water). This allows a faster approach to equilibrium

between the resin and bulk solution in situations where the kinetics of ion exchange is a significant factor.

Mixed beds are used in nuclear power plants to remove ionic contaminants that may potentially corrode the steam generator. The contaminant sources are typically metal oxides from corrosion of the materials of construction and condenser water from condenser tube leakage. The advantages of pure water are two-fold: the absence of any component in an electrochemical reaction prevents the reaction from occurring, and a low conductivity inhibits corrosion reactions by inhibiting the flow of electrons.

The removal of contaminants eliminates the reactants for a corrosion reaction in the steam power cycle. Ultrapure water has a very low conductivity, theoretically 0.055 μS/cm at 25 °C due to the self-dissociation of water. Therefore ultrapure water has a very low current capacity for electrochemical reactions.

## Mixed-bed ion exchange in ultrapure water applications

Ultrapure water has many applications, but the primary consumers of ultrapure water are the electrical power, semiconductor manufacturing, and pharmaceutical industries. This section describes the functions of ultrapure water in these industries.

### Electrical power

Steam cycle water chemistry is critical to the sustained operation of nuclear and fossil-fired power plants. Ultrapure water processing occurs in three major areas of the plant: make-up water production, condensate polishing, and reactor water clean-up. Each of these applications has specific requirements for water quality and uses different technologies to achieve these requirements.

The nuclear industry is far more interested in the production of ultrapure water than fossil-fired electrical generation plants; the replacement cost of a nuclear steam generator can exceed 250 million dollars (Bates, 1999). Many fossil plants had been constructed before a clear economic advantage in favor of condensate polishing for standard electrical power plants, but a recent analysis by the Electrical Power Research Institute (EPRI) has shown the benefits of condensate polishing for fossil plants.

Nuclear power plants use ultrapure water to minimize erosion and corrosion of materials within the steam power cycle. The erosion and corrosion of the materials of construction are complex phenomena and depend primarily upon the temperature, pH and contaminants present in the water. The Electrical Power Research Institute (EPRI) suggested maximum contaminant concentrations for each steam cycle configuration. The water chemistry is determined by the steam cycle configuration. Two steam cycle configurations are predominant in the United States nuclear industry, the Boiling Water Reactor (BWR) and the Pressurized Water Reactor (PWR).

As shown in Figure I-4, the BWR steam cycle water is in direct contact with reactor core. The steam cycle water is very close to ultrapure, occasionally hydrogen is added to prevent water radiolysis, and also very low levels of zinc may be added to suppress the formation of radioactive $Co^{60}$ on metal surfaces in the reactor. After the water is boiled in the nuclear reactor, the high-pressure steam is expanded through the turbine, and then it is condensed back to a liquid in a condenser. The condensate is then passed through condensate polishers to remove any contaminants that may have been introduced into the steam cycle.

The primary source of contaminants in a BWR plant is the condenser cooling water. The condenser tubes occasionally leak cooling water into the steam cycle, which induces corrosion in the circuit. The greatest concern is the water quality in the reactor, where the contaminants are concentrated to about 100 times the influent value.

For example, a boiler influent concentration of 200 parts per trillion (ppt) sulfate concentrates to 20 ppb sulfate, a significant concentration that can induce corrosion of iron, cobalt and nickel. Even more of a concern is the local concentration of contaminants on the boiling nucleation sites in the reactor core; contaminants concentrate to even higher levels in the pits and scratches and induce pit corrosion.

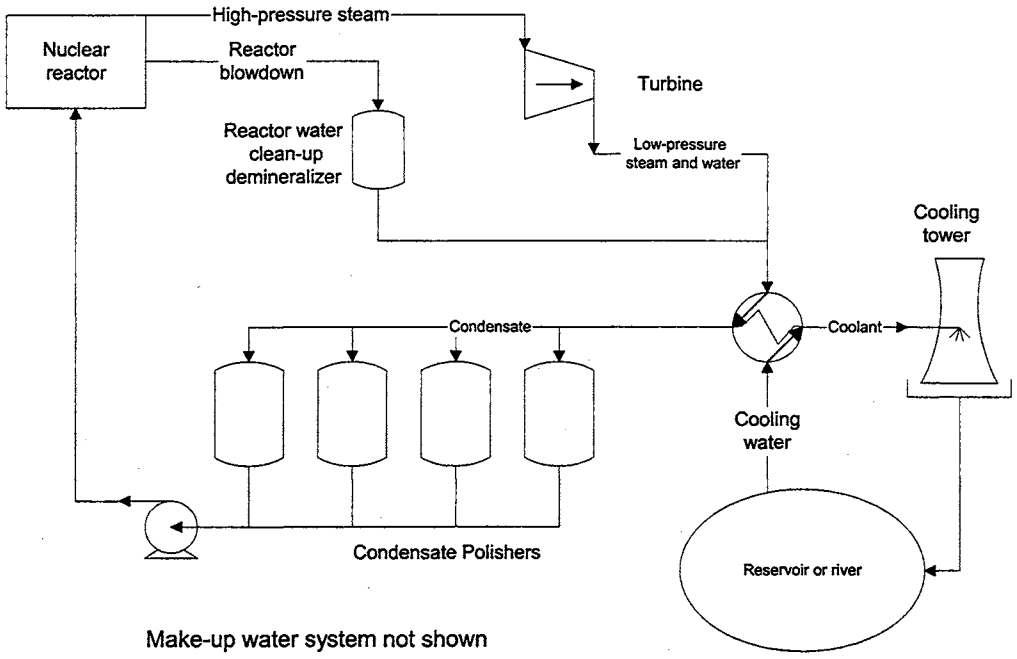


Figure I-4 Skeleton schematic of a BWR nuclear power plant

The reactor blowdown (concentrated water) is typically treated with a mixed-bed demineralizer to prevent excessive concentration in the reactor core, after which it is re-introduced into the steam cycle.

As shown in Figure I-5, the flow configuration for a Pressurized Water Reactor (PWR) is divided into two loops, the primary loop and the secondary loop. The primary loop is at very high pressure, approximately 2500 psig, and this maintains the water in its liquid phase as it contacts the reactor. The heated water is passed through a steam generator where it boils the secondary loop water. The secondary steam expands through the turbines where it is condensed and polished in a manner similar to BWR plants. Notice a steam generator blowdown demineralizer is also used after the steam generator.

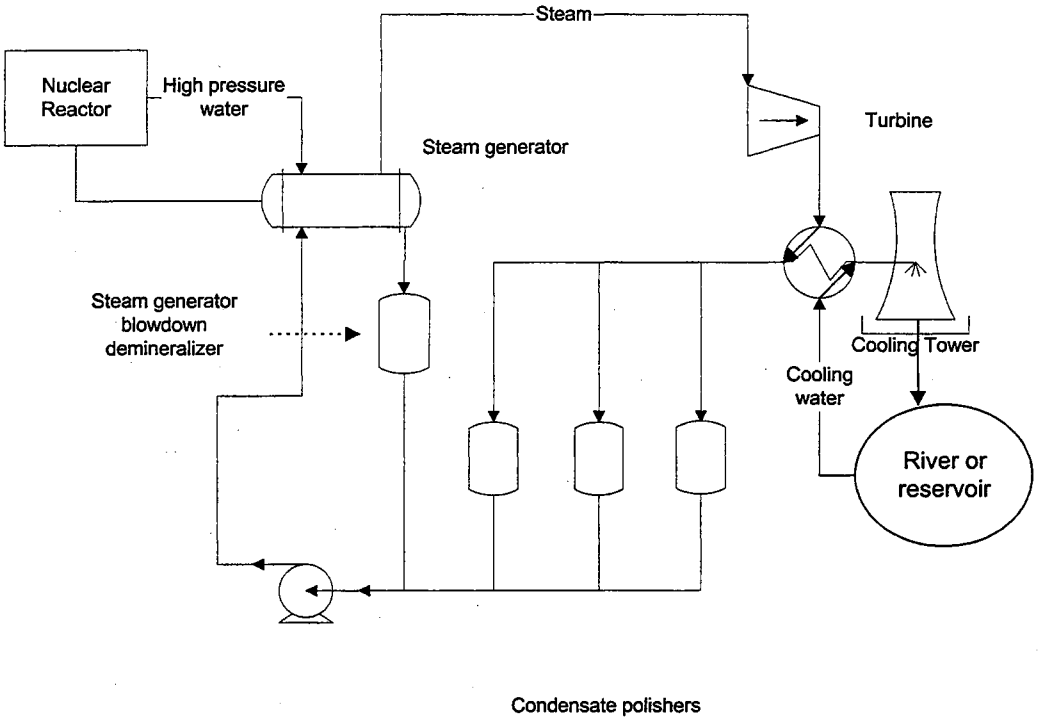


Figure I-5 Skeleton shematic for a Pressurized Water Reactor nuclear power plant

PWR plants generally do not use ultrapure water in either the primary or secondary cycles. The secondary cycle generally has an amine such as ammonia, ethanolamine or hydrazine added to the system directly after the condensate polishers to raise the pH to approximately 9.0. The addition of the amine reduces the hydrogen

concentration according to weak base dissociation chemistry, which reduces the corrosion potential between hydrogen ions and the metals of construction.

Semiconductor manufacturing

Semiconductor chips are manufactured using a complex procedure that chemically imprints a small, rectangular transistor pattern on a circular disk, or wafer. The wafer is typically 150 to 200 mm (6 to 8 inches) in diameter, although 300 mm (12-inch) wafers are currently in development. After processing, the wafer is cut into rectangular 'chips,' which are placed in a housing for attachment of pin-out connections to the silicon. Although the assembly of the chip requires some rinse water, wafer manufacturing consumes much larger quantities of ultrapure water.

The transistors are applied to the silicon wafer using a combination of film deposition, lithography, ion implantation and chemical etching in a sequence that may contain more than 100 steps. During many of these steps, chemicals or residuals are rinsed from the wafer with ultrapure water. Ultrapure water is used in many processing steps, but the major consumer is chemical etching, where acids are washed from the wafer.

Since 1985, the number of transistors on processors has doubled nearly every 18 months. This increase is accomplished, in part, by reducing the transistor line width (or size) from more than 1.0 micron to less than 0.2 microns. As the line width decreases, water purity requirements increase to reduce electrical shorting or physical destruction of the transistors during rinsing.

The water quality standards in the semiconductor industry are far more severe than nuclear applications, and several more units are required to remove all of the

contaminants before the water is used for process applications. Figure I-6 is a sample schematic for a typical semiconductor ultrapure water system, although the configuration is by no means standard.

The system is composed of a make-up water system, a primary ultrapure water loop, and a polish ultrapure water loop. The water quality improves for each sub-system. The make-up loop water typically rejects or adsorbs 99% of the ionic and organic contaminants removed from the source water. The primary loop usually has 18+ MΩ-cm water (the theoretical maximum resistivity of water is 18.25 MΩ-cm at 25 °C), but the water still contains trace amounts of organic chemicals and particles. The polish loop must maintain factory specifications at all times, the contaminant limits are determined by the process but are usually in the single part per trillion range for ionic contaminants, and less than 1 ppb for organic chemicals. Dissolved gas concentrations vary according to the process, some of the processes have no dissolved oxygen constraints, while some processes require less than 1 ppb.

The make-up system is designed to maintain the level of the reverse osmosis product storage tank, while the primary loop is designed to maintain the level of the ultrapure water storage tank.

Pharmaceutical Applications

The primary pharmaceutical applications for ultrapure water processing are Water for Injection (WFI) and manufacturing of medicines. The separation requirements for pharmaceuticals are aimed at eliminating pyrogens (low molecular weight organic molecules – typical of microbial membrane decay) that can cause fevers. In addition,

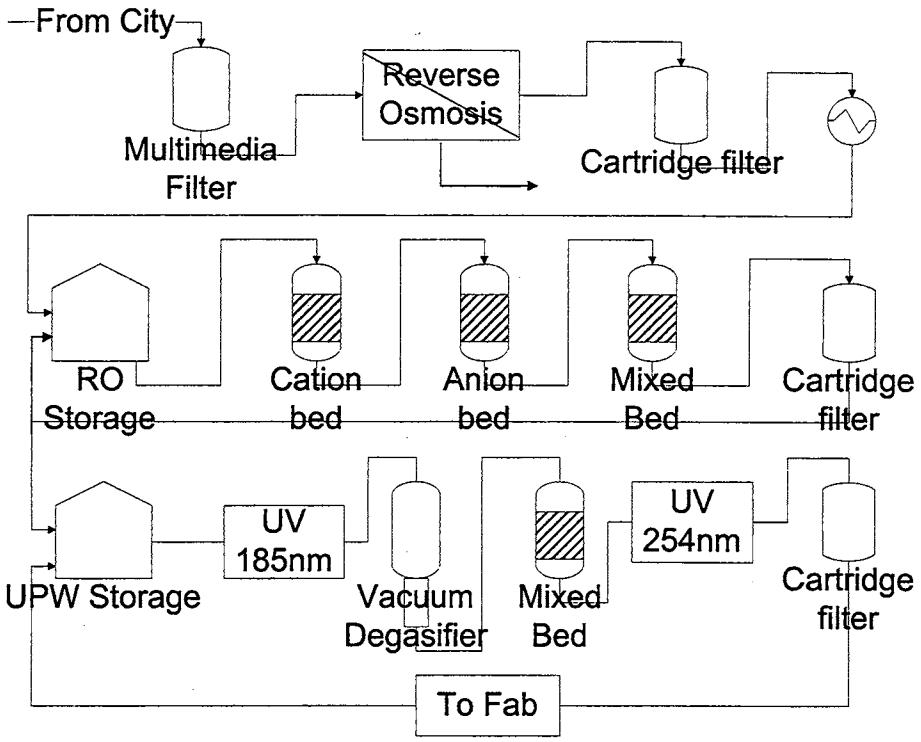


Figure I-6 Simplified configuration for a semiconductor UPW system

ultrapure water is used extensively as a diluant for dialysis. Patients with kidney failure must undergo dialysis two to three times per week. Waste products in the blood, such as urea, diffuse through hollow fiber membranes into ultrapure water. Cases have been reported where ultrapure water systems have failed, and fluoride is introduced into patients' blood streams (by back diffusion from the water source), with disastrous results.

The United States Pharmacopoeia (U.S.P.) determines the water purity requirements for the United States pharmaceutical industry. The purity requirements are typically less stringent than those for the semiconductor industry, with exception to microbial contaminants and pyrogens.

## Mixed bed ion exchange modeling objectives

This work proposes an algorithm to model the behavior of a mixed bed ion exchange column under a variety of industrial applications. The model intends to have the following options or attributes, many of which were developed in theory by Sunkavalli (1996) and Liu (1998).

- Modeling multicomponent systems to include up to eight strong base cations, eight strong base anions, five single-step dissociative monovalent weak bases, five single step dissociative monovalent weak acids, one each of a two-step dissociative base and acid and one each of a three-step dissociative base and acid.
- Strong electrolyte ion exchange with mass transfer rates calculated by an approximation of the Nernst-Planck ionic flux integrated across a thin film.
- Model weak electrolyte ion exchange with mass transfer rates calculated by either Nernst-Planck film diffusion only, or a combination of Nernst-Planck and Fickian film diffusion if possible.
- Maintain solution phase bulk neutralization for complex ionic species and resin/solution reaction equilibrium for ionic species throughout the duration of the simulation.
- Model the effect of variable influent flow rate and contaminant concentrations for step and pulse concentration experiments.
- Determine the effects of temperature on water properties, ionic diffusivities and dissociation constants, and determine the applicability of the temperature dependent parameters in the model.

- Predict the effects of fouling on the effluent quality and bed performance for both the cation or anion resins.
- Predict the effects of cation resin desulfonation on the effluent water quality.
- Predict the effects of resin heels, or layers of cation or anion resin at the top or the bottom of the mixed bed.

This chapter has introduced ultrapure water, mixed bed ion exchange, ultrapure water applications in industry and explicitly stated the modeling objectives of this work.

In Chapter 2, the development of the analytical model algorithm is discussed. Chapter 3 discusses the numerical integration of the analytical model, and Chapter 4 presents results of several industrial scenarios. Chapter 5 extends the analytical definition to radial flow mixed bed ion exchange units. Chapter 6 offers some conclusions and recommendations for future work in mixed bed ion exchange modeling.

# CHAPTER II

# DEVELOPING AN ANALYTICAL MODEL FOR MIXED BED ION EXCHANGE COLUMNS

## Introduction

Mathematical modeling of a separation process is important to industry because the model provides a tool that may be used to improve the design of a system, or allows an engineer to rate the performance of an existing system. A separation process is modeled by combining first-principles equations to model the system according to physical laws, empirically defining a relationship between the inputs and outputs, or a combination of both. First-principles models are typically very work intensive, but when successful they usually yield a generalized solution that is applicable to many systems. Empirical models are usually system-specific with limited operational flexibility.

First-principles models can be divided into two categories: equilibrium models and rate models. For a fixed-bed system, equilibrium models divide the bed into slices, or elements, and assume the solid phase (resin) and liquid phase (water) reach equilibrium that distributes the species between the two phases. The calculations are similar to vapor-liquid equilibrium distillation calculations. Equilibrium models are generally over-simplified, as they assume equilibrium concentrations in the solution

and resin phase without regard to the rates of mass transfer entering and leaving the solid phase. But, they may be useful for general trending and quick estimations.

Rate models may be significantly more accurate than equilibrium models, but they are also much more complex. Like equilibrium models, rate models also divide the bed into a number of elements. Phase equilibrium is typically assumed, but the phase equilibrium conditions are used only to calculate the mass transfer rate of each species across the phase boundary. This is the primary difference of the rate and equilibrium models, the effluent concentration of a rate model is not necessarily in equilibrium with any slice of the bed because there may not be enough time for the liquid and solid phases to reach equilibrium.

The Oklahoma State University Ultrapure Water Research Group developed a rate model for the mixed bed ion exchange column system based on the first principles of continuity. The model uses empirical correlations and constants to estimate solution, resin, and ionic properties. The model used multicomponent reaction equilibrium, Nernst-Planck diffusion, and bulk neutralization in a column material balance.

The work began with Haub and Foutch (1986) by applying a component column material balance to a strong electrolyte, single cation/single anion system in cylindrical coordinates and using a linear concentration driving force model to approximate ionic transfer. Foutch and co-workers have done much work to expand the functionality of the model, but the following elements are present in each variation (including the present work):

- Solution phase bulk neutralization and resin phase reaction equilibrium—provides boundary conditions required to calculate the ionic fluxes.

- Flux expressions—Calculates the mass flow rate per unit area of each ionic species entering and leaving the resin.
- Rate expressions—Required for material balance integration, rate expressions vary with time and distance and they are derived for each constituent from ionic and molecular fluxes and several bed parameters.
- Column material balance—Accounts for all species leaving the solution phase and entering the resin phase as a function of time and distance.

This chapter presents a literature review of the mixed bed ion exchange column model, qualitatively describes the dynamics of mixed-bed ion exchange column modeling, lists the assumptions required for completion of the model and then discusses the refinements made to each element of the model algorithm. The elements will be discussed in reverse order, i.e. the derivation of the column material balance is listed first, then the rate expressions are developed, the flux expressions are described and the chapter concludes with a discussion of the resin phase and bulk phase reaction equilibrium.

## Literature review of strong and weak electrolyte mixed bed column modeling

Haub (1984), Zecchini (1991), Bulusu (1994), Sunkavalli (1996), Chowdiah (1997), and Liu (1998) have done exhaustive literature reviews in mixed bed ion exchange column modeling. The following sections discuss first strong electrolyte ion exchange modeling and then weak electrolyte ion exchange modeling..

### Strong electrolyte mixed bed ion exchange

MBIE technology has been used for water processing for several decades; however, theoretical studies of the MBIE process are still limited. Caddell and Moison

(1954) conducted theoretical study of MBIE. They investigated the variables influencing the breakthrough of mixed-bed, and developed an empirical relationship between leakage and capacity. Their work indicated the general applicability of mixed-bed deionization over a wide range of flow rates and concentrations.

Frisch and Kunin (1960) further conducted an experimental study on the kinetics of mixed-bed deionization. The effects of influent concentration, flow rate, bed depth, and temperature on bed performance was investigated. They concluded that the ion exchange rate was controlled by a liquid-film mass transfer mechanism at low concentrations.

Studies on liquid-side mass transfer in binary ion exchange systems have been carried out by many researchers (Copeland et al. (1967); Copeland and Marchellow, (1969); Glaski and Dranoff (1963); Kataoka et al. (1968, 1971, 1973); Schlögl and Helfferich (1957); Smith and Dranoff (1964); Turner and Snowdon (1968); and Chowdiah (1996). Schlögl and Helfferich (1957) were the first to apply the Nernst-Planck (N-P) equation to describe the fluxes of ionic species. In their work, the kinetics of a binary system was studied. They showed that the electric field caused by the difference of the diffusivities has a significant effect on the ion exchange rate.

Kataoka et al. (1987) studied the film-diffusion controlled liquid-side mass transfer in a ternary system. Flux expressions for the ions with equal valences and ions with different valences were developed separately. The numerical solution of their model agreed reasonably well with the experimental results. However, the model cannot be extended to more than three species.

Haub and Foutch (1984) were the first to model rate-limited mixed-bed ion exchange at ultrapure water concentrations. They developed a model for hydrogen cycle MBIE at ultra-low concentrations with the dissociation of water considered. The major advantages of this model were the considerations of separate material balances for each resin and the inclusion of water dissociation effects. But the model was limited to only binary monovalent systems such as $Na^+$ - $Cl^-$ at 25 °C.

Divekar et al. (1987) extended this model to incorporate temperature effects, the correlations of physical properties such as diffusivity, viscosity, and dissociation constant as a function of temperature for certain species were developed and implemented in the model. Unfortunately, the temperature dependence of selectivities was not available due to lack of experimental data.

Zecchini (1990, 1991) extended the above models to simulate a ternary system of monovalent ions with amines. Pondugula (1994) extended the model to handle divalent ternary systems, and the effect of desulfonation of the cation resin on column performance was included.

Weak electrolyte mixed bed ion exchange

Samuelson (1963) studied the ion exchange with weak electrolytes. He treated the sorption of weak electrolytes, especially the molecular form, as nonionic adsorption. Helfferich (1962) also investigated the sorption of weak electrolytes. He indicated that the total moles of weak electrolytes adsorbed into resin could exceed the ion-exchange capacity of the resin, which is different from what was observed for strong electrolyte systems.

The ion exchange of weak electrolytes is complicated because the concentration distributions are pH dependent, so that the uptake of weak electrolytes into the ion exchange resin is dependent on the pH of solution. Recently, Jansen et al. (1996b, 1997) studied the effects of pH, solution concentration and dissociation equilibrium on column dynamics of weak electrolyte ion exchange. They found that changing either pH or concentration, while keeping the other variable constant, lead to considerable fluctuations of effluent concentration and pH, respectively. These phenomena, they thought, were caused mainly by the uptake of molecular form electrolytes. They concluded that the exchange of counterions and sorption of neutral species are the two major factors determining the ion exchange behavior of weak electrolytes.

Bulusu (1994) extended the OSU model to handle 3 cations and 5 anions with dissociative carbonates. The ionic flux expression developed by Franzreb et al. (1993) was incorporated in the model, which allowed the modeling of arbitrary valence systems. In addition, Bulusu added modeled the effects of resin heels. Bulusu's model was the prototype of OSU's multicomponent MBIE model. Sunkavalli (1996) developed a more generalized multicomponent MBIE model based on Bulusu's work. The number of strong electrolytes was expanded to 8 cations and 8 anions, and preliminary attempts to model carbonate were made.

Hussey (1996) modified the mass-action reaction equilibrium expressions to calculate the interfacial solution equivalent fractions for ionic species regardless of the form of the resin. A pseudo-ion concept was introduced as reference to guarantee the solution of the mass action equation system, which was necessary for robust calculation

of the interfacial concentrations. The algorithm developed was successfully incorporated in Sunkavalli's (1996) multicomponent model.

Liu (1999) added significant contributions to the OSU multicomponent model, the water chemistry was expanded to include five single-step weak dissociative bases, five single-step weak dissociative acids, one each of a two-step dissociative acid or base, one each of a three-step dissociative acid or base and also included silica exchange. The model trends appeared reasonable except for the effluent concentrations of the weak electrolyte species. The column material balance had errors with respect to both strong and weak electrolyte mass transfer, as will be demonstrated later in this chapter.

## Mixed-bed ion exchange column dynamics

Mixed-bed ion exchange columns are very complex systems because there are two sets of parallel reactions occurring on the cation and anion resin. The reaction products (typically hydrogen and hydroxyl ions) interact with each other in solution. If the cation and anion resin capacities are not balanced to the cation and anion equivalents in solution, the exhaustion of one resin affects the kinetics and equilibrium of the other.

Fixed beds have the advantage of contaminants loading from the top to the bottom of the column. During a service run, three 'zones' develop in the bed and change as a function of time. This is illustrated in Figure II-1.

Exhausted zone—Defined in this work as the region where the cation and anion exchange resins have reached equilibrium with the solution and the mass transfer rates are zero.

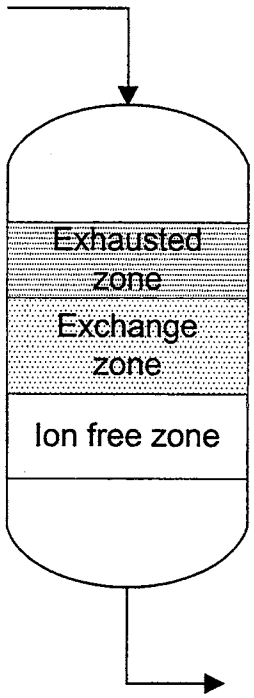


Figure II-1 Exchange zones developed during MBIE service run

Exchange zone—Defined as the zone of the bed where the mass transfer rates are significantly non-zero. Almost all of the ionic contaminants are removed from the water in this section of the bed. The depth and behavior of the exchange zone during the simulation is system dependent.

Ion free zone—Defined as the zone following the exchange zone with near-zero mass transfer rates. The quality of the effluent water is determined in part by the amount of ions loaded on the resin at the bottom of the ion-free zone because contaminants may leach into the water via reaction equilibria.

Suppose the anion resin at the top of the bed were to exhaust more quickly than the cation resin (this is expected, anion diffusivities and selectivities are generally higher than cations). Even if the anion resin loading does not change, implying the anion

exchange rate is zero, the anion resin is still considered to be in the exchange zone as long as the cation exchange rates are non-zero.

## Criteria for successful mixed-bed eon exchange column model

External verification of the model is a topic that has received little attention in the previous works by Foutch and co-workers. It needs to be addressed because of the nature of numerical computing. Every calculation has an associated error, and at times the error may propagate throughout the run and significantly affect the results. It is also quite possible, and in the author's experience quite probable, to 'correctly' enter the necessary equations into a computer program and generate incorrect results. A detailed discussion of the sources of error for the model is described in Chapter 3, but the author has established the following criteria to define proper model function.

- The column material balance must be maintained—This criterion is paramount. Stated plainly, over a given time period the mass of an ionic species removed from the solution phase must be accounted for in the resin phase. As will be discussed in Chapter 3, the column material balance can be checked externally by inspection of the resin equivalent loading as a function of bed depth and the effluent concentration as a function of time.
- Ions must chromatographically elute through the bed as a function of time according to valence, selectivity, and diffusivity criteria—Each ionic species has an affinity to the ion exchange resin defined by reaction equilibrium. For multicomponent systems with parallel reactions, ions with a strong affinity to remain attached to the resin will displace ions with a weak affinity to the resin. This effect essentially stratifies the concentrations of the individual ions throughout the length of the bed as time varies.

The diffusivity in part defines the sharpness of the exchange zone for a particular species. Low diffusivity ions have long exchange zones at UPW service flow rates, high diffusivity ions have narrow exchange zones.

- Smooth solution concentration, resin loading and mass transfer rate profiles without discontinuity or oscillation—The definition of these profiles will be given in Chapter III, but this criterion simply states the numerical integration of the system of differential equations must be stable with few, if any, external constraints applied.
- Infinite time runs gradually settle to effluent concentrations equal to the influent concentrations, and resin loadings settle to the final loadings predicted by mass action equilibrium with the feed—In practice, if a constant contaminant concentration influent is added to a mixed bed and allowed to flow for an infinite time, the effluent concentration will eventually equal the influent concentration because the resin will be completely exhausted. The exhaustion occurs when the resin is in equilibrium with the feed, which leads to zero ionic flux into or out of the resin.
- Effluent contaminant concentrations should correspond reasonably well to industrial data—Most industrial sponsors would prefer this criterion be placed higher on the list; however, it has been the author's experience that it is relatively easy to generate effluent concentrations that show reasonable trend behavior while failing to satisfy the column material balance. If the previous criteria are satisfied and the effluent results do not appear reasonable, several parameters in the model can be used to tune the model to a more correct value.

## Model assumptions

Many simplifying assumptions are required to satisfy physical requirements of the system and make the algorithm calculation feasible. They are listed below in no particular order with commentary about the impact to the model when appropriate.

- Process is film-diffusion controlled—Helfferich (1962) validated the assumption by noting the mass transfer coefficient increased with increasing flow rate
- No net current flow and no net coion flux within the film—no net current flow is required because there is no flow of electrical current in a mixed bed
- The Nernst-Planck film diffusion model predicts all interactions between diffusing ionic species
- The non-ionic (molecular) form of weak electrolytes can be adsorbed through the film and use exchange capacity by direct protonation—Fickian diffusion has been commonly used for molecular diffusion by many resources
- Fick's law models the transfer rate of molecular species into the resin
- Pseudo steady state exchange—variations of concentration with space are much more important than with time
- An ion with a higher valence is preferred to an ion with a lower valence by the ion-exchange resin—assumption is verified experimentally
- Local equilibrium at solid-film interface defined by mass action reaction equilibrium—possibly the weakest assumption of the model, ion exchange thermodynamics is complex and ideal mass action only approximates the equilibrium conditions

- Selectivity coefficients are constant—the assumption necessary for implementation of the thermodynamics, selectivity coefficients are known to vary with resin loading and temperature
- Binary selectivity coefficients can be used for multicomponent ion exchange—a thermodynamic assumption that facilitates the solution of the equations, but only approximates the system
- Activity coefficients are constant and unity—reasonable for solution phase with concentrations less than 0.002 N, most likely inaccurate in resin phase because selectivity is known to vary with resin loading
- Curvature of the film is negligible—the ratio of the stagnant film thickness to the diameter of the particle is extremely small, which justifies the assumption
- Ideal bulk phase neutralization—activity coefficients are near unity at ultrapure water concentrations
- Uniform bulk phase concentrations in each time-distance node—a by-product of no axial dispersion, and valid if no channeling in the bed is occurring
- Isothermal, isobaric operation—the ion exchange reaction is only slightly exothermic and diffusion of ions in water is not a function of pressure

## Mixed bed ion exchange continuity equations

The mixed bed ion exchange column material balance is developed with theory analogous to adsorption modeling. The fundamental equations of the column material balance are written below for a single cation species and a single anion species in a cylindrical packed bed assuming no radial or axial dispersion. Throughout this document,

the subscripts 'i' and 'j' are used to represent ion/counter-ion systems, for this discussion the subscripts 'i' and 'j' refer to a cation and anion constituent, respectively.

$$\frac{\partial C_i^T}{\partial t}+\frac{u}{\varepsilon}\frac{\partial C_i^T}{\partial z}+(FCR)\frac{1-\varepsilon}{\varepsilon}\frac{\partial q_i^T}{\partial t}=0 \qquad \text{(II.1)}$$

$$\frac{\partial C_j^T}{\partial t}+\frac{u}{\varepsilon}\frac{\partial C_j^T}{\partial z}+(FAR)\frac{1-\varepsilon}{\varepsilon}\frac{\partial q_j^T}{\partial t}=0 \qquad \text{(II.2)}$$

where $C_i^T$ and $C_j^T$ are the total constituent solution concentrations, and $q_i^T$ and $q_j^T$ are the total constituent resin concentrations. The constants FCR and FAR are the volume fractions of cation resin and anion resin, respectively, allow the use of the total bed volume for capacity calculations.

The total constituent concentration is a term borrowed from Matthias Franzreb (2000) representing the total concentration of a weak electrolyte. The species of a weak electrolyte is defined as the molecular form that is not a protonation/hydrolysis product. For example, the species associated with ammonia dissociation are

$$NH_3 + H_2O \Leftrightarrow NH_4^+ + OH^- \qquad \text{(II.3)}$$

The constituent species of the ammonia reaction is $NH_3$. Similarly, for carbonic acid,

$$H_2CO_3 \Leftrightarrow H^+CO_3^- + H^+ \Leftrightarrow CO_3^{2-} + H^+ \qquad \text{(II.4)}$$

the constituent is $H_2CO_3$.

The self-dissociation of $H^+$ and $OH^-$ ions makes a mass balance of the constituent species impractical. The constituent definition is very useful. All of the contaminant atoms that are not a component of water are included in the mass of the constituent, regardless of the dissociative behavior of the constituent. Throughout this document the

ionic dissociation products are called the ionic sub-species, or species, of their respective constituent.

Although the system of partial differential equations is homogeneous, the equations cannot be easily integrated because there are three differential quantities: the variation of solution concentration with respect to time; the variation of solution concentration with respect to the length of the bed; and the variation of resin phase concentration with respect to time.

These equations are written separately for each component, but the system is coupled because the equations share a common variable that varies with time and space, the solution pH. An external charge balance is required to adjust the $C_{OH}$ and $C_H$ concentrations with respect to distance and time, which effectively negates an analytical solution of the mixed bed column equation set.

The column material balance for both cation and anion species is solvable by applying the method of characteristics, which combines the time and space variation of the solution concentration and the time variation of the resin phase concentrations into two dimensionless variables. This method can only be performed if the combined differential quantities (the solution concentration variation with time and space) share a common initial condition.

Kataoka (1976) proposed combining the time and distance variables of the solution fraction with the following dimensionless time ($\tau$) and distance ($\xi$) variables (written below for cations).

$$\tau_i = \frac{k_i C_i^f}{Q_i \varepsilon}\left(t - \frac{z\varepsilon}{u_s}\right) \qquad \text{(II.5)}$$

$$\xi_i = \frac{k_i (1-\varepsilon) z}{d_{p,i} u_s} \qquad \text{(II.6)}$$

where $k_i$ is the mass transfer coefficient of species 'i,' and $d_p$ is the diameter of the ion exchange resin bead (cation resin diameter for cations, anion resin diameter for anions).

Kataoka (1973) also proposed the following definitions for a single species model to convert concentration and capacity to dimensionless terms (again the anion definitions are omitted).

$$X_i = \frac{C_i}{C_i^f} \qquad \text{(II.7)}$$

$$Y_i = \frac{q_i}{Q_i} \qquad \text{(II.8)}$$

where $C_i$ is the solution concentration of species 'i,' $C_i^f$ is the feed concentration of ion 'i,' $q_i$ is the resin phase concentration of ion 'i,' and $Q_i$ is the total capacity of the ion exchange resin (cation resin capacity for cations, anion resin capacity for anions). It should be noted the subscript 'i' was not present in Kataoka's concentration definitions.

Previous derivations of the mixed bed ion exchange column model by Zecchini (1991), Sunkavalli (1996), Chowdiah (1997) and Liu (1998) used the following definitions for dimensionless concentrations and capacities,

$$X_i = \frac{C_i}{C_T^f} \qquad \text{(II.9)}$$

$$Y_i = \frac{q_i}{Q} \qquad \text{(II.10)}$$

where $C_i$ is the concentration of a particular ionic species (including sub-species of weak electrolytes) and $C_T^f$ is the total ionic feed concentration. The total ionic feed

concentration is equal for cations and anions because of electroneutrality requirements. They also applied the following definitions for the dimensionless time and distance variables.

$$\tau_i = \frac{k_i C_T^f}{Q_i \varepsilon}\left(t - \frac{z\varepsilon}{u_s}\right) \tag{II.11}$$

$$\xi_i = \frac{k_i (1-\varepsilon) z}{d_{p,i} u_s} \tag{II.12}$$

The dimensionless time and length variable definitions are usable for reduction of the continuity equation, but the solution fraction definition is not usable for integration because the hydrogen ion concentration is the independent solution variable for solving the charge balance, hence the total concentration of the feed is a function of time, distance, and the pH, i.e.

$$X_i = X_i\left(\tau, \xi, C_H^+\right) \tag{II.13}$$

The next section proposes alternative dimensionless variable definitions for reduction of the constituent continuity equation.

## Dimensionless variable definitions

In this work the author has chosen to redefine the dimensionless variables by using ratios instead of solution fractions for constituent mass accounting. The ratios of interest are the solution concentration of the constituent to the total feed concentration of that species, and the ratio of the resin concentration of the individual species to the final equilibrium loading of the species at the given influent concentration.

The total solution concentration of a constituent species is defined as the following,

$$C_i^T = \sum_{k=1}^{n} C_{ik} + C_i^* \qquad \text{(II.14)}$$

where $C_{ik}$ is the concentration of the ionic species of a constituent molecule in mol/l (equivalents are used in most of the solution calculations), 'k' is the index of the ionic sub-species, 'n' is the total number of ionic species of a constituent (e.g. for carbonic acid, n equals two for bicarbonate and carbonate), $C_i^*$ is the molecular species concentration, and $C_i^f$ is the total constituent feed concentration. The total concentration reduces to ionic concentration for a strong electrolyte because 'n' is unity and the molecular concentration is zero.

The total constituent solution concentration is a function of time and bed length only, i.e.,

$$C_i^T = C_i^T(t,z) \qquad \text{(II.15)}$$

For weak electrolyte species, the constituent solution ratios are defined as

$$x_i = \frac{\sum_{k=1}^{n} C_{ik} + C_i^*}{C_i^f} = \frac{C_i^T}{C_i^f} \qquad \text{(II.16)}$$

The resin phase counterpart to the solution constituent concentration is the total constituent capacity. The total constituent capacity combines the individual ionic capacities of a dissociative species, as well as any molecular species in the resin matrix that does not use exchange capacity, into one lump sum. The quantity is required for the material balance and is defined as,

$$q_i^T = \sum_{k=1}^{n} q_{ik} + q_i^* \qquad \text{(II.17)}$$

In this work, the molecular constituent capacity is assumed to be zero. The analytical definition is included for future work. Notice the total constituent capacity is also only a function of time and distance,

$$q_i^T = q_i^T(t,z) \qquad \text{(II.18)}$$

The constituent resin ratios are redefined in terms of the total constituent capacity, $q_i^T$, and the equilibrium constituent capacity $q_i^e$. The equilibrium constituent capacity is found by solving the mass-action equilibrium expressions for the resin loadings at a given feed concentration and multiplying the loadings by the total capacity.

$$y_i = \frac{q_i^T}{q_i^e} = \frac{\sum_{k=1}^{n} q_{ik}}{q_i^e} \qquad \text{(II.19)}$$

Throughout this work, the lowercase 'x' and 'y' refer to the ratio of the total solution or resin phase concentration of a particular species, and the uppercase 'X' and 'Y' refer to the equivalent fraction of an ion with respect to the total number of ions in the solution and resin, respectively.

The column material balance for a fixed packed-bed is now re-written for each cation and anion species based on the constituent solution concentrations and constituent resin capacities.

$$\frac{\partial C_i^T}{\partial t} + \frac{u}{\varepsilon}\frac{\partial C_i^T}{\partial z} + (FCR)\frac{1-\varepsilon}{\varepsilon}\frac{\partial q_i^T}{\partial t} = 0 \qquad \text{(II.20)}$$

$$\frac{\partial C_j^T}{\partial t} + \frac{u}{\varepsilon}\frac{\partial C_j^T}{\partial z} + (FAR)\frac{1-\varepsilon}{\varepsilon}\frac{\partial q_j^T}{\partial t} = 0 \qquad \text{(II.21)}$$

Dividing the each element of the differential equation vector by the respective scalars $\frac{C_i^T q_i^e}{q_i^e}$ and $\frac{C_j^T q_j^e}{q_j^e}$ yields the following system of equations with dimensionless concentrations and capacities varying with dimensional time and length.

$$\frac{\partial x_i}{\partial t} + \frac{u}{\varepsilon}\frac{\partial x_i}{\partial z} + (FCR)\frac{1-\varepsilon}{\varepsilon}\frac{\partial y_i}{\partial t} = 0 \qquad \text{(II.22)}$$

$$\frac{\partial x_j}{\partial t} + \frac{u}{\varepsilon}\frac{\partial x_j}{\partial z} + (FAR)\frac{1-\varepsilon}{\varepsilon}\frac{\partial y_j}{\partial t} = 0 \qquad \text{(II.23)}$$

The new definitions of the solution and resin fractions must be greater than zero, but they are not constrained to a maximum limit of 1.0 because they are referenced to the initial concentrations and final capacities, and not referenced to the total concentration and capacity. Accumulation of species in the bed leads to concentrations and capacities greater than (and less than) the initial and final values throughout the run.

As time approaches infinity; the final value of '$x_i$' and '$y_i$' is unity. This provides a defined final value boundary condition for the model, a benefit that is used to speed the numerical integration of the model.

The new dimensionless variables are used with the method of characteristics because the time and distance variation of the constituent ratio share the common initial conditions, the feed concentration of the constituents, $C_i^f$ and $C_j^f$. The dimensionless time and distance variables shown below in Equations (II.24) and (II.25) are similar to the variable proposed by Kataoka (1973), but the time variable uses the influent concentration and final equilibrium capacity of the particular species. The dimensionless variables for constituent 'i' are defined below

$$\tau_i = \frac{k_i C_i^f}{q_i^e \varepsilon}\left(t - \frac{z\varepsilon}{u_s}\right) \tag{II.24}$$

$$\xi_i = \frac{k_i (1-\varepsilon) z}{d_{p,i} u_s} \tag{II.25}$$

The third order differential equations are reduced to second order differential equations by applying the chain rule to scale the coordinate axes from time and length to dimensionless time and length. The derivation is presented in Appendix D, resulting in the following equation set for cations and anions.

$$\frac{\partial x_i}{\partial \xi_i} + FCR \cdot \frac{\partial y_i}{\partial \tau_i} = 0 \tag{II.26}$$

$$\frac{\partial x_j}{\partial \xi_j} + FAR \cdot \frac{\partial y_j}{\partial \tau_j} = 0 \tag{II.27}$$

For a single species, there is only one species feed concentration and equilibrium capacity, and the dimensionless time and distance variables translate directly to real time and distance by applying the method of separation of variables. However, for each ionic species to be integrated along the same real time and distance axis, appropriate constants must be applied to scale each constituent to a reference constituent.

For this work, the constituent with the largest dimensionless time ion is chosen as the reference constituent; however, selection of the reference constituent deserves discussion. The author concedes there may be more elegant selection algorithms, as he is not aware of a rigorous proof for the optimum reference constituent. Experience with the numerical integration of the equation set shows the species with the largest dimensionless time will have largest rates. The constituent with the largest rate is most likely to over-

predict the change in resin capacity ratio as the resin loading nears equilibrium if the time integration increment is too large.

Another consideration for using the constituent with the largest $\tau$ as the reference is the dimensionless distance variable is directly related to the dimensionless time variable by means of the mass transfer coefficient, bed length, and fluid velocity. The dimensionless distance is not sensitive to influent concentration and equilibrium capacity.

The derivation demonstrating the change of integration variables from $\partial\tau_i$ and $\partial\xi_i$ to the reference constituent integration increments, $\partial\tau_r$ and $\partial\xi_r$, is in Appendix D. The result is the following sets of equations.

$$\frac{\partial x_i}{\partial \xi_r} + FCR \cdot \frac{C_r^f}{C_i^f} \frac{q_i^e}{q_r^e} \frac{\partial y_i}{\partial \tau_r} = 0 \qquad \text{(II.28)}$$

$$\frac{\partial x_j}{\partial \xi_r} + FAR \cdot \frac{C_r^f}{C_j^f} \frac{q_j^e}{q_r^e} \frac{\partial y_j}{\partial \tau_r} = 0 \qquad \text{(II.29)}$$

Note Equations (II.28) and (II.29) reduce to Equations (II.26) and (II.27) when constituent 'i' or 'j' is the reference constituent.

The initial conditions for integration are as follows,

$$x_i = 1 \text{ at } t = 0$$

$$y_i = \frac{Y_i^{init}}{y_i^e} \text{ at } t = 0$$

$$R_i^T = R_i^T (t = 0, z = 0)$$

The term $Y_i^{init}$ is the initial resin phase equivalent fraction (also known as the initial loading) at $t = 0$ and $z = 0$.

For the remainder of this discussion the expressions will be developed for the cations only, the reader is asked to recognize analogous expressions are derived for the anion species.

A single element of this partial differential equation set is integrated by applying separation of variables. This technique recognizes that when the differentials must equal to a constant at each time and space coordinate. The two differentials are equated by subtracting one term from both sides of the equation,. In our case, the constant is directly proportional to the constituent mass transfer rate, $R_i^T$.

$$\frac{\partial x_i}{\partial \xi_r} = -FCR \cdot \frac{C_r^f}{C_i^f} \frac{q_i^e}{q_r^e} \frac{\partial y_i}{\partial \tau_r} = R_i^T(\tau, \xi) \qquad \text{(II.30)}$$

Analytical solutions for this differential equation exist when $R_i^T$ is constant, but in our system the rates vary with time and distance because solution concentrations, solution pH and resin loadings change. This forces simultaneous numerical integration first in the length direction to calculate the solution ratio profiles, then in the time direction to calculate the changes in the constituent capacity profiles. An algebraic definition of $R_i^T$ is required that varies according to Nernst-Planck and Fickian diffusion principles when equations are varied with distance and time.

Perhaps the greatest strength (and weakness) of this model is that the column material balance is as accurate as the rate expressions developed for the particular system. Foutch and co-workers arguably have developed the most advanced rate expressions for ion exchange rate calculations, as they have incorporated the multicomponent ionic flux expressions developed by Franzreb (1993) with temperature dependence, solution chemistry and reaction equilibrium. They also considered the effects of molecular

species transfer into the resin. The development of the exchange rates is complex and is discussed later in this chapter and in Appendices A, B and C.

The mass transfer can be written for an arbitrary dissociative species by combining the ionic and molecular fluxes for integration along the distance path. The ionic and molecular fluxes, $J_{ik}$ and $J_i^*$ respectively, are defined in the next section. For cations,

$$\frac{\partial x_i}{\partial \xi_r} = R_i^T = \frac{6(FCR)}{C_i^f}\frac{d_{p,r}}{d_{p,i}}\left[\sum_{k=1}^{n}\left(\frac{J_{ik}}{k_e}\right)\frac{k_e}{k_r} + \frac{J_i^m}{k_r}\right] \qquad \text{(II.31)}$$

where $J_{ik}$ represents the individual ionic fluxes of constituent 'i,' $J_i^m$ is the molecular flux of species 'i,' and $k_e$ is the effective mass transfer coefficient calculated from the effective diffusivity in the flux expressions.

The solution constituent ratios in Equation (II.31) are easily converted to absolute concentrations by multiplying by the respective reference values, and a separate dissociation equilibrium routine calculates the resulting ionic concentrations. The equations may be integrated by using one of several numerical methods, but for this work, Gear's backward difference method has been shown to be reliable (Zecchini 1991). The procedure is optimal because it requires only one function evaluation of $R_i^T$ per distance increment.

The loading profiles are changed by relating the differential $\partial y_i/\partial \tau_r$ and $R_i^T$ to the loading profile $Y_i$. Note $y_i$ is the ratio of species 'i' capacity to its equilibrium capacity, while $Y_i$ is the fraction of the total capacity. These quantities are related according to Equation (II.32).

$$Y_i = y_i \frac{q_i^e}{Q_i} = y_i Y_i^e \qquad \text{(II.32)}$$

Differentiating Equation (II.32) with respect to $y_i$ yields

$$\frac{dY_i}{dy_i} = Y_i^e \qquad \text{(II.33)}$$

The differential is then used in the chain rule to relate the total rate to the change in resin equivalent fraction as below in Equation (II.34). The details are given in Appendix D, the final form is

$$\frac{dY_i}{d\tau_r} = Y_i^e \frac{C_r^f}{q_r^e} \frac{q_i^e}{C_i^f} R_i^T \qquad \text{(II.34)}$$

The preceding equations analytically define the column material balance, but the numerical integration of the differential equations requires dividing the bed length into a finite number of elements. The algorithm requires extending the vector equations to matrix equations, where the concentrations of each time and space node are determined from the previous distance and time slices. The detailed solution algorithm for the model is presented in Chapter 3.

## Rate expression development

The constituent mass transfer rate, $R_i^T$, physically represents the amount of a constituent entering or leaving the resin at a specific point in time and space. The mass transfer mechanisms are characterized by Nernst-Planck diffusion of ions and Fickian diffusion of molecular species through a stagnant film.

Figure II-2 below pictorially describes the possible mass transfer mechanisms across the stagnant film. There are three routes for a species to enter the resin:

- Reversible ionic diffusion with the mass transfer mechanism calculated with the Nernst-Planck expressions
- Irreversible molecular diffusion of a species with Fickian diffusion that results in the protonation/hydrolysis of the molecular species that uses exchange capacity
- Irreversible molecular diffusion of a species with Fickian diffusion that results in the molecular species being adsorbed into the resin matrix without using exchange capacity.

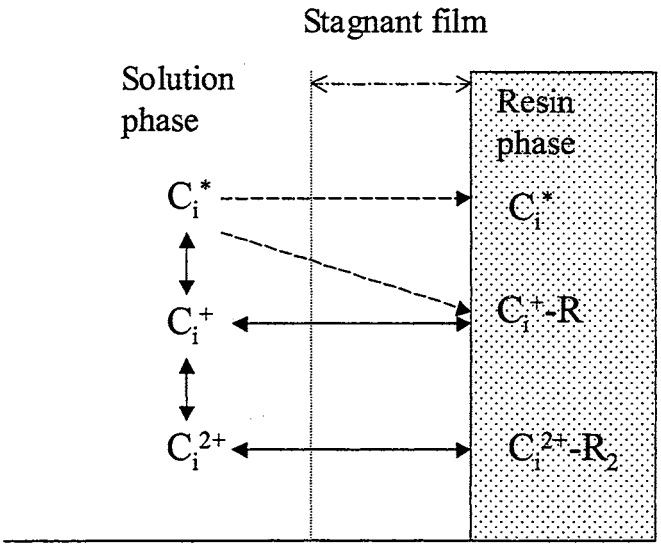


Figure II-2 Possible constituent mass transfer mechanisms for weak electrolytes

Ionic flux expressions

Helfferich (1962) has shown that ultrapure water modeling requires a film diffusion model to calculate the ionic fluxes. Film diffusion assumes the ionic mobility in the resin phase is much faster than across the stagnant film, and was experimentally verified by several authors who noted the mass transfer coefficient increased with increasing flow rate, which implies a decreasing film thickness. The concept is illustrated in Figure II-3 below.

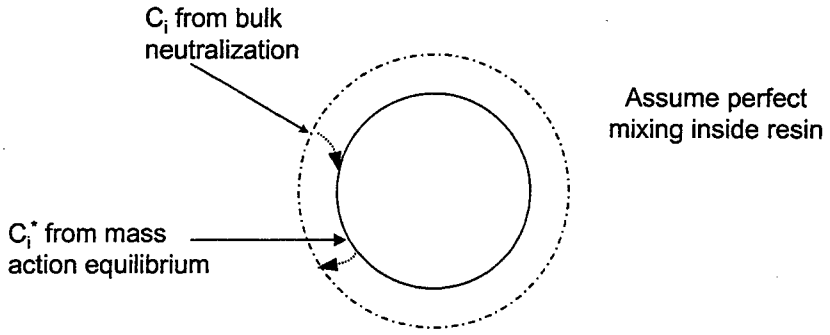


Figure II-3 Ionic fluxes diffusing into and out of an ion exchange resin bead

The bulk phase and interfacial concentrations are required to determine the concentration gradient. An early model by Gluekauf (1947) assumed a linear driving force flux expression; however, the model did not account for the effects of electric potential. Schogl and Helfferich (1957) were the first to apply the Nernst-Planck equation for the derivation of the flux expression.

$$J_i = -D_i\left(\frac{\partial C_i}{\partial r} + \frac{z_i C_i F}{RT}\frac{\partial \phi}{\partial r}\right) \qquad \text{(II.35)}$$

where R is the ideal gas constant, $\phi$ is the electric potential, and F is Faraday's constant.

Franzreb (1993) manipulated the Nernst-Planck equation to form a true multicomponent flux expression by differentiating Equation (II.35) with respect to 'r,' and setting the left-hand side equal to zero. This gave a homogeneous second-order differential equation that was solved analytically. The resulting flux expression is exact for monovalent species, and an approximation for divalent species. The derivation is quite complex and is presented in Appendix C; the final form of the flux expression is

$$\frac{J_i}{k_e} = \frac{D_i}{D_e}\left(\left(1-\frac{N_i}{P}\right)\left(C_i^* - C_i^b\right) + N_i A_i\left(1+\frac{1}{P}\right)\left(C_T^* - C_T^b\right)\right) \qquad \text{(II.36)}$$

where,

$$N_i = -\frac{z_i}{z_Y} \tag{II.37}$$

$$P = \frac{\sum_{i=1}^{n} N_i D_i \left(X_i^* - X_i^b\right)}{\sum_{i=1}^{n} D_i \left(X_i^* - X_i^b\right)} \tag{II.38}$$

$$C_T^* = \left( \frac{\sum_{i=1}^{n} (1+N_i) D_i X_i^b}{\sum_{i=1}^{n} (1+N_i) D_i X_i^*} \right)^{\frac{1}{P+1}} C_T^b \tag{II.39}$$

$$A_i = \frac{1}{C_T^b}\left( z_i C_i^b - B_i \left(C_T^b\right)^{-P} \right) \tag{II.40}$$

$$B_i = \omega \frac{X_i^* - X_i^b}{\left(C_T^*\right)^{-P-1} - \left(C_T^b\right)^{-P-1}} \tag{II.41}$$

The mass transfer coefficient $k_e$ is calculated by using the effective diffusivity to calculate the Schmidt number and applying the Dwivedi and Upadhyay (1979) correlation.

$$k_e = \frac{D_e}{d_{p,i}} Sc^{1/3} Re \left[ \frac{0.765}{(\varepsilon Re)^{0.82}} + \frac{0.365}{(\varepsilon Re)^{0.386}} \right] \tag{II.42}$$

Chowdiah (1996) chose the Dwivedi and Upadhyay correlation to use for flux calculations. His decision was based on correlating experimental mass transfer coefficient data at ppb levels using a j-factor analysis analogous to heat transfer theory. The correlation predicted ionic properties to within 10 %.

Molecular flux expressions

The second and third mechanisms use molecular diffusion for the constituent species to cross the film. Molecular diffusion is known to occur with weak electrolytes, and the proposed model for calculating the fluxes is a linear concentration driving force model presented below.

$$J_i^m = \frac{D_i^m}{\delta}(C_i^m - C_i^{m*}) = k_i^*(C_i^m - C_i^{m*}) \qquad \text{(II.43)}$$

In this work, the molecular fluxes were not implemented successfully because the calculation of the molecular interfacial concentrations did not yield a result that gave a stable solution in the column material balance. This is a recognized weakness of this work because molecular transfer has been shown to be significant by Dranoff et al (1967) and Janzen et al (1997), who both recognized the amount of species adsorbed was greater than the available ion exchange capacity.

Solution phase neutralization for weak and strong electrolyte systems

The assumption of no net current flow states the sum of the positive charge will always equal the sum of the negative charge. Current flow does not spontaneously occur in water systems without an externally applied potential, hence the system is always electrically neutral. The charge balance relationship expressed in terms of ion concentrations and valences is

$$\sum_{i=1}^{m} z_i C_i = \sum_{j=1}^{n} z_j C_j \qquad \text{(II.44)}$$

where $C_i$ is the ionic species concentration of a cation, $C_j$ is the ionic species concentration of the anions, $z_i$ is the positive cation valence, and $z_j$ is the negative anion valence.

If the hydrogen and hydroxyl ions are written separately, Equation (II.44) becomes.

$$\sum_{i=1}^{m} z_i C_i + C_H = \sum_{j=1}^{n} z_j C_j + C_{OH} \qquad \text{(II.45)}$$

Inserting the self-dissociation of water, $k_w = C_H C_{OH}$, for the hydroxyl ion concentration yields Equation (II.46).

$$\sum_{i=1}^{m} z_i C_i + C_H = \sum_{j=1}^{n} z_j C_j + \frac{k_w}{C_H} \qquad \text{(II.46)}$$

For strong electrolyte systems, the right hand side of Equation (II.46) can be subtracted from both sides, giving a second order polynomial that can be solved with the quadratic equation.

$$C_H^2 + \left( \sum_{i=1}^{m} z_i C_i - \sum_{j=1}^{n} z_j C_j \right) C_H - k_w = 0 \qquad \text{(II.47)}$$

Equation (II.47) becomes a higher order polynomial if the $C_i$ and $C_j$ terms are dependent upon the hydrogen/hydroxyl ion concentrations, such as weak electrolytes. Table II-1 summarizes the dissociation equilibrium equations applied for weak electrolytes in this model. The nomenclature for the weak electrolyte types is as follows:

- 'D' indicates a dissociative species
- The number indicates the number of hydrolysis/ protonation products
- The letter 'A' indicates anions (or acid) and 'C' stands for cations.

For example, D1C indicates a single-step dissociative cation, such as ammonia

$$NH_3 + H_2O \Leftrightarrow NH_4^+ + OH^-$$

D2A indicates dissociative two-step acid, such as carbonic acid

$$H_2CO_3 + H_2O \Leftrightarrow H^+CO_3^- + H^+ \Leftrightarrow CO_3^{2-} + H^+$$

The nomenclature system can be applied to a variety of strong and weak acids.

By inspection of the equations in Table II-1, it can be shown the charge balance can be up to a fifth order polynomial if a three-step dissociative base is modeled. Fifth order polynomials require a numerical algorithm that selects the appropriate root for a given simulation. The details of the root selection are in Chapter 3.

The weak acid and base equations are similar in form as they describe step-wise hydrolysis and protonation of dissociative bases and acids, respectively. The dissociation constants are unique for each species, and they are temperature dependent. Temperature dependent parameters are presented in Appendix E.

The ionic concentration expressions are substituted into a charge balance calculation routine. A one-dimensional root-finding numerical method varies the hydrogen ion concentration until the charge balance is zero. A simple heuristic algorithm is applied to select the correct root if multiple roots are present. The numerical solution of the dissociation expressions is discussed in Chapter III.

There are six general categories of weak electrolytes considered in this work: monovalent dissociative acids (chemistry is similar to formic or acetic acids), monovalent dissociative bases (ammonia or ethanolamine), two-step dissociative acids (carbonic acid), two-step dissociative bases (hydrolysis products of zinc, iron or cobalt), three-step

dissociative acids (phosphoric acid), and three-step dissociative bases (metal hydrolysis products). The details of the dissociation chemistry are presented in Appendix B.

Table II-1 Dissociation equilibrium expressions applied in the mixed-bed model

| Weak electrolyte | Anions | Cations |
|---|---|---|
| Monovalent single-step dissociative species | $C^{-}_{D1A} = \frac{C^{T}_{D1A}}{\left(1+\frac{C^{+}_{H}}{K_1}\right)}$ | $C^{+}_{D1C} = \frac{C^{T}_{D1C}}{\left(1+\frac{C^{-}_{OH}}{K_1}\right)}$ |
| | $C^{*}_{D1A} = \frac{C^{-}_{D1A}C^{+}_{H}}{K_1}$ | $C^{*}_{D1C} = \frac{C^{+}_{D1C}C^{-}_{OH}}{K_1}$ |
| Divalent two-step dissociative species | $C^{-}_{D2A} = \frac{C^{T}_{D2A}}{\left(1+\frac{C^{+}_{H}}{K_1}+\frac{K_1}{C^{+}_{H}}\right)}$ | $C^{+}_{D2C} = \frac{C^{T}_{D2C}}{\left(1+\frac{C^{-}_{OH}}{K_1}+\frac{K_1}{C^{-}_{OH}}\right)}$ |
| | $C^{2-}_{D2A} = \frac{K_2 C^{-}_{D2A}}{C^{+}_{H}}$ | $C^{2+}_{D2C} = \frac{K_2 C^{+}_{D2C}}{C^{-}_{OH}}$ |
| | $C^{*}_{D2A} = \frac{C^{-}_{D2A}C^{+}_{H}}{K_1}$ | $C^{*}_{D2C} = \frac{C^{+}_{D2C}C^{-}_{OH}}{K_1}$ |
| Trivalent three-step dissociative species | $C^{-}_{D3A} = \frac{C^{T}_{D3A}}{\left(1+\frac{C^{+}_{H}}{K_1}+\frac{K_2}{C^{+}_{H}}+\frac{K_3K_2}{\left(C^{+}_{H}\right)^2}\right)}$ | $C^{-}_{D3C} = \frac{C^{T}_{D3C}}{\left(1+\frac{C^{-}_{OH}}{K_1}+\frac{K_2}{C^{-}_{OH}}+\frac{K_3K_2}{\left(C^{-}_{OH}\right)^2}\right)}$ |
| | $C^{2-}_{D3A} = \frac{K_2 C^{3-}_{D3A}}{C^{+}_{H}}$ | $C^{2+}_{D3C} = \frac{K_2 C^{3+}_{D3C}}{C^{-}_{OH}}$ |
| | $C^{3-}_{D3A} = \frac{C^{2-}_{D3A}C^{+}_{H}}{K_3}$ | $C^{3+}_{D3C} = \frac{C^{2+}_{D3C}C^{-}_{OH}}{K_3}$ |
| | $C^{*}_{D3A} = \frac{C^{-}_{D3A}C^{+}_{H}}{K_1}$ | $C^{*}_{D3C} = \frac{C^{+}_{D3C}C^{-}_{OH}}{K_1}$ |

Resin phase reaction equilibrium

Two key assumptions allow the application of mass-action reaction equilibrium: 1) the reaction equilibrium of the exchange reaction is ideal and 2) binary selectivity coefficients represent the behavior of multicomponent systems. Mass action is applied for two purposes in this model: 1) to calculate the solution fractions on the surface of the resin and 2) to calculate the equilibrium capacities of the ionic species at a given feed concentration. A summary derivation of the solution fraction algorithm developed by Hussey (1996) is presented below.

The mass-action reaction equilibrium expression for an arbitrary cation 'i' and hydrogen is given below in Equation (II.48).

$$K_H^i = \left(\frac{q_i}{C_i^*}\right)^{z_H} \left(\frac{C_H^*}{q_H}\right)^{z_i} \tag{II.48}$$

Expressing Equation (II.48) in terms of solution equivalent fractions, resin equivalent fractions, total capacity and total interfacial concentration yields the following.

$$K_H^i = \left(\frac{Y_i}{X_i^*}\right)^{z_H} \left(\frac{X_H^*}{Y_H}\right)^{z_i} Q^{(z_H - z_i)} C_T^{*(z_i - z_H)} \tag{II.49}$$

Solving Equation (II.49) for $X_i^*$,

$$X_i^* = Y_i \left(K_H^i\right)^{-1/z_H} \left(\frac{X_H^*}{Y_H}\right)^{z_i/z_H} \left(\frac{Q}{C_T^*}\right)^{1-z_i/z_H} \tag{II.50}$$

and inserting into the solution fraction constraint,

$$\sum_{i=1}^{n} X_i^* \tag{II.51}$$

yields the following polynomial that can be solved with a one-dimensional root finding numerical method with $X_H^*$ as the independent variable

$$f\left(X_H^*\right) = 1 - \sum_{i=1}^{n} \lambda_i \left(X_H^*\right)^{z_i/z_H} \tag{II.52}$$

where $\lambda_i$ represents the constants in the mass action expression for ion 'i,'

$$\lambda_i = Y_i \left(K_H^i\right)^{-1/z_H} \left(Y_H\right)^{-z_i/z_H} \left(\frac{Q}{C_T^*}\right)^{z_i/z_H} \tag{II.53}$$

Equation (II.53) has an inherent flaw. The reference ion loading ($Y_H$) has a negative exponent, and the equation becomes undefined if the reference ion loading is zero. Hussey (1996) circumvented this problem by changing the reference ion to a pseudo-ion with properties defined by the ions loaded on the resin. The pseudo-ion selectivity with respect to hydrogen is defined by

$$K_H^{ref} = \prod_{i=1}^{n} K_H^{i\ y_i} \tag{II.54}$$

and the mean ion valence is calculated from an algorithm similar to that developed by Franzreb (1993) for the mean coion valence.

$$z_{ref} = \frac{\sum_{i=1}^{n} z_i q_i}{\sum_{i=1}^{n} q_i} \tag{II.55}$$

The reference ion for each species is switched to the pseudo-ion by changing the reference ion of the selectivity coefficient with the following expression.

$$K_{ref}^{i} = \frac{\left(K_H^i\right)^{z_{ref}}}{\left(K_H^{ref}\right)^{z_i}} \tag{II.56}$$

Equations (II.52) and (II.53) are then written in terms of the pseudo-ion.

$$f\left(X_{ref}^{*}\right) = 1 - \sum_{i=1}^{n} \lambda_i \left(X_{ref}^{*}\right)^{z_i/z_{ref}} \tag{II.57}$$

$$\lambda_i = Y_i \left(K_{ref}^{i}\right)^{-1/z_{ref}} \left(Y_{ref}\right)^{-z_i/z_{ref}} \left(\frac{Q}{C_T^{*}}\right)^{z_i/z_{ref}} \tag{II.58}$$

and the solution fractions are found by back-substitution of $X_{ref}^{*}$ into the vector generated by Equation (II.58) and normalizing the vector to 1.0. Normalization can be done because the solution fractions of each ion are correct in proportion to each other, even if they do not sum to unity.

Calculation of the total interfacial ionic concentrations

The individual and total interfacial concentrations are not known, but are calculated by an iterative procedure that uses the preceding flux expression combined with mass-action reaction equilibrium. The procedure is outlined in Table II-2.

Table II-2 Procedure to calculate the total interfacial ionic concentration and ionic fluxes

| *Step number* | *Procedure action* |
|---|---|
| 1. | Assume $C_T^{*} = C_T^{b}$ |
| 2. | Calculate $X_i$'s using Equations (II.57) and (II.58) |
| 3. | Calculate $C_T^{*}$ using Equation (II.39) |
| 4. | If the difference between new and old $C_T^{*}$ exceeds the specified tolerance, repeat steps 2 and 3 |
| 5. | Calculate the ionic fluxes using Equation (II.36). |

Derivation of the rate expression

Ionic and molecular fluxes have been developed theoretically, and although molecular fluxes are not used in this work, the rate expressions are developed to include them for future reference. From the assumption that the mass flow rate per unit area of a constituent is equal to the sum of its ionic species fluxes plus the molecular flux, the constituent flux is defined.

$$J_i^T = \sum_{k=1}^{n} J_{ik} + J_i^m \qquad \text{(II.59)}$$

The constituent flux is incorporated into the column material balance by relating the change in constituent capacity with respect to time to the product of the constituent flux and the specific surface area.

$$\frac{dq_i^T}{dt} = -J_i^T a_s \qquad \text{(II.60)}$$

The variable $a_s$ is the specific surface area per unit volume. For spherical particles in film diffusion, only the external surface area of the sphere is considered.

$$a_s d_{p,i} = \left( \frac{4\pi r^2}{\frac{4}{3}\pi r^3} \right)(2r) = 6 \qquad \text{(II.61)}$$

The change in loading ratio with respect to time is found by applying Equation (II.61) and the definition of the loading ratio and substituting into Equation (II.60).

$$\frac{dy_i}{dt} = \frac{-6J_i^T}{q_i^e d_{p,i}} \qquad \text{(II.62)}$$

In order to include the particle rate into the column material balance, dt must be changed to $\partial\tau_r$ by successive applications of the chain rule. The details are in Appendix D, the final result is below in Equation (II.63).

$$\frac{\partial y_i}{\partial \tau_r} = -\frac{6J_i^T}{C_i^f k_i}\left(\frac{d_{pr}}{d_{pi}}\frac{q_r^e}{q_i^e}\frac{k_i}{k_r}\right) \tag{II.63}$$

Inserting Equation (II.63) into Equation (II.30) yields the following expression after manipulation.

$$R_i^T = \frac{6(FCR)}{C_i^f}\frac{d_{p,r}}{d_{p,i}}\left[\sum_{k=1}^{n}\left(\frac{J_{ik}}{k_e}\right)\frac{k_e}{k_r} + \frac{J_i^m}{k_r}\right] \tag{II.64}$$

where $R_i^T$ is the dimensionless mass transfer rate for constituent 'i.'

The analytical derivation of the mixed bed model has been presented. Each equation is not needed for integration of the model. Equation (II.30) is the final form of the solution ratio material balance that is integrated, and Equation (II.34) is the differential equation integrated to calculate the change in loading with respect to time. Both equations require the total constituent mass transfer defined by Equation (II.64) to be integrated.

# CHAPTER III

# NUMERICAL INTEGRATION OF THE MIXED-BED ION EXCHANGE COLUMN MODEL

## Introduction

This chapter discusses the numerical integration of the analytical equations of the mixed bed column system and discusses the numerical methods and approximations that were required to implement the analytical mathematics into a computer program. The time-distance node calculation is defined and discussed.

The correct analytical equations are required before numerical calculations can begin, but round-off, extrapolation and interpolation have associated error that may significantly affect the results. An external analysis of the model results is used to prove the closure of the species material balances.

## Column material balance

In Chapter 2, the analytical derivation of the mixed bed model developed a set of partial differential equations of the form;

$$\frac{\partial x_i}{\partial \xi_r} = -\alpha \frac{\partial y_i}{\partial \tau_r} = R_i^T(\tau_r, \xi_r) \qquad \text{(III.1)}$$

where $\alpha_i$ is a constant defined by,

$$\alpha_i = (FR)\frac{q_r^e}{q_i^e}\frac{C_i^f}{C_r^f} \tag{III.2}$$

After defining the initial time and space boundary conditions and integration limits, Equation (III.1) can be separated into two related ordinary difference equations.

$$\Delta x_i = R_i^T \Delta \xi_r \tag{III.3}$$

$$\Delta y_i = -\frac{R_i^T}{\alpha_i}\Delta \tau_r \tag{III.4}$$

Consider Figure III-1.

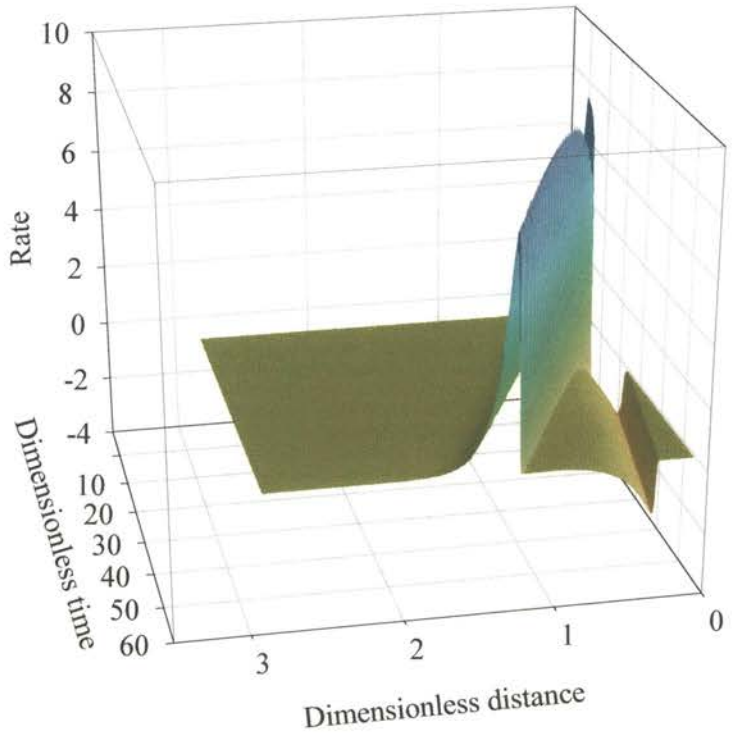


Figure III-1 Example rate surface for integration of Equation (III.1)

Equations (III.3) and (III.4) can be integrated using ordinary differential equation solvers such as Euler's method if the value of the rate is known or can be calculated at each time and distance, but the rate is not known for mixed beds.

Figure III-1 shows a rate surface as a function of time and space for a constituent exchanging in a multicomponent mixed-bed column. The distance is zero at the top of the bed and the service run begins at time equals zero. The value of the rate is positive for constituent entering the resin, and negative for constituent leaving the resin.

From a mathematical perspective, the surface is difficult to predict. There are peaks and valleys that appear to follow orderly rules, but there is no real indication of how the surface was generated. Furthermore, from a mixed-bed modeling perspective, the rate surface of a constituent varies with different initial loadings, influent concentrations, flow rates, and kinetic factors. Almost every rate surface is unique, and there is a rate surface for each constituent.

There are no established rules or boundary conditions derived from the ion properties or bed dynamics to define the surface, especially considering the interactions of other species and service parameters (temperature, fraction of cation/anion resin, etc). This indicates an *a priori* calculation of the rate profiles, though highly desirable, is not practical for mixed bed columns. Therefore we are forced to calculate the exchange rates simultaneously with the column material balance.

As shown in Chapter II, the rate expressions are not written in terms of time and distance, instead the rates are calculated from the thermodynamic equilibrium concentrations of the bulk solution phase and interfacial concentrations calculated from resin phase reaction equilibrium.

The solution and resin thermodynamics are determined from the solution phase concentrations of the constituents and the resin phase ionic concentrations (or resin loadings). The resin loading and solution concentrations vary with time and distance in a fixed coordinate system, hence we have a method to calculate $R_i^T$ at a local point in time and distance based on the local resin and solution concentrations.

The numerical integration of the equations is accomplished by determining the integration limits $\tau_{max}$ and $H_d$, dividing the time and distance axes into a grid, and determining the initial conditions and boundary conditions for the solution phase and resin phase.

Integration limits and increments

Dividing the distance axis by the integration increment effectively splits the bed into a number of slices, or elements. The resin bed is transformed into a finite number of resin disks, as pictured below in Figure III-2. The resin loadings and solution constituent concentrations are assumed to be uniform throughout the element.

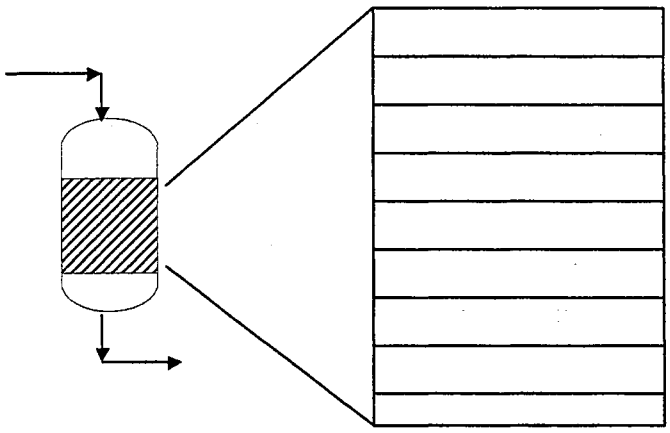

Figure III-2 Dividing resin column into distance elements

The number of distance elements is calculated by dividing the dimensionless column height by the distance step-size,

$$N_S = \frac{H_d}{\Delta\xi_r} \tag{III.5}$$

where the dimensionless column height is found from,

$$H_d = \frac{k_r(1-\varepsilon)L}{u_s d_{p,r}} \tag{III.6}$$

The maximum dimensionless time does not have a definite boundary like the dimensionless column height. Instead, the maximum time is usually user-specified. The number of dimensionless time elements is found from Equations (III.7) and (III.8).

$$N_T = \frac{\tau_{max}}{\Delta\tau} \tag{III.7}$$

$$\tau_{max} = \frac{k_r C_r^f t_{user}}{d_{p,r} q_r^e} \tag{III.8}$$

The integration axes, $\tau_r$ and $\xi_r$, when placed perpendicular to each other form a two-dimensional grid that becomes the integration plane, as shown in Figure III-3.

Time-distance node calculation

Time-distance nodes, or nodes, are the intersection points of the dimensionless time-distance integration increments. The time-distance node calculation links the constituent mass transfer with the column material balance by calculating the exchange rate for each slice at variable loadings and solution concentrations. The node calculation is summarized in Figure III-4.

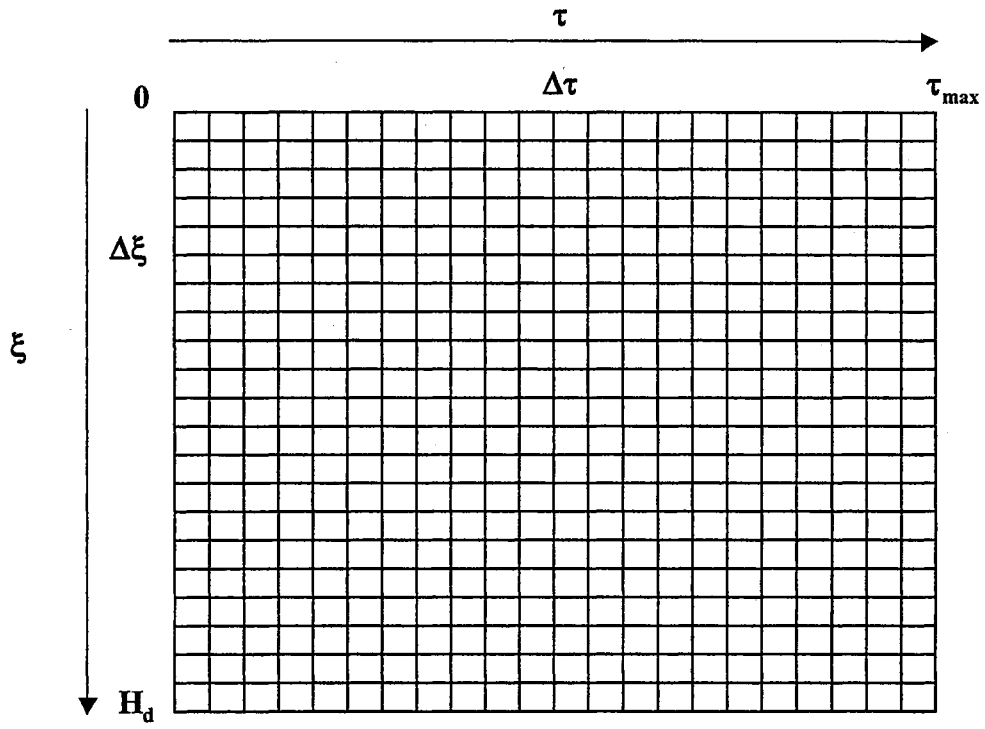


Figure III-3 Integration plane for MBIE system

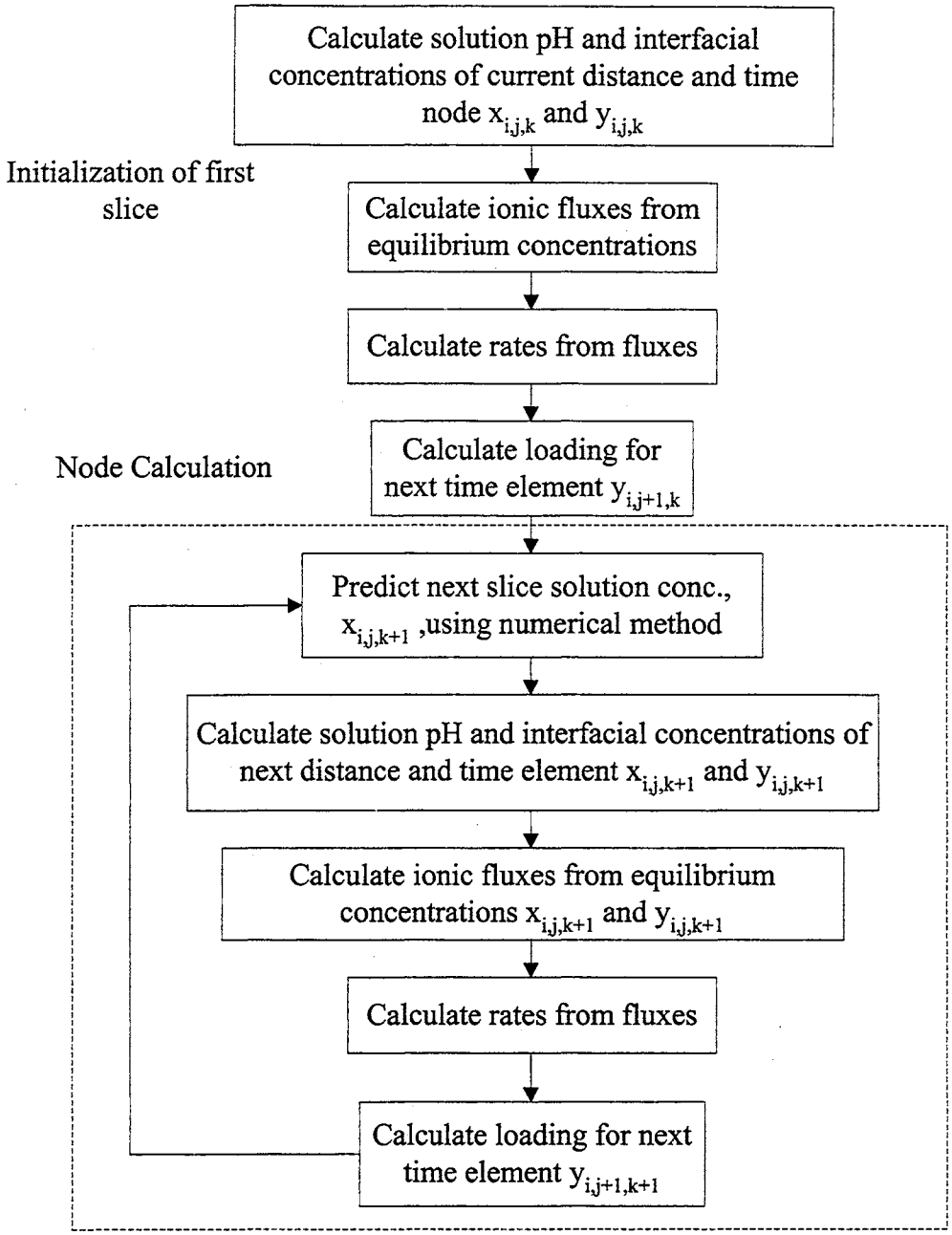


Figure III-4 Flowchart for a node calculation

The indices refer to the constituent 'i,' time coordinate and distance coordinate, respectively. The node calculation incrementally manipulates several sets time-

space dependent matrices, solution concentration ratio matrix, $x_{i,N_T,N_S}$, and the resin capacity ratio $y_{i,N_T,N_S}$. The subscripts '$N_T$' and '$N_S$' are replaced with 'j' and 'k' when referring to an arbitrary position in time and space. Figure III-5 graphically demonstrates the role of the node calculation with respect to the solution and resin constituent ratios $x_{i,j,k}$ and $y_{i,j,k}$.

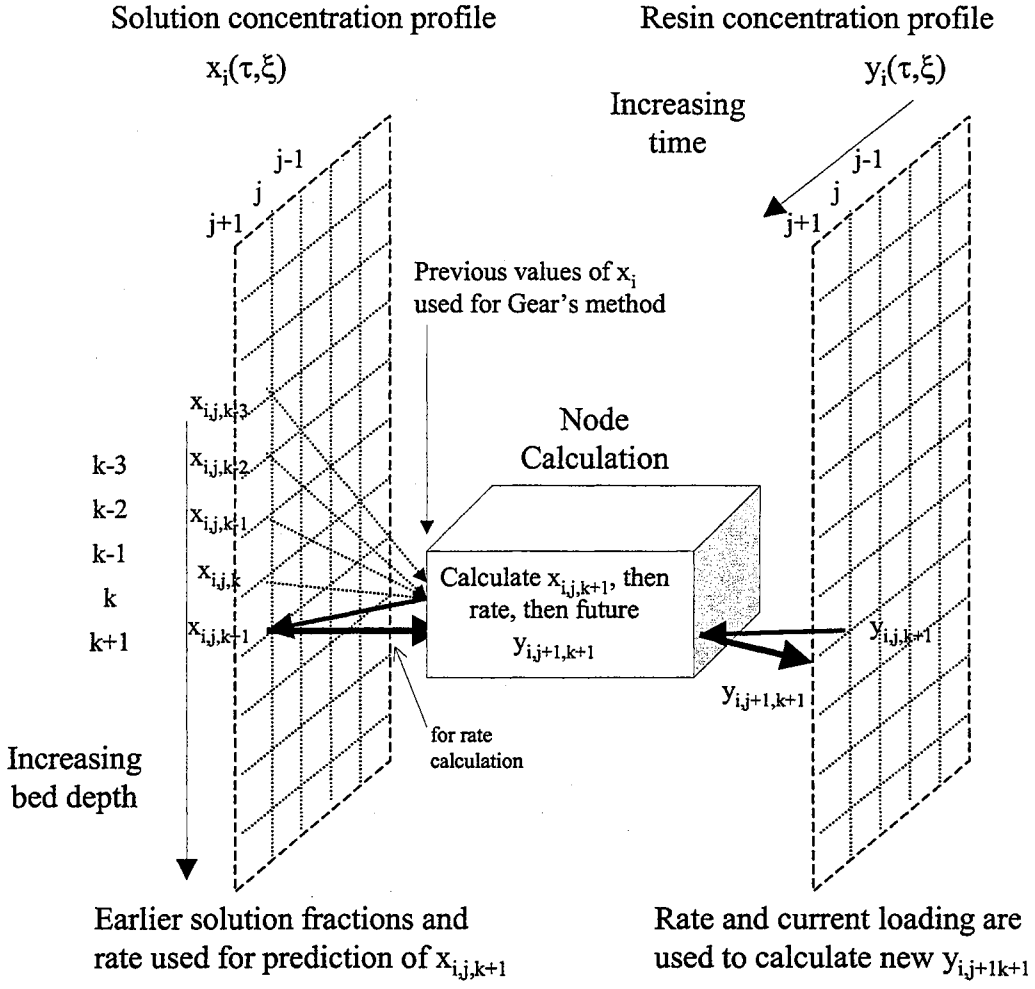


Figure III-5 Interaction of solution and capacity ratio profiles with node calculation for a single constituent

The node calculation is complex; it requires several iterative computations and also uses variable dimension arrays. The following sections describe the numerical calculation of the elements of a node calculation presented in Figure III-4.

Prediction of the next slice solution ratio

Equation (III.3) is the solution ratio differential equation written for integration using the Euler's method. Expanding for integration,

$$x_{i,j,k+1} = x_{i,j,k} + R^{T}_{i,j,k}\Delta\xi_r \qquad \text{(III.9)}$$

Euler's method is an effective approximation for simple functions, but the error term is second order with respect to the step-size h, written as $O(h^2)$, and high accuracy is obtained only with very small step-sizes. The mixed-bed equation system is stiff; some variables change quickly while some change slowly, because variables change with different time scales (Gerald, 1992). Higher order accuracy is required for stiff systems, or the integration becomes unstable.

The fourth-order Runge-Kutta method of numerical integration is popular, it has a fifth order local error, $O(h^5)$, and a global fourth order accuracy, $O(h^4)$. But the application to the mixed-bed system is difficult. It requires four function evaluations per calculation node, and the future values of the rate function are not available as a function of $\tau$ and $\xi$. The rate evaluations require an Euler's method prediction of the solution ratio, which may introduce more local error to the method and also require a lot of computational time.

Several multi-step methods integration methods such as Milne's, Adams-Moulton, and Gear's method have fourth-order accuracy. Of the multi-step methods studied, the Gear's backward difference method was chosen because it requires only one

function evaluation per integration step, and only requires the current value of the rate (typically the 'k' index) and the current and three previous values of the solution ratio. The updating formula is below.

$$x_{i,j,k+1} = -\frac{12}{25}\Delta\xi(FR)R_{i,j,k} - \frac{C_1}{25} \qquad \text{(III.10)}$$

where

$$C_1 = 3x_{i,j,k-3} - 16x_{i,j,k-2} + 36x_{i,j,k-1} - 48x_{i,j,k} \qquad \text{(III.11)}$$

Gear's method is initiated with three Eulers integration steps.

Milne's method was not chosen because of unreliable stability while integrating stiff equation systems. The Adams-Moulton method was not chosen because it requires an estimation of the k+1 rate function, which may increase error and run-time.

Gear's method has a high order accuracy, $O(h^4)$, and it is reliable in stiff systems, The primary disadvantage of Gear's method is the difficulty in implementing a variable step-size. Variable step-sizes are desired for run-time optimization. The integration increments required for Gear's method are spaced equally distant, which causes difficulties when changing the size of the increment. Varying the step-size for a multi-step method requires an interpolation of the previous values when going to a smaller step size, or averages the range of previous values when going to a larger step size.

The variable step-size must be active when the rates are significantly non-zero in order to be effective. Liu (1998) attempted to use a small step-size for the first three slices past the Euler integration. The algorithm was not implemented correctly, because it did not activate with the exchange zone of the bed. The distance elements that were reduced remained at the top of the bed. Variable step-sizes were not used in this work,

but they may be useful for future model optimization. Chapter 6 has recommendations for implementing variable step-size algorithms.

The solution ratio is created each time slice with only the top slice concentration as the boundary condition, i.e. the values of $x_{i,j,k}$ are only used in the working time slice, and the previous time slice values do not need to be stored. This reduces computer memory considerably, and the variables arrays are declared as $x_{i,k}$ in the computer program.

Rate calculation

The rate calculation combines all of the ionic and molecular fluxes of a constituent into a total constituent flux term. The total constituent flux is multiplied by constants to transform the absolute concentration that varies with real time to a dimensionless concentration that varies with dimensionless time.

The rate at a specific time and distance is found from the following equation.

$$R_i^T = -k_e\left(\frac{J_i^T}{k_e}\right)\left(\frac{6d_{p,r}}{C_i^f k_r d_{p,i}}\right)(FR) \qquad \text{(III.12)}$$

The effective mass transfer coefficient, $k_e$, is included because the flux expressions are derived to include it in the denominator.

Ionic fluxes

The ionic flux equations are defined in Chapter II, and their implementation is straightforward after the bulk solution and resin-solution interfacial concentrations have been defined. The flux equations also calculate the effective diffusivity, which is used to calculate the effective mass transfer coefficient of an ion exchange resin. The calculation of the bulk and interfacial concentrations is described in the next two sections.

An effective check to determine if the flux expressions are correctly programmed is to check for the sum of the fluxes being equal to zero, $\sum_{i=1}^{m} J_i = 0$. If the sum does not equal zero, continuity in the resin fluxes is violated and the code is in error.

Dissociation equilibrium of the bulk solution

As stated previously, the charge balance must be satisfied in the solution phase at all times. In Chapter 2, the equation describing the charge balance was defined as,

$$C_H^2 + \left( \sum_{i=1}^{m-1} z_i C_i - \sum_{j=1}^{n-1} z_j C_j \right) C_H - k_w = 0 \qquad \text{(III.13)}$$

An analytical solution exists for strong electrolytes where $C_i$ and $C_j$ are not functions the hydrogen ion concentrations, but for weak electrolytes the constituent ionic concentrations are distributed according to the hydrogen ion concentration. By substituting concentration values of the equation system listed in Table 2-1 into Equation (III.13) and expanding, the following general polynomial form is obtained.

$$a_o + a_1 C_H + a_2 C_H^2 + a_3 C_H^3 + a_4 C_H^4 + a_5 C_H^5 + a_6 C_H^6 = 0 \qquad \text{(III.14)}$$

where the $a_i$ are coefficients determined from the concentrations and dissociation constants of all constituents. The domain of $C_H$ to be evaluated is from $1.0 \times 10^{-14}$ mol/L to 1.0 mol/L, which corresponds to a pH range of 0 to 14.

The coefficients can be either negative or positive, and we have the possibility of six roots for the equation. A one-dimensional root finding numerical method is appropriate for solving higher-order polynomial. The numerical method selection is important. The selection criteria are robustness, accuracy, and speed.

The Newton-Raphson gradient search methods have quadratic convergence when the analytical derivatives are available. These methods were discarded because the analytical derivatives of the polynomial are not readily available for every possible combination of constituents, nor do they guarantee convergence.

By excluding the gradient search methods, most of the remaining available algorithms are bracketed root-finding methods. The global domain is basically between zero and one for water systems, but the possibility of multiple roots within the global bracket suggests the domain should be split into several smaller domains and evaluated. Sunkavalli (1996) developed the algorithm in Figure III-6 for determining the brackets for the root finding methods.

Several globally convergent methods were considered, and their relative advantages and disadvantages were compared. The choices compared were the bisection method, false position, Ridders' method and Brent's method (Press et al, 1994).

The bisection method has guaranteed convergence and is very simple to implement. However, the absolute tolerance for this equation is $1x10^{-16}$ (larger tolerances had propagating errors that caused instabilities in the column material balance), and would require a large number of function evaluations for convergence. The bisection method converges harmonically; the number of iterations required for the tolerance can be shown to be

$$\frac{\varepsilon_o}{\varepsilon} = 2^n \qquad \text{(III.15)}$$

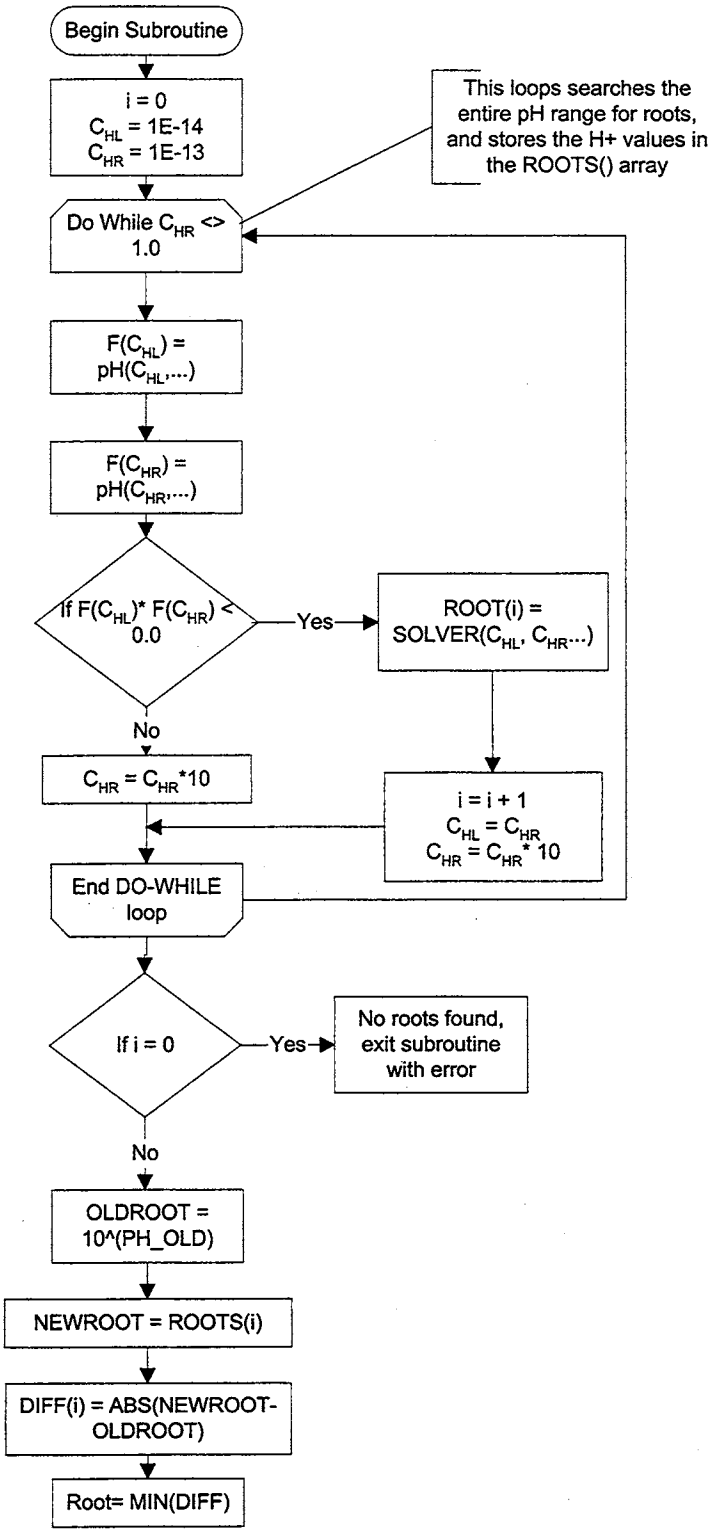


Figure III-6 Algorithm for finding roots throughout entire pH range

where $\varepsilon_o$ is the bracketing interval and $\varepsilon$ is the tolerance. Assuming the pH was 7.5, the bracket would be between $1x10^{-8}$ and $1x10^{-7}$, hence 30 iterations are needed, each requiring a function call, regardless of the complexity of the equation.

The false position method (regula-falsi, or method of interpolation) generally converges more rapidly than bisection and is quite stable, but its convergence is determined by the second derivative value of the function, which may lead to less than linear convergence for functions with near-zero second derivatives (Gerald, 1989).

Ridders' method is an extension of the false position method. It fits a quadratic exponential function to the functional values at the endpoints ($x_1$ and $x_3$) and midpoint of the bracket ($x_2$), i.e.,

$$f(x_1) - 2f(x_3)e^{Q} + f(x_2)e^{2Q} = 0 \qquad \text{(III.16)}$$

The $e^{Q}$ variable is found with the quadratic formula, and used to derive the following updating formula that is applied with the false position algorithm. The 'sign' function is +1 if the argument is positive, -1 if the argument is negative

$$x_4 = x_3 + (x_3 - x_1)\frac{\text{sign}(f(x_1) - f(x_2))f(x_3)}{\sqrt{f(x_3)^2 - f(x_1)f(x_2)}} \qquad \text{(III.17)}$$

Ridders' method has been used effectively in the model, but superior convergence performance was achieved using the Van Wijngaarden-Dekker-Brent method. The algorithm combines two numerical algorithms to guarantee rapid and stable convergence. Brent's method uses inverse quadratic interpolation for sections of the interval that have high curvature, while using the bisection algorithm for intervals with near zero second derivatives.

Multicomponent reaction equilibrium

The interfacial concentration algorithm is discussed in Chapter 2, but the author notes the algorithm is basically a two step method; calculation of the interfacial solution equivalent fractions, and iterating with the solution fractions to calculate the total interfacial concentration. The interfacial solution fractions are discussed in this section, the total interfacial concentrations are discussed in the next section.

The interfacial solution fractions are found by combining the solution fraction constraints and the reaction equilibrium expressions. The resulting equation is a polynomial with fractional exponents, as shown below.

$$f\left(X^*_{ref}\right) = 1 - \sum_{i=1}^{n} \lambda_i \left(X^*_{ref}\right)^{z_i / z_{ref}} \qquad \text{(III.18)}$$

Equation (III.18) is defined if $X^*_{ref}$ is not negative. The root of interest is bounded between zero and one, $\lambda_i$ is always positive and the equation is defined throughout the entire domain. This allows the use of a bracketing root-finding method. Brent's method is also a reliable, convergent algorithm for the reasons discussed in the previous section.

The application of mass action reaction equilibrium in ultrapure water ion exchange equilibrium has not been studied sufficiently. It is arguable that the mass action reaction equilibrium expressions do not accurately represent the equilibrium isotherm of an ultrapure water system. Consider the mass action expression.

$$K_A^B = \left(\frac{Y_B}{X_B^*}\right)^{z_A} \left(\frac{X_A^*}{Y_A}\right)^{z_B} \left(\frac{Q}{C_T}\right)^{(z_A - z_B)} \qquad \text{(III.19)}$$

Notice for monovalent binary systems the $Q/C_T$ term has a zero exponent, making the value of that term 1.0, and the equation reduces to the familiar separation factor expression;

$$K_A^B = \left(\frac{Y_B}{X_B^*}\right)\left(\frac{X_A^*}{Y_A}\right) \qquad \text{(III.20)}$$

For divalent systems, the mass action and separation factor equations no longer resemble each other because of the squared solution to resin concentration ratio, and the exponent for the $Q/C_T$ term for a divalent system is -1.0.

$$K_A^B = \left(\frac{Y_B}{X_B^*}\right)\left(\frac{X_A^*}{Y_A}\right)^2\left(\frac{Q}{C_T}\right)^{-1} \qquad \text{(III.21)}$$

At normal solution concentrations, this factor influences the equilibrium significantly, but it is not dominant. However, for ultrapure water systems, $Q/C_T$ is dominant. The total resin capacity is generally 2.0 meq/ml for strong acid cation resin, and 1.0 meq/ml strong base Type I anion resin. The value of $C_T$ for ultrapure water systems at 25 °C is usually $1x10^{-7}$ eq/L because of the hydrogen/hydroxyl ion concentrations, which gives a value of $Q/C_T$ of about $1.0x10^7$ eq/L.

Consider the right hand sides of Equation (III.20) and Equation (III.21), if the $Q/C_T$ term of Equation (III.21) is moved to the left hand side of the equation, an effective separation factor is developed (noting the squared $X_A^*/Y_A$ term and assuming the magnitude is not large). The $Q/C_T$ term effectively multiplies the selectivity by 10,000,000 at ultrapure water concentrations.

$$K_A^B\left(\frac{Q}{C_T}\right) = \left(\frac{Y_B}{X_B^*}\right)\left(\frac{X_A^*}{Y_A}\right)^2 \approx 10,000,000 \qquad \text{(III.22)}$$

When solving for the loading of a divalent ion 'B' at ultrapure water concentrations, the value is typically greater than 0.99999. This is too close to 1.0 for a numerical column material balance to distribute the remaining monovalent species as the resin approaches equilibrium.

Experience with the model has shown the maximum monovalent mass-action equilibrium constant (equivalent to the separation factor) is approximately 5,000 before instabilities occurred in the column material balance integration. Decreasing the distance step-size can increase the maximum separation factor limit, but run-time considerations preclude any benefit of reducing the distance step-size to less than 0.0001, which was the distance step-size used when finding the 5,000 separation factor limit.

As Equation (III.22) demonstrates, the effective separation factor can be much higher than 5,000 for divalent and trivalent ions. Therefore the mass-action equilibrium model is not compatible with the column material balance for multivalent systems.

Many ion exchange equilibrium models are present in the literature, but the author could not find a multicomponent equilibrium model that could be readily implemented into the model. A simple algorithm was developed to approximate the multivalent exchange properties with monovalent separation factors.

1. The ion with the highest valence and selectivity is chosen as a reference and is assumed to have a separation factor of 5,000.
2. The selectivity of each multivalent ion is found by the following relationship.

$$K_A^i = 5000 \cdot \frac{K_A^{i\ z_i/z_{ref}}}{K_A^{ref}} \qquad \text{(III.23)}$$

3. Divalent and trivalent ions are assumed to be monovalent in the mass action expressions.

The author recognizes the equilibrium model is not rigorous and requires more research; equilibrium model research is a primary conclusion in Chapter VI. However, the approximation generates reasonable results, and is usable for preliminary MBIE modeling.

Ionic flux calculation

The flux expressions developed by Franzreb (1993) require the equivalent fraction resin loading, ionic solution equivalent fraction, valence, diffusivity, selectivity, mass transfer coefficients, and equivalent weight of every ion in solution for input. Note the constituent concentration is not considered in the calculations; the fluxes must be converted to constituent concentrations in the rate expressions.

The ionic data are more readily manipulated by forming separate, combined concentration, loading and property arrays for cations and anions. The combined arrays are sorted according to valence from highest to lowest, and then sorting within each valence category by selectivity. The index used for combined ion arrays is $i_p$, where 'p' denotes the exchange priority of the ion.

The exchange priority index was used in earlier versions of the model where an external constraint was applied (Liu, 1998). The constraint set the flux of a practically non-exchanging ion to zero. Non-exchanging ions were typically the last on the exchange priority list, and the ion calculation would essentially be dropped from the model calculations to avoid exceeding loading constraints.

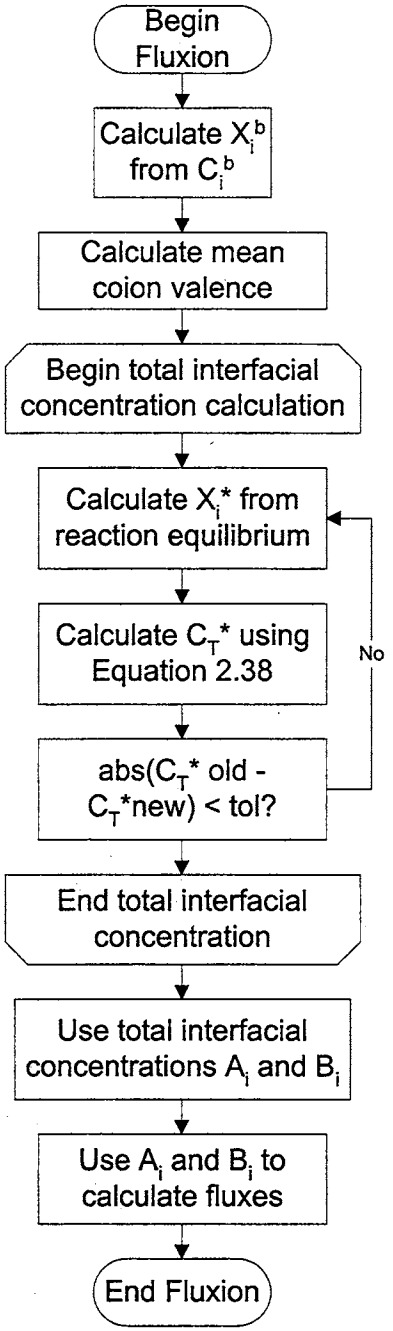


Figure III-7 Flowchart for ionic flux calculation

The constraint was unnecessary, but the exchange priority index is still useful in the model calculations because it provides the elution order of the ionic species as a

function of bed depth, and usually places the reference ion after the contaminants. The flow chart for the ion exchange flux calculations is in Figure III-7.

Resin loading calculation

Figure III-5 shows the interaction of the rates and the solution and resin constituent ratio profiles. The resin constituent ratio is not the resin loading used to calculate the fluxes, the value must be transformed to the resin loading using some variant of Equation (III.24).

$$Y_{i_p} = y_i \frac{q_i^e}{Q_i} = y_i Y_{i_p}^e \qquad \text{(III.24)}$$

where the '$i_p$' subscript is the exchange index of an ionic species of the constituent.

This expression is valid when the constituent uses only ion exchange capacity, and does not include molecular adsorption into the matrix. A different expression is needed when the constituent is loaded on the resin in the molecular form. The overall loading change equation is written below for a single-ion constituent.

$$Y_{i_p,j+1,k+1} = Y_{i_p,j,k+1} + \alpha_i \Delta\tau Y_i^e R_{i,j,k+1}^T \qquad \text{(III.25)}$$

Equation (III.25) is the updating formula for constituents with multiple ions, but the equilibrium loading is that of the ionic species only, as in Equation (III.26).

$$Y_{i_p,j+1,k+1} = Y_{i_p,j,k+1} + \alpha_i \Delta\tau Y_{i_p}^e R_{i,j,k+1}^T \qquad \text{(III.26)}$$

The hydrogen or hydroxyl ion loading is found explicitly by noting the sum of the resin phase ionic equivalent fractions (loadings) must always equal 1.0.

$$\sum_{i=1}^{m} Y_{i_p} = 1.0 \qquad \text{(III.27)}$$

For cation resin, Equation (III.27) is written for the hydrogen loading explicitly to separate the contaminant ions from the reference ion.

$$Y_{H,j+1,k+1} = 1 - \sum_{i=1}^{m-1} Y_{i_p,j+1,k+1} \qquad \text{(III.28)}$$

Inspection of Equations (III.25) and (III.28) show that if the sum of the future contaminant ion loadings is greater than 1.0, then the hydrogen loading would be negative. This is clearly physically impossible, but numerically a possibility during the integration. An external constraint or an algorithm must be developed to prevent the loading constraint from being violated. Equation (III.25) shows the new contaminant loadings can be prevented from summing greater than 1.0 by changing one of three variables: $Y_{i_p,j+1,k+1}$, $R_i^T$ and $\Delta\tau$.

The author has attempted to find an external constraint that can be applied to the loading fractions $Y_{i,j+1,k+1}$ to prevent violating the loading fraction constraints. Several methods were tried to force the sum to equal 1.0. These included normalizing the loadings, harmonic damping of the change in loading, or developing factors based upon equilibrium assumptions to distribute the ions while leaving capacity for the hydrogen ions. All efforts resulted in column material balance instabilities induced by unreasonable fluxes that eventually led to negative bulk concentrations.

Two variables may be altered to manipulate the change in loading; the time step-size, $\Delta\tau$, and the rate, $R_i^T$. The rate appeared to be an attractive variable to manipulate. The exchange rates for all constituents were reduced by multiplying all of the fluxes by a damping constant, such as 0.99, and gradually reducing the rates until the contaminant loadings sum to less than 1.0. Note that changes in the loadings must be accounted for in

the solution phase. These attempts also failed as they induced instabilities in the material balance.

The remaining variable to be varied is the time step-size, $\Delta\tau$. The time step-size was reduced at the beginning of the simulation, and for this work it cannot be changed during the simulation. Decreasing the time step-size had successful results and leads to the following postulate for mixed-bed modeling: If the resin loading constraints are exceeded, the time step-size needs to be reduced.

To the author's knowledge, no constraint may be applied to Equations (III.25) or (III.28) without causing instabilities in the integration. The author notes that it 'feels' correct to not manipulate the equations externally; they are allowed to integrate naturally without disturbances.

### Adapting the material balance to industrial applications

The model developed so far simulates the behavior of a cylindrical, homogeneous, virgin resin mixed-bed vessel at a constant temperature, flow rate and influent concentrations. Industry does not typically have constant flow rate or influent concentrations for the entire service run. Additionally, the resin may foul, or the resin may segregate into heels because of terminal settling velocity differences between anion and cation resin. The properties of water also have known temperature effects, as do selectivities, ionic dissociation constants, and diffusivities.

Industry also requires the model output to be presented in forms that may be correlated to plant data. Typically plants use conductivity measurements compensated to 25 °C.

Several additions need to be added to the model in order to more accurately simulate industrial scenarios. Many of the options were developed by Liu (1998) and are changed only slightly in this work.

Variable influent flow rates and concentrations

The need for variable concentration and flow rates is apparent when viewing the conditions of a mixed bed column. Consider the service conditions of an ion exchange bed in a nuclear power plant. The flow rate through the polishers may be reduced when the power demand decreases in the winter, if the bed had been challenged by a condenser leak, or the source water may vary in concentration if a condenser tube leak should occur.

The season may be significant if the cooling water is drawn from a local river. For example, if it is drought season in the summer, the volumetric flow rate of the river generally decreases while maintaining the approximately the same contaminant mass. Therefore the concentrations increase and challenge the cycle water more with a single tube leak.

The multicomponent model is derived using dimensionless time and distance variables that assume constant feed concentrations, equilibrium capacities, mass transfer coefficients, and superficial velocity.

The dependence of the integration variables on the flow rate and concentration prevents changing the values of the variables without resetting the simulation with new dimensionless variables. Consider the dimensionless height, Equation (III.29).

$$H_d = \frac{k_r(1-\varepsilon)L}{u_s d_{p,r}} \qquad \text{(III.29)}$$

The value of $H_d$ changes with the reference mass transfer coefficient and superficial velocity, which changes the number of distance elements. The dimensionless

height is not a function of the influent concentrations. If we keep the flow rate constant, the number of distance elements does not change.

The dimensionless time (Equation (III.30)) is dependent on the flow rate and influent concentrations, which guarantees the time scale will shift with any influent change. However, this does not necessarily hinder the variable influent algorithm because time is held constant during the distance coordinate integration.

$$\tau_{max} = \frac{k_r C_r^f t_{user}}{d_{p,r} q_r^e} \qquad \text{(III.30)}$$

The model simulates variable influent concentrations and flow rates by importing and exporting the equivalent fraction loading profiles of each ionic species for the cation and anion resin at user-specified times.

The loading profiles are the only extra input required to restart the model because the solution profile is calculated incrementally by the distance integration starting from the top slice boundary condition, while the loading profiles are held constant and are used to calculate the constituent rates. The rate is calculated with the solution and resin concentrations only,

Each ionic species has a unique loading value for each distance element of the bed. The number of slices varies with influent conditions; therefore an interpolation method is required for exporting and importing profiles with different flow rates.

The cubic spline was chosen, because it is less likely to become erratic at sharp changes in the function. The number of data points for an exported profile was arbitrarily chosen to be 300 for this work.

The procedure for exporting the loading profiles follows:

1. Run the model for the user defined time
2. Copy each species loading profile as a function of bed depth, e.g. $Y_{1,500,k}$, to an individual data set D(z,L) with the loading L varying as a function of bed depth, z.
3. Spline the data set D(z,L) to create a second derivative vector, D''(z,L).
4. Use the second derivative vector and an interpolation routine to estimate the N data points at equidistant bed depths.
5. Write and export the time and interpolated loadings to an external loading matrix L(i,z).

Importing the profiles has a similar procedure. The import time is required.

1. Read the import time and calculate the time iteration index.
2. Import the loading matrix L(i,z) and generate the spline D''(z,L) for each ionic species.
3. Used the spline to generate the data set D(z,L) that has a loading for each dimensionless height increment.
4. Copy each D(z,L) to the proper element in $Y_{i,j,k}$.

Occasionally, the sum of the contaminant loadings exceeds 1.0 because of interpolation error. Dividing the loading vector by the sum of the contaminant loadings can normalize the loadings.

Resin heels

The importance of resin heel modeling was discussed in Chapter 2. The model is readily adapted to model resin heels by varying two parameters with respect to distance: the volume fraction of cation and anion resin. The bed is divided into three sections; the

top heel, middle heel and bottom heel. The user is prompted to specify the cation and anion resin volume fractions (FCR and FAR) for each section of the bed, as well as the depth.

The heels are simulated by choosing the appropriate values of FCR and FAR at the beginning of each node calculation. The volume fractions of cation and anion resin are varied in the column material balance according to bed depth. No instabilities in the integration were detected during the test cases; the sudden shift in resin fractions did not cause any oscillations in the solution fraction profiles.

Temperature compensated pH

The dissociation of water is temperature dependent. As is easily seen in Equation (III.31), increasing temperature increases the dissociation constant $k_w$, which increases the concentrations of hydrogen and hydroxyl ions,

$$k_w(T) = C_H C_{OH} \qquad \text{(III.31)}$$

The pH (which equals $-\log_{10}(C_H)$) is often used as an effluent quality indicator. The sample stream from the effluent of a condensate polisher generally cools to near room temperature before it is in contact with the pH probe, and generally the pH meter software compensates for temperature difference from 25 °C.

The model uses the pH at actual temperature for the calculations, but a calculation is needed to report the pH at 25 °C for arbitrary contaminant concentrations for any effluent temperature. The first step is to take the ratio of the dissociation constants.

$$\frac{k_w(25°C)}{k_w(T)} = \frac{C_{H_{25}} C_{OH_{25}}}{C_{H_T} C_{OH_T}} \qquad \text{(III.32)}$$

Equation (III.32) has one equation and two unknowns, the hydrogen and hydroxyl concentration at 25 °C. Assuming the cation and anion contaminant concentrations are equal at both temperatures,

$$\sum_{i=1}^{m-1} C_{i25} = \sum_{i=1}^{m-1} C_{iT} \tag{III.33}$$

$$\sum_{j=1}^{n} C_{j25} = \sum_{j=1}^{n} C_{jT} \tag{III.34}$$

allows the charge balance equations at both temperatures to be equated.

$$\begin{aligned} &\sum_{i=1}^{m-1} z_i C_{i25} + \sum_{j=1}^{n-1} z_j C_{j25} = \sum_{i=1}^{m-1} z_i C_{iT} + \sum_{j=1}^{n-1} z_j C_{jT} \\ &= C_{OH25} - C_{H25} = C_{OHT} - C_{HT} \end{aligned} \tag{III.35}$$

That gives another equation for solving Equation (III.32). Substituting Equation (III.35) into Equation (III.32) and expanding yields the following polynomial in terms of $C_{H_{25}}$.

$$C_{H_{25}}^2 + \left(C_{H_T} - C_{OH_T}\right) C_{H_{25}} - \frac{C_{H_T} C_{OH_T} k_{w25}}{k_{wT}} = 0 \tag{III.36}$$

Equation (III.36) is easily solved for $C_{H_{25}}$ with the quadratic formula, and is used for the temperature compensated pH calculation.

Conductivity

On-line conductivity sensors are standard equipment in an ultrapure water facility, because they provide a real-time indicator of the total ionic solids in the ultrapure water stream. Conductivity meters do not indicate the specific concentrations of ions; instead they indicate the total ionic contaminant concentration. Many of the meters are subject to calibration zero error when measuring ~18.2 MΩ water, but they are very useful as a trending tool.

Theoretically pure water has a conductivity of 0.055 μS/cm. Water is not a perfect insulator because of the self-dissociation of water to hydrogen and hydroxide ions, both of which have a significant conductivity. The theoretical conductivity is calculated by summing the product of the equivalent concentrations and the equivalent conductivity, i.e.

$$\Lambda = \sum_{i=1}^{m} z_i C_i \lambda_i^o + \sum_{j=1}^{n} z_j C_j \lambda_j^o \qquad \text{(III.37)}$$

Many of the specific ionic equivalent conductivities, $\lambda_i^o$, are found in the Handbook of Chemistry and Physics (1999).

Like the pH, industry measures conductivity at 25 °C. Conductivity is also temperature dependent primarily because of the increase in the hydrogen and hydroxyl ion concentrations with increasing temperature. A quick method for compensating for temperature is simply using the same contaminant concentrations with the hydrogen and hydroxyl concentrations found from the temperature dependent pH algorithm.

### External column material balance

The primary criterion for a successful mixed bed model is closure of the material balance. Previous multicomponent models had not checked the constituent balance, and this led to error in some cases. As will be shown in Chapter IV, the mass balance is a primary indicator of the performance of the model with a given influent.

The requirement that constituent mass removed from the solution must equal the constituent mass retained in the resin is used to externally check the mass balance.

$$\Delta m_i^{solution} = -\Delta m_i^{resin} \qquad \text{(III.38)}$$

The change in solution constituent mass can be shown to be the flow rate times the area between the influent and effluent concentration profile, and is shown graphically in Figure III-8.

$$\Delta m_i^{solution} = F\int_0^t \left(C_i^{inf} - C_i^{eff}\right)dt \qquad \text{(III.39)}$$

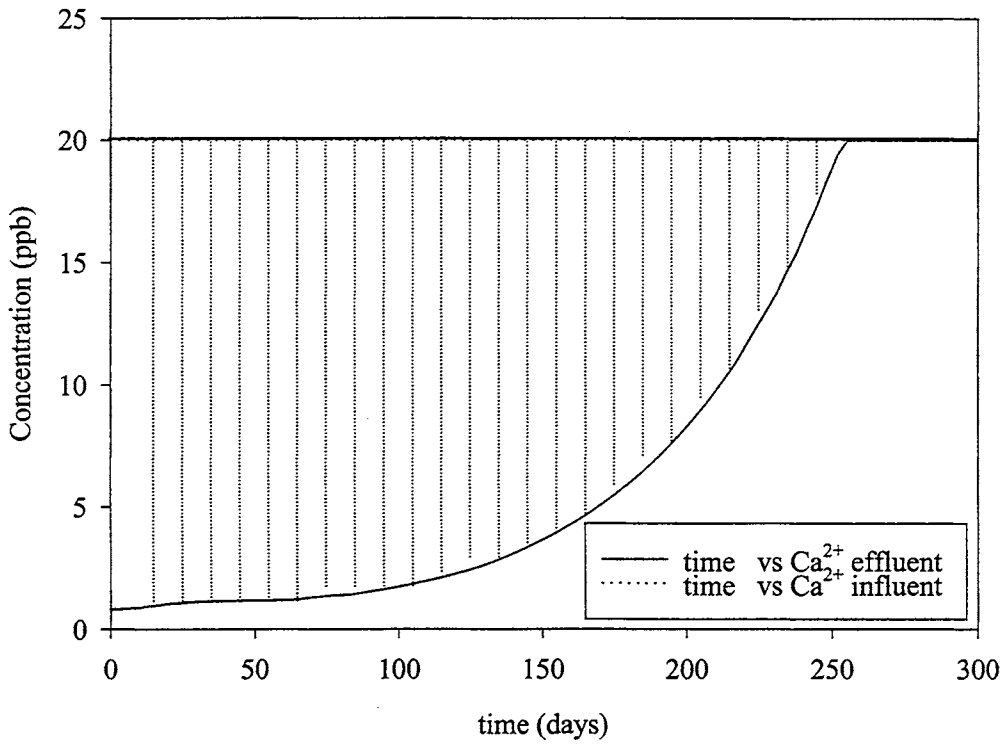


Figure III-8 Calculation of the constituent solution mass using the concentration history

It is computationally tedious to numerically integrate the area between the curves. If a large number of time steps are calculated, large amounts of memory are required to store entire concentration history, and significant processor time is required to apply Simpson's rule or an equivalent numerical integration. The task is simplified by applying the mean value theorem of calculus.

$$\bar{y}(b-a) = \int_a^b y\,dx \qquad \text{(III.40)}$$

Defining the concentration difference as $C_i^R = C_i^{inf} - C_i^{eff}$, and rewriting Equation (III.39) in terms of the mean value theorem yields,

$$F\overline{C_i^R}\Delta t = F\int_0^t C_i^{inf} - C_i^{eff}\,dt \qquad \text{(III.41)}$$

The average value of the concentration difference still requires the complete concentration history as time progresses, which still requires a lot of program memory. Applying a running average algorithm to maintain the average mass of contaminant removed reduces the memory requirement,

$$\left(\overline{C_i^R}\right)_j = \frac{(j-1)\left(\overline{C_i^R}\right)_{j-1} + \left(C_i^R\right)_j}{j} \qquad \text{(III.42)}$$

where 'j' is the time slice index.

A similar method is used to calculate the mass of ions retained in the resin phase. The total contaminant mass in the resin phase at a particular time is found from the following relationship

$$\Delta m_i^{resin} = Q_i V_T (FR_i)(1-\varepsilon) \qquad \text{(III.43)}$$

Assuming uniform radial concentrations and substituting the bed area, length and loading profile as a function of length into Equation (III.43) yields,

$$\Delta m_i^{resin} = Q_i (FR_i)\frac{\pi D_B^2}{4}(1-\varepsilon)\int_0^L Y_i\,dL \qquad \text{(III.44)}$$

Applying the mean value theorem to eliminate the integral reduces Equation (III.44) to the following.

$$\Delta m_i^{resin} = Q_i (FR_i)\frac{\pi D_B^2}{4}(1-\varepsilon)\overline{Y_i}L \qquad \text{(III.45)}$$

## Programming issues

The model is programmed in FORTRAN 90/95 (F90) using the Compaq Visual Fortran Version 6.1 (formerly Digital Visual Fortran) compiler. FORTRAN 90/95 was selected over FORTRAN 77, Visual Basic, and C++ for the following reasons.

- Translation—Much of the previous code was in Fortran, translation to C provides no speed benefit at the expense of much effort.
- Speed—F90 is much faster for numerical computing than Visual Basic.
- Dynamically allocated arrays—Optimizes array sizes for profile variables.
- Code readability—FORTRAN 77, though functional, is limited to 72 characters before a continuation character on the sixth column is required. F90 allow 132 characters, and the continuation character is an ampersand at any location on the line, and another ampersand at the beginning of the next line.
- FORTRAN 90 array formulas—Array formula syntax is very flexible and eliminates many DO loops. It also allows direct assignment statements of an array to a constant or another array of common dimensions, i.e. if each element of X(10) is to be assigned to a value of one, the following statement is acceptable.

  $$X = 1.0 \tag{III.46}$$

  If each element of Y(10) needs to be assigned to X(10), the following is used

  $$Y = X \tag{III.47}$$

- Type variables—Though not implemented in this version, F90 has derived type variables, which will be useful when generalizing constituents (see Chapter 6).

All real variables are double precision, which means they are eight byte numbers that calculate values to 16 significant digits. The default compiler options are usable for

the model as programmed, except the default stack-size (memory reserved for calculations) needs to be increased to at least 32 megabytes, perhaps more if necessary. Insufficient stack size is indicated by a STACK OVERFLOW error.

Array sizes are no longer static as they were in F77. All profile variables are declared as ALLOCATABLE, the number of slices determines the array sizes (variable NOSLICE in the code). The loading arrays are three dimensional, one dimension for the ionic species, one for time slice, and one for distance. The time slice array has only four elements, the memory locations are re-used throughout the simulation. The allocation statement is used for loading arrays, yrc() and yra(). For example,

ALLOCATE(yrc(18,4,noslice),yra(18,4,noslice))

The project is built as a QuickWin application, which allows the program to access the swap file in 32-bit Windows operating systems. The required memory is a function of the number of ionic species and the number of calculation slices. The author notes if the program is regularly accessing the swap file (implying not enough RAM), the model run-time is greatly increased. Excessive swap file access is indicated by either the memory usage in a performance monitor (found in the Task Manager of Windows NT and 2000), or by continuous hard drive activity during the simulation running in Windows 98. In both cases, the system response for other applications is extremely slow.

# CHAPTER IV

# RESULTS AND VALIDATION OF THE MIXED-BED ION EXCHANGE COLUMN MODEL

## Introduction

The previous two chapters developed the analytical concepts and numerical algorithms necessary to model the mixed bed ion exchange column. In this chapter, the results of the modeling effort are presented, and the model is benchmarked to limited experimental data. The following topics are described.

- Results are presented that demonstrate the model satisfies the criteria in Chapter II.
- A parametric analysis to show the flexibility and limitations of the model.
- Ammonia cycle operation is modeled under different temperatures and conditions
- The model is compared to service data presented by Pennsylvania Power and Light.

## Verification of the mixed bed modeling criteria

Five criteria were specified in Chapter II in order for the modeling effort to be considered successful. The following sections described the methods and results used to

verify the criteria were satisfied for this effort. The criteria are not in the order listed in Chapter II.

Ion elution according to ionic properties

Each ionic species has a different affinity to the functional group attached to the ion exchange resin. The affinity is quantified with the selectivity coefficients or separation factors. The observed trend is that given equal concentrations in the solution; the equilibrium loading of the species on the resin varies directly with the separation factor.

Assume a mixed bed column with an influent containing 10 μmol each of calcium sulfate, potassium nitrate and sodium chloride and assume complete dissolution in the aqueous phase. The separation factor order for the cations is calcium, potassium, and sodium; while for the anions it is sulfate, nitrate, and chloride. The diffusivities and selectivities are listed in Table IV-1.

Table IV-1 Ionic property data for elution example

| *Ion* | *Diffusivity ($cm^2/s$)* | *Selectivity* |
|---|---|---|
| *Cations* | | |
| Calcium | $0.79 \times 10^{-5}$ | 4 (5000) |
| Potassium | $1.96 \times 10^{-5}$ | 2.5 |
| Sodium | $1.33 \times 10^{-5}$ | 1.5 |
| *Anions* | | |
| Sulfate | $1.07 \times 10^{-5}$ | 18 (5000) |
| Nitrate | $1.90 \times 10^{-5}$ | 58 |
| Chloride | $2.10 \times 10^{-5}$ | 21 |

Consider a single element of contaminants entering the bed with a uniform velocity. If the mass transfer coefficients are of the same magnitude, but the concentration driving forces are much different according the reaction equilibria; the

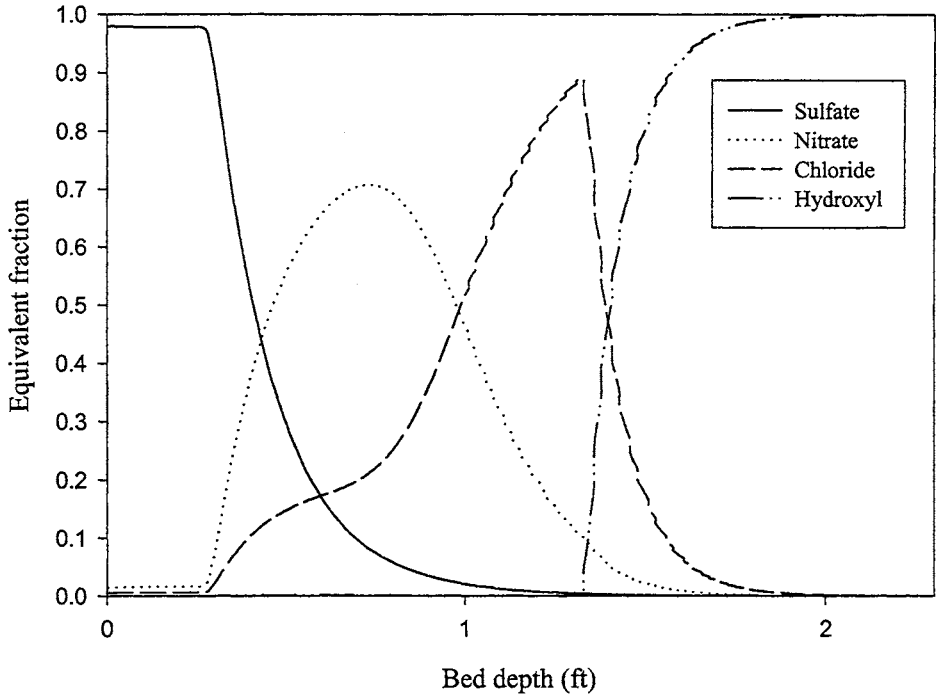


Figure IV-1 Anion resin equivalent fraction elution through mixed bed

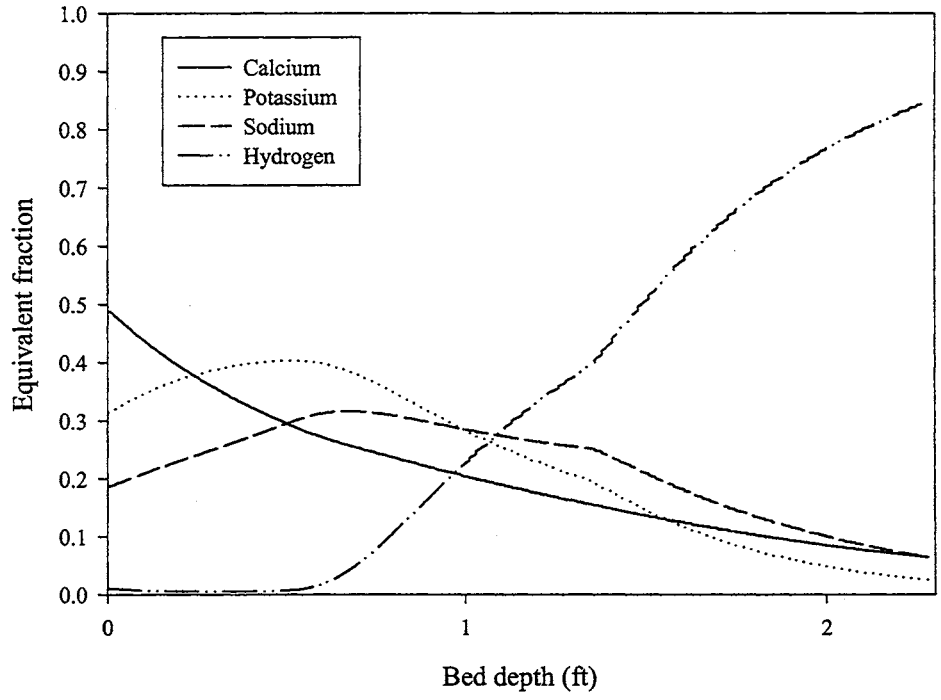


Figure IV-2 Cation equivalent fraction elution through the mixed bed

highest separation factor ion attaches to the resin much more tightly and displaces all other counterions. For the anions described above, as the element of fluid moves through the bed, all of the sulfate ions exchange with the resin at the top of the bed but nitrate and chloride remain in solution. Sulfate is now absent in solution, so nitrate will then preferentially exchange. Finally, chloride exchanges after nitrate.

The concept was demonstrated using the model by exporting the loading profile at an arbitrary time. The results for the anion and cation system described above are in Figure IV-1 and Figure IV-2. The anions appear to follow the concept exactly; there are rather clearly defined sections where the sulfate, nitrate, and chloride are dominant.

The cation system is not as clearly defined. The calcium does displace potassium and sulfate, but even though it is divalent (and has a separation factor of 5000), it has a very long exchange zone and does not displace the sodium and potassium.

This appears to be an error, but it is actually a good demonstration of mixed bed column dynamics. Figure IV-3 shows solution pH as a function of bed depth at several time intervals. The solution pH varies with the length of the bed and is a function of mass transfer rates of cations or anions. If the pH is greater than 7.0 at 25 °C, then the anion resin is providing more hydroxyl ions to solution than the cation resin is supplying hydrogen ions.

In general, anions have higher mass transfer rates than cations, as is indicated in Figure IV-3. The cations are not clearly separated because of the low mass transfer coefficient for calcium and the low selectivities of sodium and potassium. This results in longer exchange zones for cations, because the residence time in a distance element is not long enough to exchange a large fraction of the constituent. Also note the hydrogen and

hydroxyl ions have different diffusivities, and may impact the relative kinetics of the cations and anions.

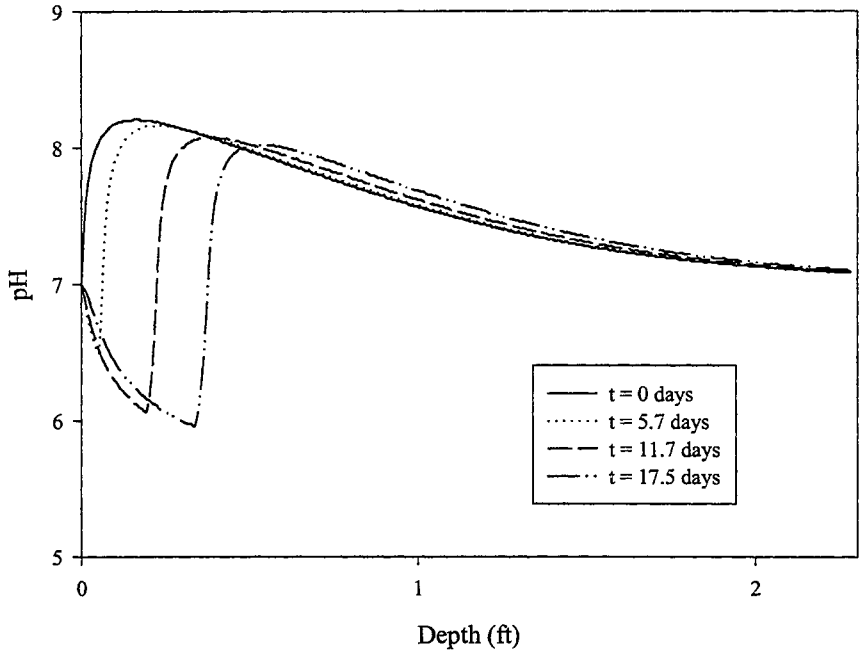


Figure IV-3 Solution pH varying with time and distance in a strong electrolyte system

A nitrate pulse experiment was performed to see the elution of nitrate with ultrapure water feed. Of particular interest is the spreading or tailing of the nitrate peak as time progresses. Figure IV-4 shows that while some spreading does occur, ultrapure water does not elute the nitrate through the bed very quickly, over three years of service were required to change the general shape of the curve, while the effluent quality remained nearly constant.

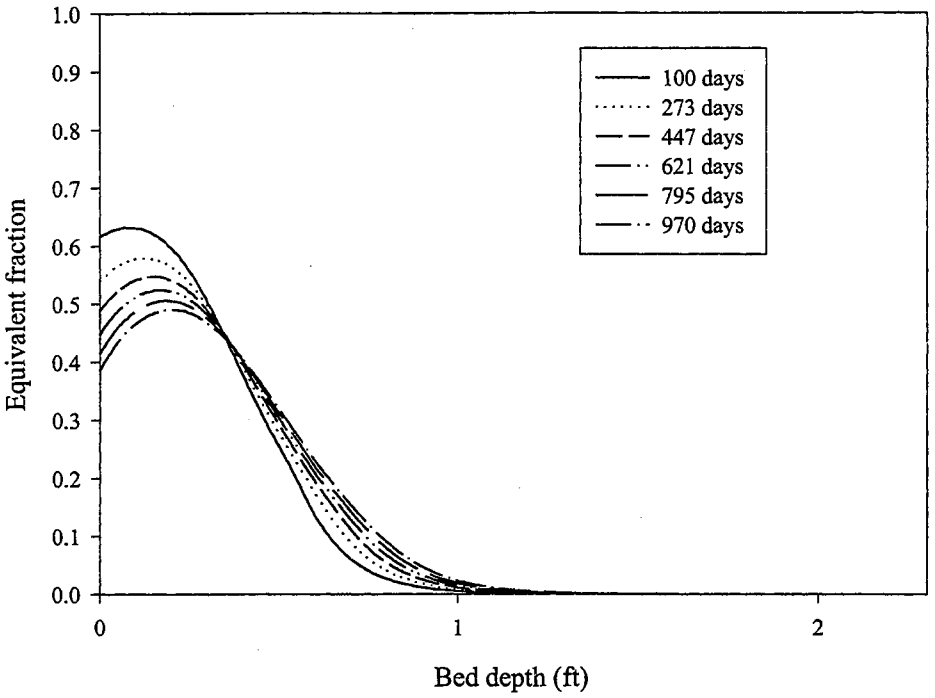


Figure IV-4 Elution of a nitrate peak through a mixed bed with UPW eluent over 1000 days

The following elution trends are observed with respect to selectivity and diffusivity.

- Ions with the highest selectivity elute through the bed more slowly because they displace other ions, hence they are nearest the top of the bed. The order of elution is consistent with theory.
- Ions with high selectivities and high diffusivities generally have sharper delineations between the equilibrium, exchange and ion-free zones than ions with high selectivities and low diffusivities.

Effluent concentration histories

The effluent concentration histories followed expected trends and in general gave reasonable results. Some of these are discussed in the following paragraphs.

Ionic throw—In a multicomponent system, when an ion of lower selectivity breaks through, the effluent concentration of the ionic species becomes greater than the influent concentration because the bed is releasing not only the influent concentration, but also the accumulated ions in the resin phase. Refer to Figure IV-5 for an illustration of sodium throw caused by calcium displacement.

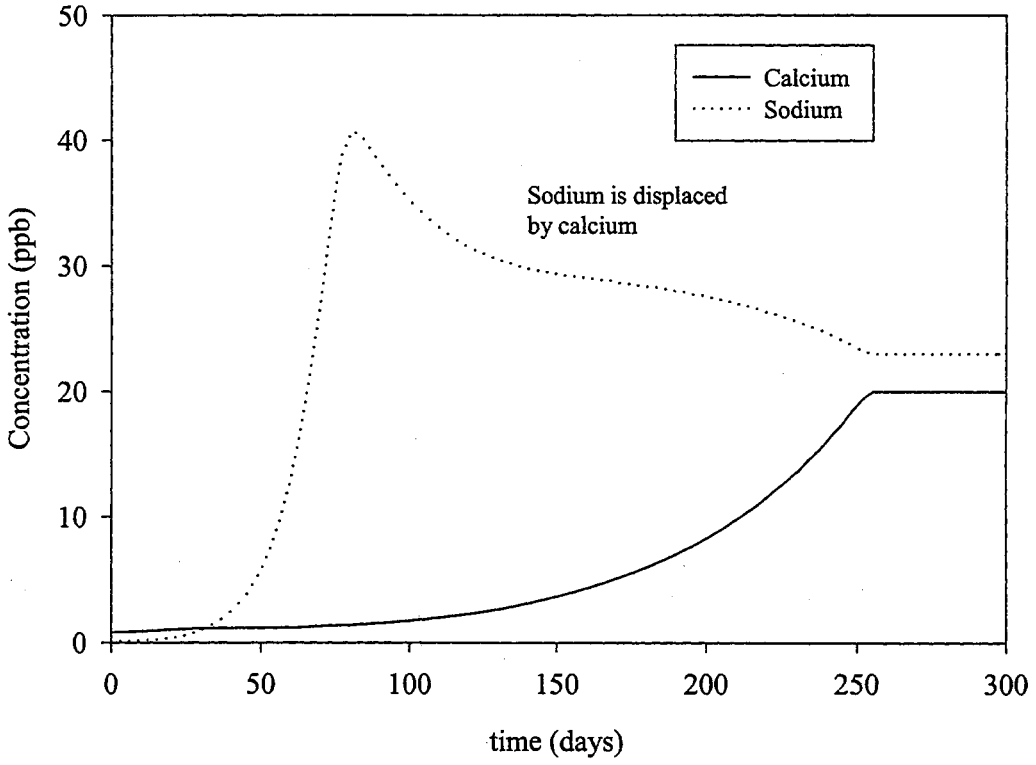


Figure IV-5 Illustration of ionic throw and return to influent concentrations at infinite time

Industrial data illustrating ionic throw are quite rare because the usual protocol for a mixed bed that is leaking ions is to remove it from service before it damages the

system, hence modeling ionic throw has virtually no application in the ultrapure water industry. However, ionic throw is useful to demonstrate the concept of ionic accumulation in the resin phase and, in part, confirms the model is functioning correctly.

Also note the calcium and sodium concentrations in Figure IV-5 eventually became constant. These concentrations equal the influent concentrations and satisfy one of the criteria stated in Chapter II. For most cases tested, the effluent concentrations settled to the influent values.

Effluent concentrations near ultrapure water levels— ultrapure water concentrations are difficult and expensive to measure on-line, and even the best off-line methods have only part per trillion (ppt) resolution. Therefore, it is difficult to determine if the model generates reasonable effluent concentration histories at the beginning of the service run, when the concentrations are less than 1 ppt. However, the results presented in the later examples show the effluent concentrations, if not perfect, are reasonable for the modeled scenarios.

Weak electrolyte modeling—Bulusu (1994), Sunkavalli (1996) and Liu (1998) first attempted multicomponent weak electrolyte ion exchange modeling. The work produced results that followed most of the expected trends, but a mathematical error in the column material balance resulted in a 'bump' for weak electrolytes at the beginning of the run that did not behave properly (see Figure IV-6).

The 'bump' is not present in the current model because the dimensionless variables have been redefined. However, as will be shown in later sections, the dissociative species mass transfer mechanism needs further refinement.

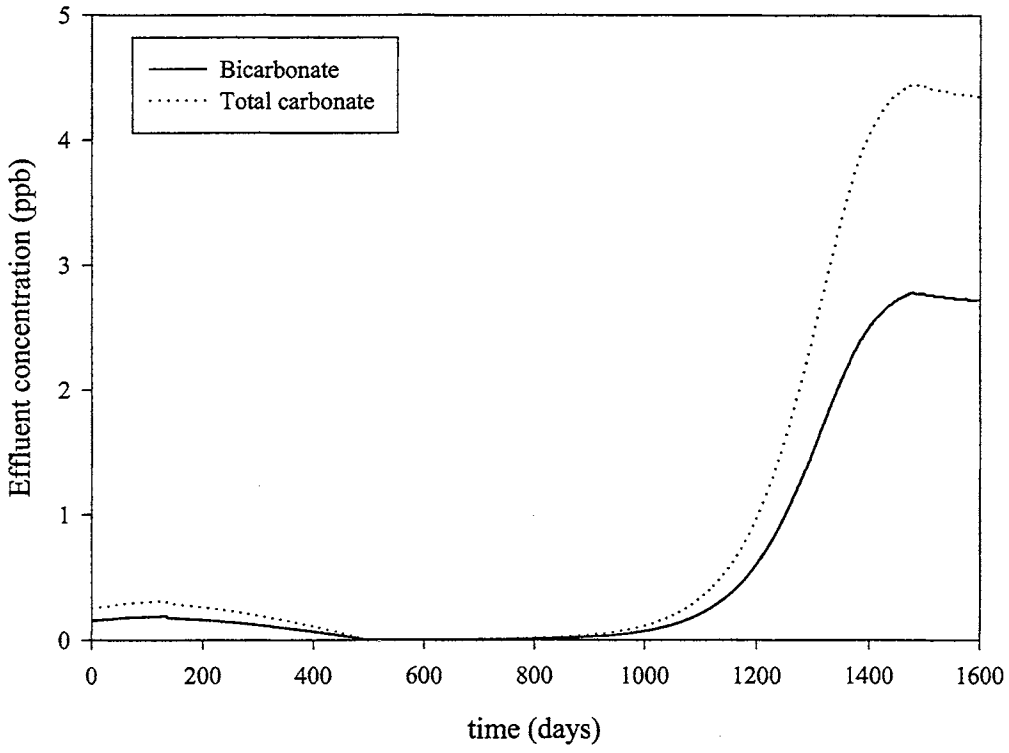


Figure IV-6 Dissociative species bump present in earlier versions of OSUMBIE model

Solution, loading and rate surfaces

As stated in Chapter III, the mixed bed model uses three matrices per constituent to maintain the column material balance. The matrices represent the solution ratio, $x_{i,N_T,N_S}$, resin equivalent fraction, $Y_{i,N_T,N_S}$, and exchange rate profiles, $R^T_{i,j,k}$, that vary with dimensionless time and distance as the independent variables. The constituent capacity ratio matrix, $y_{i,N_T,N_S}$, is not needed for calculations, and it is not stored by the computer program to conserve memory.

The simulator stability is most affected by the rate profiles. If the distance step-size is too large, the rate profiles are the first variable to develop oscillations and discontinuities caused by overestimation of the solution ratio.

Profile variables are generated at each time element. These profiles are exported and the constituent data are collated to form surfaces describing the solution, resin, and exchange rate behavior.

Figure IV-7 is the loading surface for calcium in a calcium-sodium-chloride-sulfate equivalent mixture with equal capacity mixture of cation and anion resin. Consider times slightly above zero. The loading of calcium near the top of the bed (distance is equal to zero) is at the highest point for that particular time, then decays to almost zero near the end of the bed.

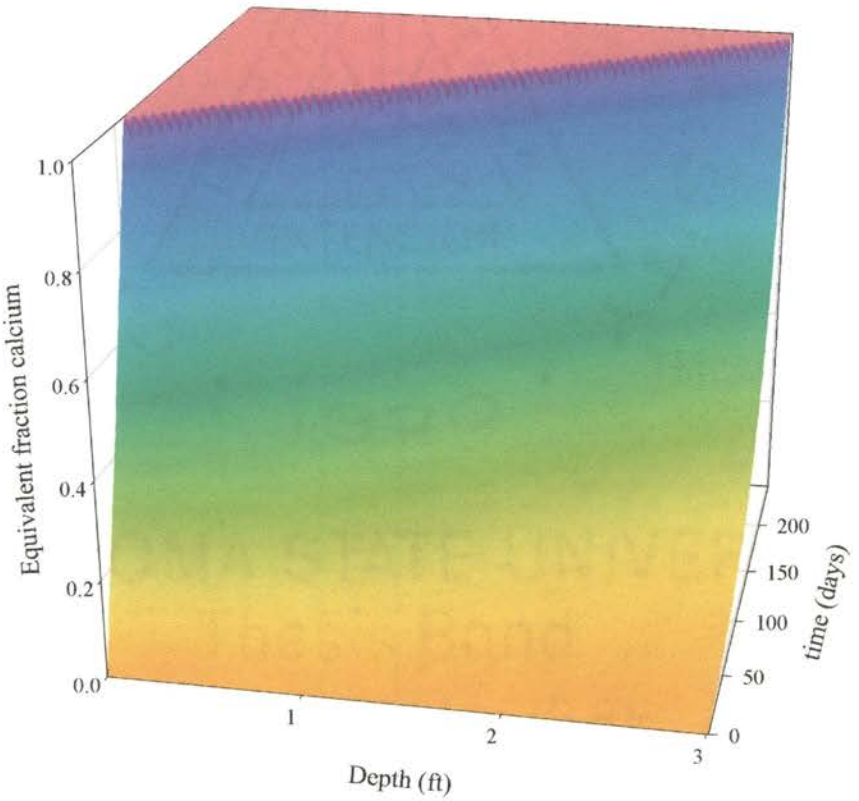


Figure IV-7 Loading surface for calcium in a strong electrolyte system

As time increases, the calcium loading at the top of the bed increases until it approaches 1.0 at approximately 60 days, where it remains constant at a plateau as time

reaches infinity. Eventually the bottom of the bed has a loading of 1.0 when time reaches approximately 245 days. The plateau is an indicator that the ion has the highest exchange priority for a given system because no ions are displacing it.

Figure IV-8 is the sodium loading surface for the same system. Unlike calcium, sodium loading does not reach a plateau at the top of the bed, instead the sodium ions form a 'hill' with a critical line (the line formed by the ridge of the surface) at some point in time between t = 0 and t = 245 days.

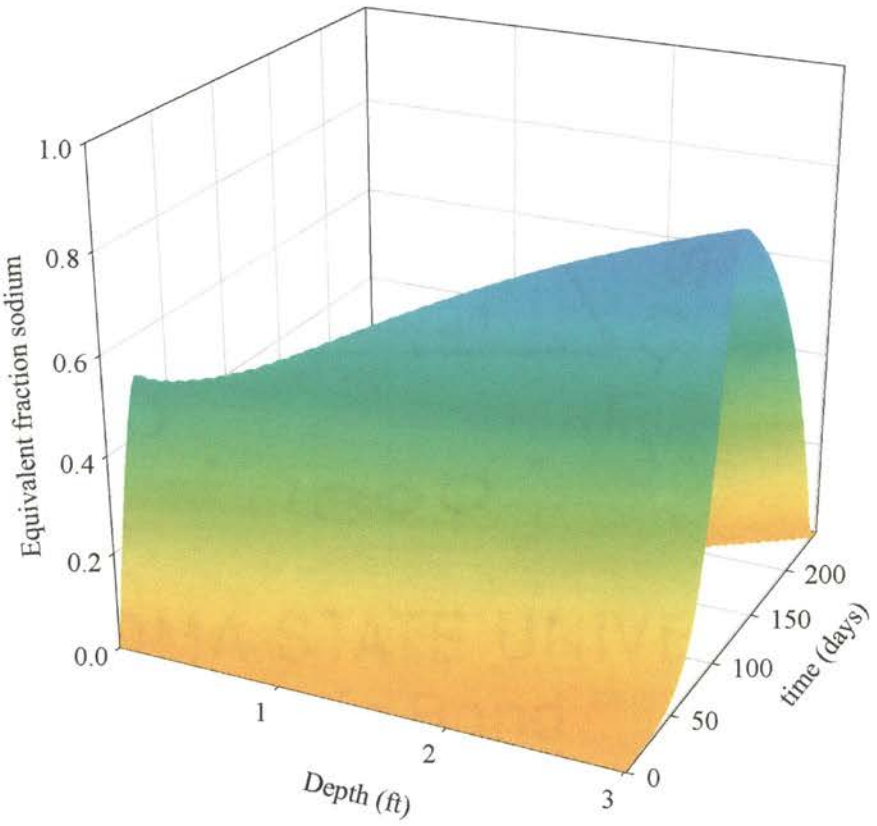


Figure IV-8 Loading surface for sodium in a strong electrolyte system

The critical line value first decreases, and then it smoothly increases. The decrease in loading is an entrance effect that is attributed to the displacement of sodium by calcium. The critical line value increase is the effect of displaced sodium mixing with

the influent sodium, and therefore a higher resin loading. Sulfate and chloride loading profiles are available, but they are similar in form and are omitted for brevity.

The rate surfaces are more complex than the loading profiles. The values may be positive or negative, and they are not bounded between 0.0 and 1.0. Multicomponent rate surfaces may have several peaks and valleys for each species. Figure IV-9 is a rate surface for sulfate in a calcium-sodium-sulfate-chloride system (the potassium nitrate is not considered in this plot).

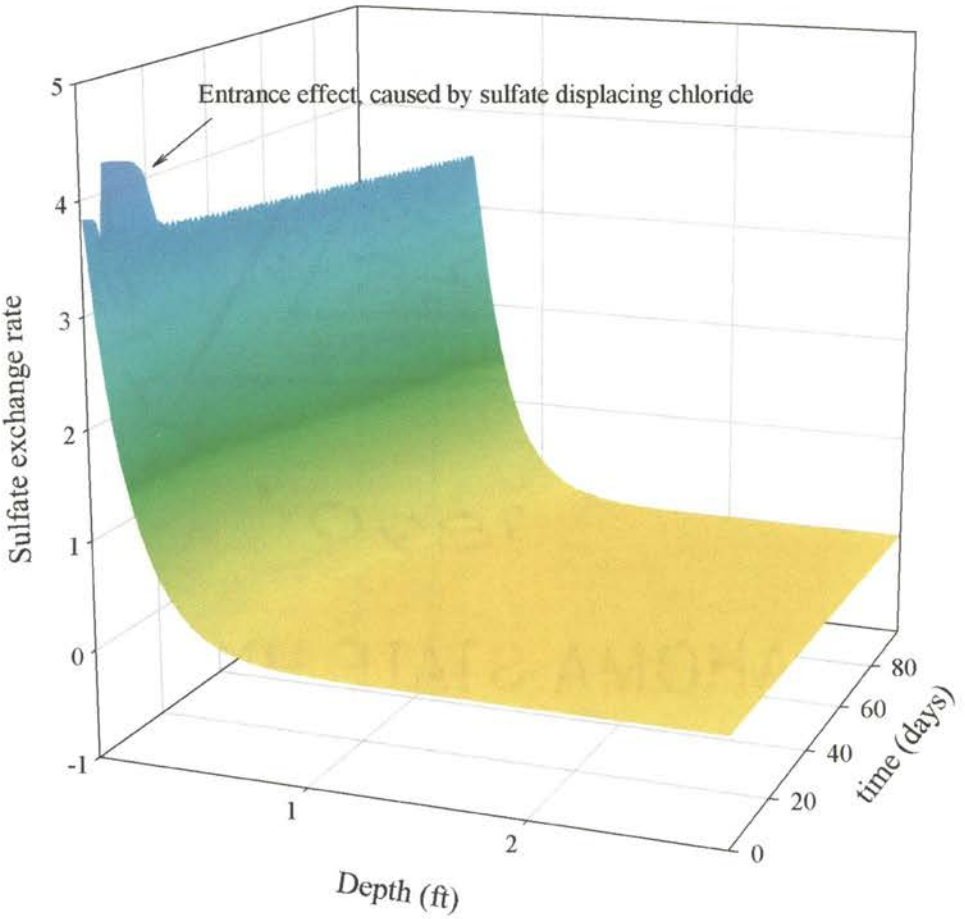


Figure IV-9 Sulfate rate surface in a multicomponent strong electrolyte system

Holding the initial time at zero, the sulfate rate is positive (ions entering the resin) at the top of the bed, and falls off sharply as the bed length increases. This corresponds

with the physical situation because most of the contaminant is exchanged at the top of the fresh bed. Notice the increase in the sulfate rate as at the top of the bed due to the displacement of chloride at approximately 10 days. When the time is approximately equal to 30 days, the resin becomes completely loaded at the top of the bed, the sulfate exchange rate abruptly drops to zero, creating a 'hill' throughout the rest of the surface. The sulfate rate is never negative (for this case), indicating that sulfate has the highest exchange priority.

The rate surfaces of constituents that do not have the highest exchange priority are complex. Consider Figure IV-10. The view of the 3-D coordinate system has

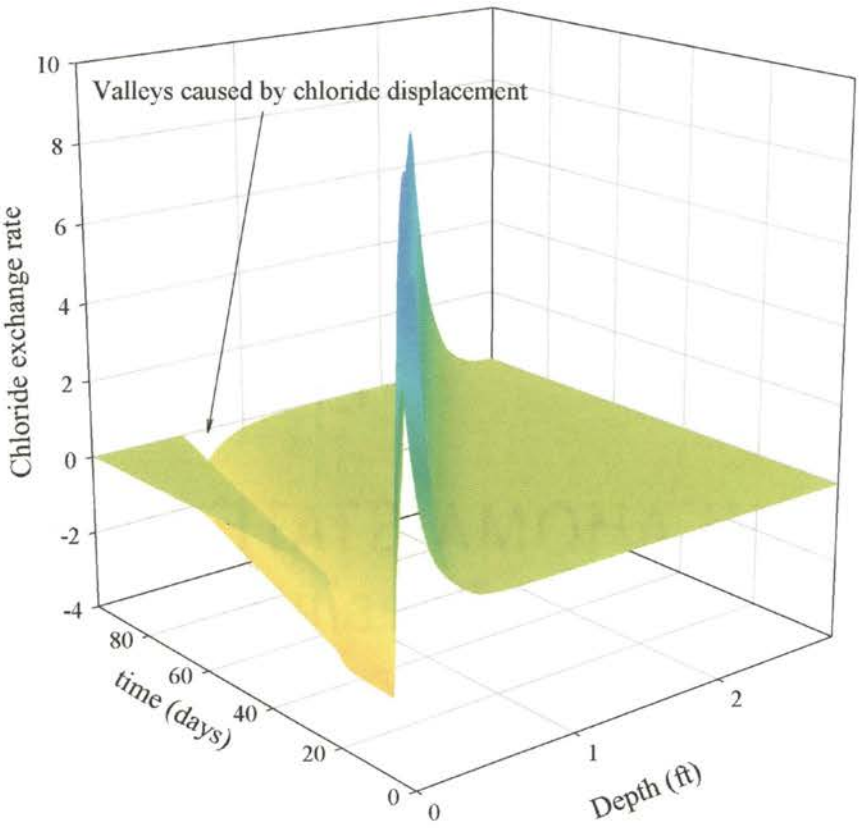


Figure IV-10 Chloride rate surface for multicomponent system

been rotated to enhance the surface features. Notice chloride has a peak similar to the sulfate peak that follows somewhat diagonally along the integration plane, but after the time reaches approximately 10 days (when the sulfate begins to displace chloride), the rate becomes negative, and the surface develops a valley.

The solution ratio surface for chloride in the calcium-sodium-chloride sulfate system is presented in Figure IV-11. The solution ratio value exceeds one because the sulfate displaces the chloride from the resin, and the influent chloride is added to the displaced chloride inside the bed. The surface returns to a value of unity after all of the chloride ions on the resin are displaced. The profiles are smooth, which satisfies the criterion established in Chapter II.

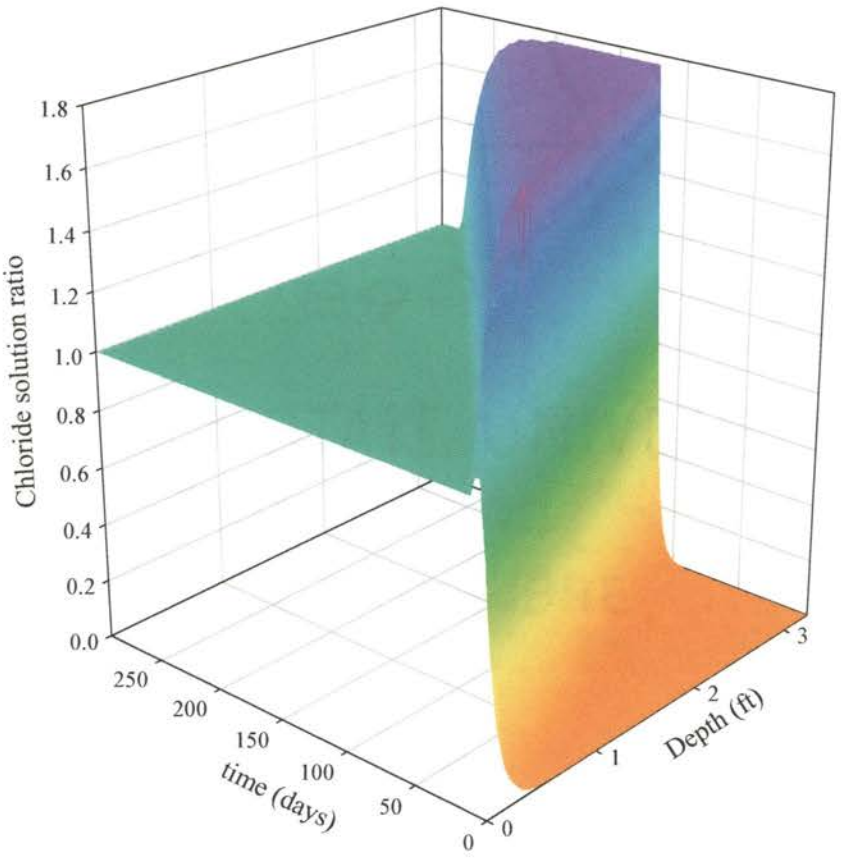


Figure IV-11 Solution ratio surface for chloride in strong electrolyte system

External column material balance

The external column material balance algorithm described in Chapter III was implemented to update the material balance throughout the simulation. The mass balance has been satisfied for all of the constituent types in the model, but an important trend was discovered relating the accuracy of the mass balance to the distance step-size. Figure IV-12 below shows a bar chart of both cation and anion mass balances with respect to distance step-size for the calcium-sodium-sulfate-chloride system.

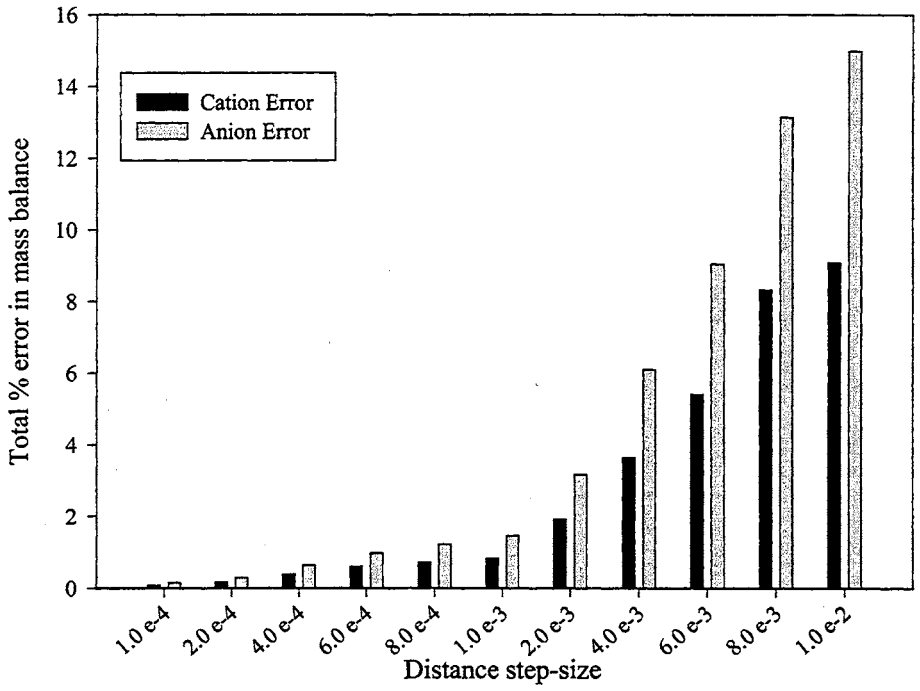


Figure IV-12 Overall mass balance as related to distance step-size

It is clear from the figure that the lower the distance step-size, the better the mass balance closure. The relationship between them appears asymptotic. This is useful to determine the optimum step-size for a particular scenario, the author recommends

reducing the step-size until the largest error is approximately one percent. If a smaller step-size is chosen, the model requires more run-time for little gain in accuracy.

The anion and cation errors are not equal, and for this scenario the cation error was larger than the anion error. A cause for the error difference has not been found; however, it is noted the ion type with the smallest error is the same ion type as the reference constituent. The mass balance was not sensitive to the time step-size, and there was no correlation with any other model parameters.

## Parametric analysis and model tuning

A working model has been developed that satisfies the criteria established in Chapter II. Now the model sensitivity to parameter changes needs to be evaluated, so the model can be applied to industrial scenarios. The model is tuned by using the chemical engineering principles of thermodynamics and kinetics. First, determine the equilibrium distribution of ions on the resin by properly choosing the selectivity coefficients; then approximate the rate of mass transfer by manipulating kinetic parameters.

### Selectivity coefficients

The selectivity coefficients serve two purposes in the model; they calculate the interfacial ionic concentrations given an equilibrium loading distribution, and they calculate the ionic equilibrium capacities at given influent contaminant concentrations. The ion exchange rates are affected by the selectivities of the exchanging species because they help determine the concentration driving force, but they do not correlate directly to ion exchange rates.

Selectivities vary with several parameters including temperature, cross-linkage and the resin functional group. The selectivity is also not constant; the observed

separation ratio varies with the loading of the particular ion. If the equilibrium loadings are known, then the selectivity coefficients can be adjusted to yield the desired equilibrium loadings. Figure IV-13 shows how the variation of the sodium selectivity changes the equilibrium distribution.

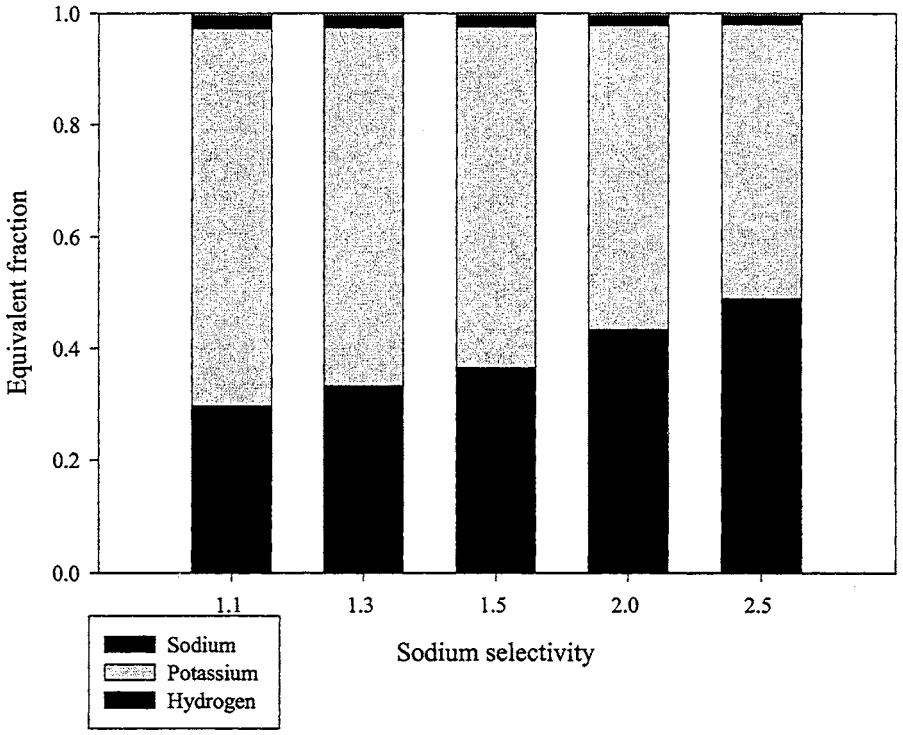


Figure IV-13 Equilibrium loadings of potassium, sodium and hydrogen with varying sodium selectivity

Divalent and trivalent ions generally completely displace monovalent ions, but if more than one multivalent ion is present, they distribute themselves according to the same principles monovalent ions. Figure IV-14 shows how varying the magnesium selectivity can alter the distribution of calcium and magnesium.

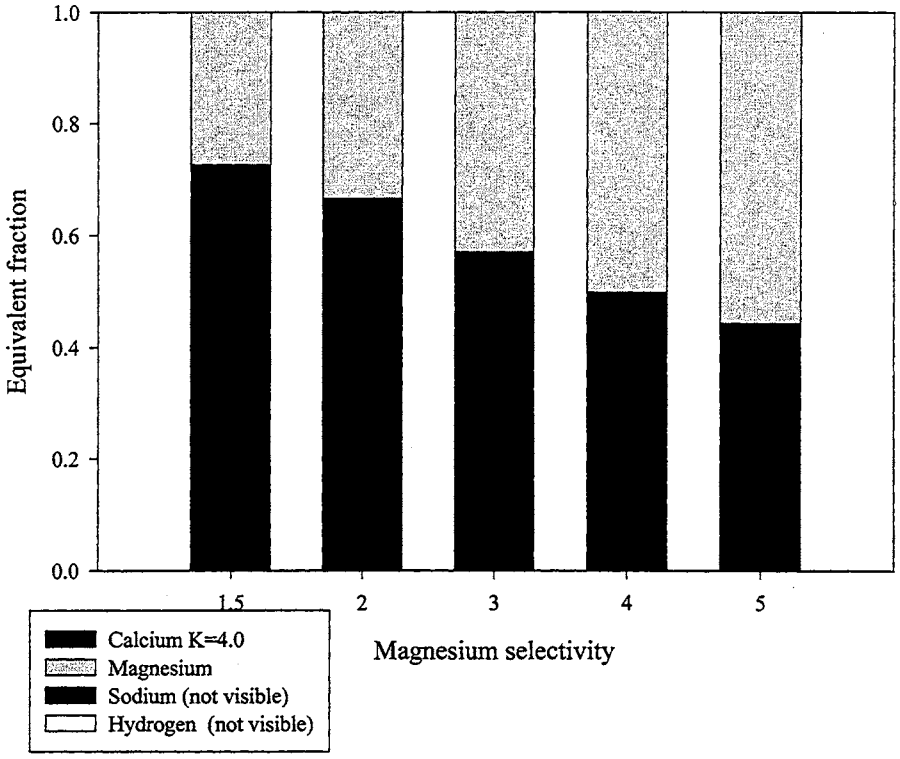


Figure IV-14 Manipulation of calcium and magnesium loading distribution by changing selectivities

Diffusion coefficients and fouling

The constituent mass transfer rate is calculated using a combination of the ionic fluxes and an effective mass transfer coefficient. The ionic fluxes are found using the ionic concentrations and diffusivities; while the effective mass transfer coefficients are calculated from ionic properties, hydrodynamic properties and fouling factors that ratio the mass transfer characteristics of the service resin with new resin.

The fouling mechanism is analogous to insulation in heat transfer; two objects in contact will eventually reach thermal equilibrium, but insulation between the two objects slows the rate of heat transfer.

Fouling results in the spreading of the exchange zone for all exchanging species without reducing exchange capacity. The exchange zone spreads because the residence time of water remains constant while the constituent mass transfer rate decreases. Therefore more constituent is remaining in solution and exchanges further down the bed. Figure IV-15 shows the effect of 50% fouling on the resin loading of a sulfate-nitrate-chloride system.

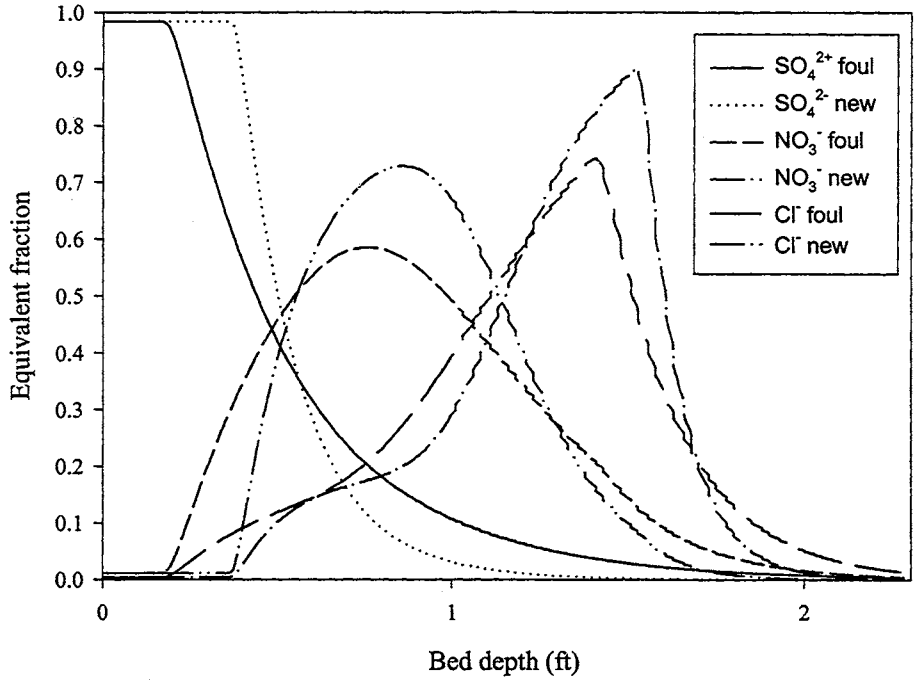


Figure IV-15 The effects of 50% fouling on the loading profiles of anions

Observing the top of the bed shows the equilibrium capacity of sulfate, nitrate and chloride are the same regardless of the mass transfer coefficient, as expected. The spreading of the loading profiles results in an increased loading at the bottom of the bed, which increases the effluent leakage. This is demonstrated in Figure IV-16. The initial loading for all ions was set to 0.0, and the desulfonation term was not used.

The initial leakage for all ions is far below the detection limits of modern equipment; however, the trends appear to follow expectations. The diffusivity order for the ions is chloride, nitrate, and sulfate, while the selectivity order is sulfate, nitrate, and chloride. Sulfate has the lowest leakage for new resin, but also has the highest leakage for fouled resin because the small diffusion coefficient coupled with the fouled resin impeded mass transfer greatly. The chloride effluent concentration only increased an order of magnitude, compared to four orders for nitrate and nine for sulfate.

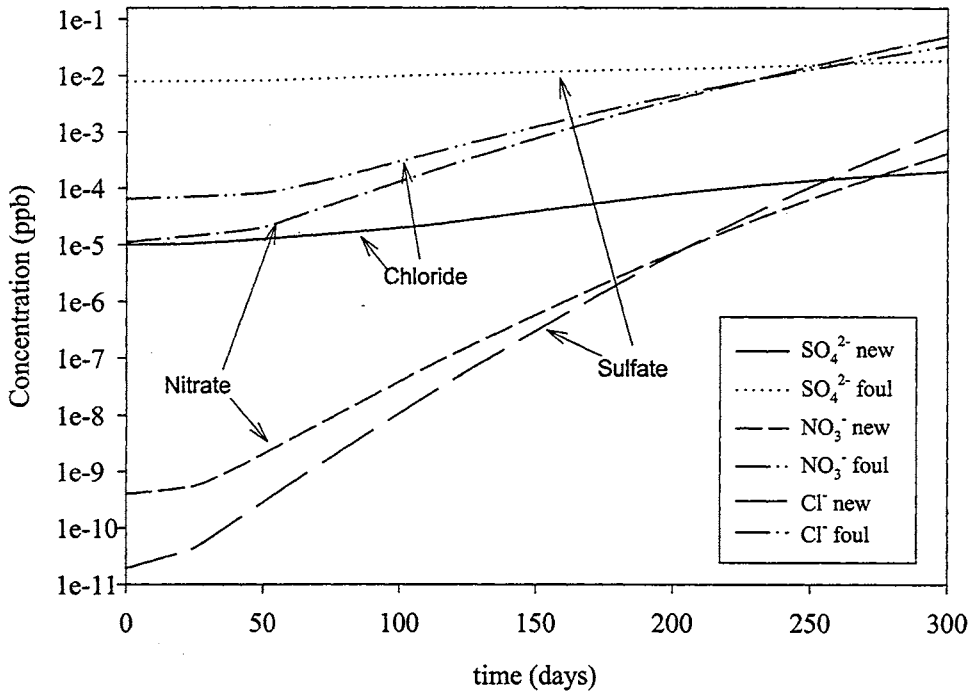


Figure IV-16 Effects of fouling on the equilibrium leakage of an anion system

There may be cases where the performance of the multicomponent system is reasonable except for the kinetics of a single constituent. In such a case, the diffusivity of the ionic species may be changed to modify the kinetic performance. The author concedes the manipulation of the diffusivity is akin to 'twisting facts to suit theories,' but

considering a correlation is used to calculate the mass transfer coefficient, it is reasonable to assume the behavior of a particular ion may not be correlated well and may require an adjustment. Figure IV-17 demonstrates how the effluent leakage of an ion may be manipulated by varying the ionic diffusivity.

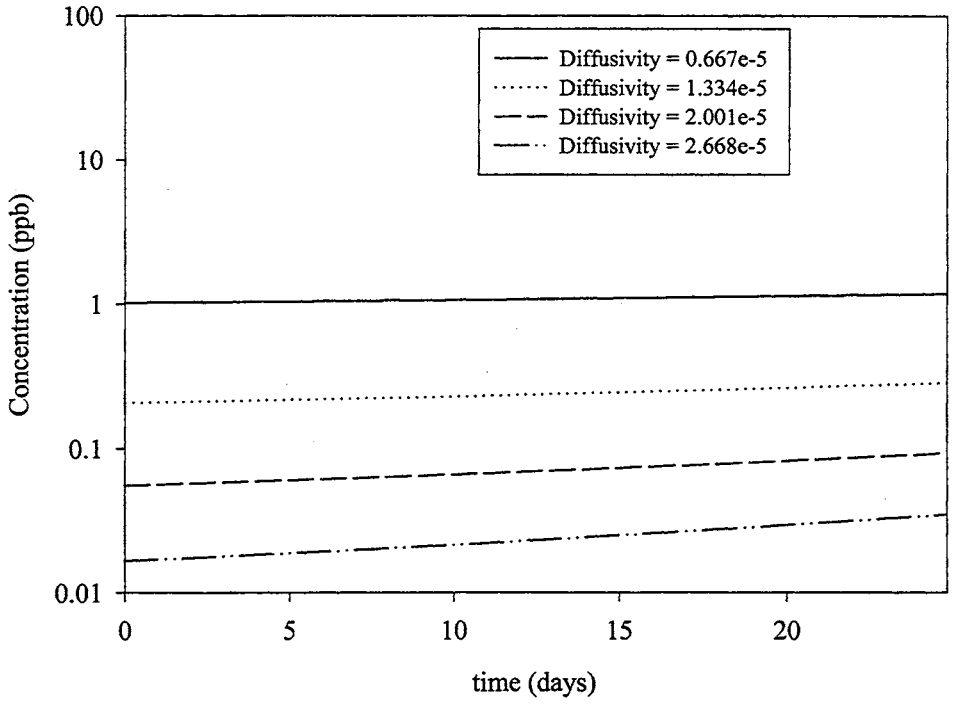


Figure IV-17 Initial effluent concentration variation with ionic diffusivity

Flow rate and influent concentration

Helfferich (1960) has shown the mass transfer mechanism for many ion exchange processes to be film diffusion controlled by demonstrating an increase in the average mass transfer coefficient (and therefore an increased removal efficiency) of an ion with increasing flow rate. The theoretical explanation is that the stagnant film thickness decreases with increasing Reynolds numbers, while the ionic diffusivity remains constant. According to the mass transfer coefficient definition,

$$k_i = \frac{D_i}{\delta} \qquad \text{(IV.1)}$$

Several researchers, including Harries (1984), McNulty (1993), Lee (1993) and Arunachalam (1996), have reproduced the experiment evaluating ion exchange mass transfer coefficients with respect to flow rate and influent concentration.

All authors noted at near ppm concentrations the mass transfer coefficient was independent of the influent concentration, but at very low concentrations the mass transfer coefficient decreased with decreasing influent concentration. The mechanism for the reduced efficiency is not clearly understood, experimental error and flow dynamics have been proposed (Arunachalam, 1996).

The model sensitivity to influent concentration was modeled by varying the calcium-sodium-chloride-sulfate concentrations holding all other variables constant. Figure IV-18 shows the calcium removal efficiency,

$$\eta = \left(1 - \frac{C_i^{eff}}{C_i^{inf}}\right) x100 \qquad \text{(IV.2)}$$

increasing with increasing influent concentration until a maximum value is obtained. This trend is concurrent with experimental results obtained by Arunachalam (1996), where the low concentration removal efficiencies increased with increasing concentration until a limit was obtained. Further work is required to validate the trend with respect to flow rate and other ionic species.

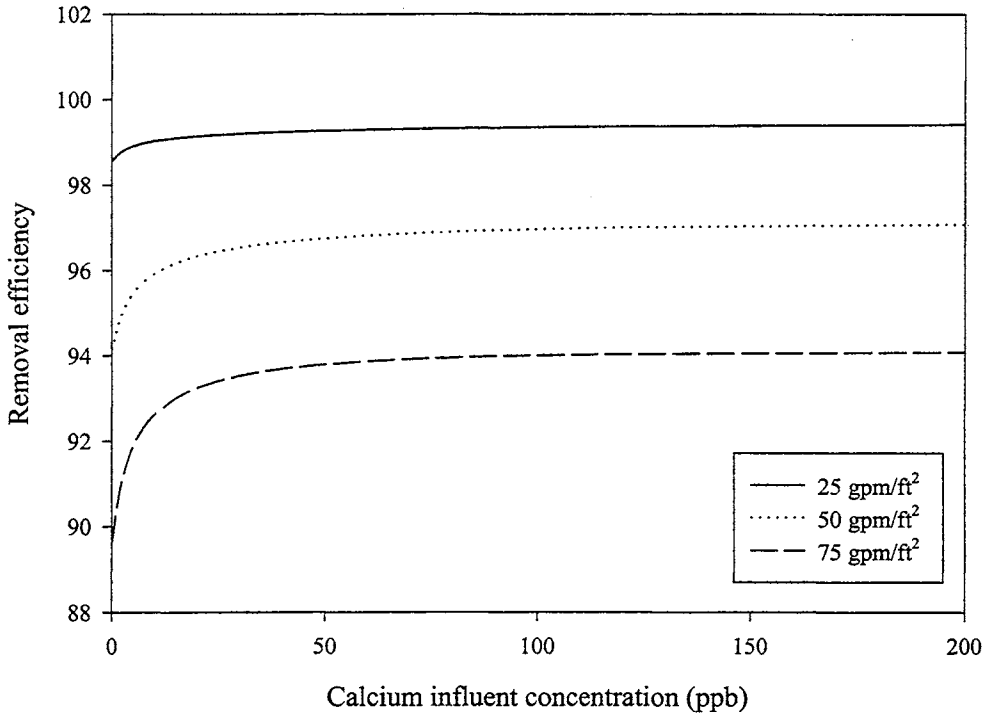


Figure IV-18 Increased calcium removal efficiency with increased influent concentration

The effect of flow rate on removal efficiency was also compared. Increasing the flow rate reduces the residence time of a single element of fluid in the mixed bed; however, the film thickness also decreases with increasing flow rate. It has been shown by several authors that at higher concentrations the increase in rate from the reduced film thickness dominates over decreased residence time and increases the removal efficiency. However, industrial experience has shown at very low influent concentrations that the reduced residence time is dominant, and increasing the flow rate reduces removal efficiency.

Figure IV-19 reproduces industrial experience of decreasing removal efficiency with increasing flow rate. The curve was generated for calcium with an influent

concentration of 20 ppb. As is expected for low concentrations, the removal efficiency decreases with increasing flow rate because the exchange rate is not fast enough to remove the ions within the residence time of the reactor.

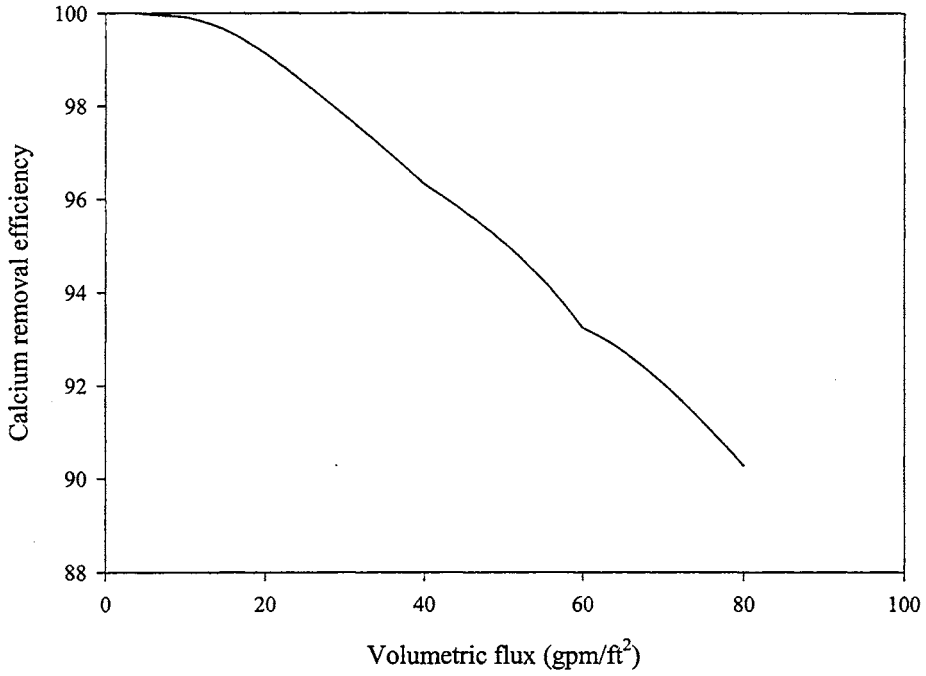


Figure IV-19 Reduced removal efficiency of calcium at 20 ppb with increasing flow rate

Pennsylvania Power and Light service runs

Pennsylvania Power and Light nuclear power plant in Susquehanna, Pennsylvania is a BWR with seven full-flow condensate polishers. Each polisher has an anion resin layer at the bottom of the bed to capture sulfate released from the cation resin because of desulfonation. The bed geometry and resin parameters are listed in Table IV-2.

Table IV-2 Bed geometry and service parameters for PP&L polishers

| *Parameter* | *Value* |
|---|---|
| Bed diameter (feet) | 10.8 |
| Total bed depth (feet) | 3 |
| Flow rate (gpm) | 4800 |
| Anion resin heel depth (inches) | 3 |
| Volume fraction of cation resin (in non-heel section) | 0.38 |
| Volume fraction of anion resin (in non-heel section) | 0.62 |
| Void fraction | 0.35 |
| Flow rate (service, gpm) | 4800 |
| Temperature (°C) | 60 |
| Cation resin: | |
| Bead diameter (mm) | 0.63 |
| Capacity (meq/ml) | 2.0 |
| Form | Hydrogen |
| Anion resin: | |
| Bead diameter (mm) | 0.525 |
| Capacity (meq/ml) | 1.1 |
| Form | Hydroxyl |
| Desulfonation | Yes |
| Fouling | No |

The PP&L mixed bed influents generally have three phases of operation; typical, drought and upset conditions. Typical operation is during the winter, spring and fall months, when rainfall is plentiful, while drought operation occurs in some dry summers when the river level drops during the summer and the contaminant concentrations increase, although the conductivity is similar because the carbonate concentration decreases. Occasionally, a condenser tube will spring a leak and challenge the mixed beds with high conductivity water. The concentrations for each river condition are assumed using the average equivalent fraction of contaminants present in the Susquehanna River water.

Table IV-3 Influent contaminant scenarios for PP&L vessels

| Ion | typical | drought | upset |
|---|---|---|---|
| $Cl^-$ | 0.73 | 0.77 | 730.9 |
| $SO_4^{-2}$ | 1.07 | 1.57 | 1072.8 |
| $NO_3^-$ | 0.21 | 0.05 | 213.1 |
| $Ca^{+2}$ | 0.95 | 0.77 | 946.9 |
| $Mg^{+2}$ | 0.21 | 0.25 | 208.8 |
| $Na^+$ | 0.43 | 0.50 | 434.5 |
| $K^+$ | 0.11 | 0.10 | 100.8 |
| $H_2CO_3$ | 3.01 | 2.11 | 3013.8 |
| PH | 7 | 7 | 8.1 |
| Conductivity (μS/cm) | 0.065 | 0.065 | 10 |

Figure IV-20 shows the cation concentrations of the PP&L bed under normal operation (assuming no drought) for a full service run. Observe the initial breakthrough of the contaminants. Sodium effluent concentration is approximately 5 ppt. The cause is primarily equilibrium leakage as the initial loading of sodium is 0.1%. Calcium and magnesium have zero loading, the <1.0 ppt leakage is kinetic leakage caused by the slow diffusivities of $0.79 \times 10^{-5}$ and $0.70 \times 10^{-5}$ $cm^2/s$, respectively. Potassium is assumed to have a zero initial loading, and its diffusivity is high enough ($1.9 \times 10^{-5}$) to allow it to exchange to virtual completion. Sodium is the first cation to breakthrough a 100 ppt threshold at approximately 500 days.

The strong electrolyte anions (sulfate, chloride and nitrate) did not break through to detectable levels during the simulation, but carbonate breaks through at approximately 500 days operation.

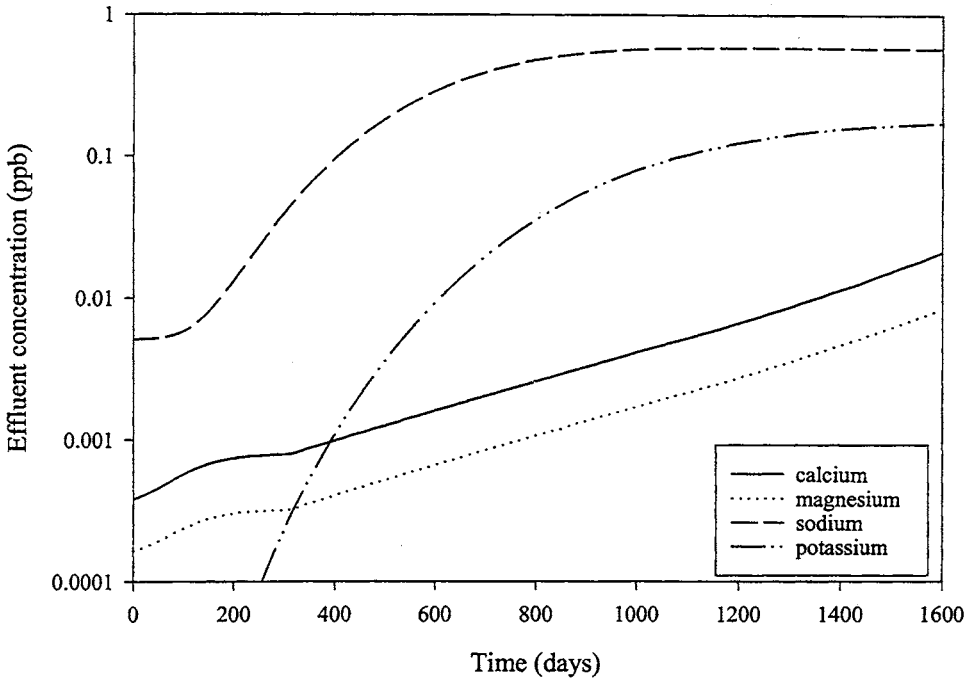


Figure IV-20 PP&L cation effluent history for normal run

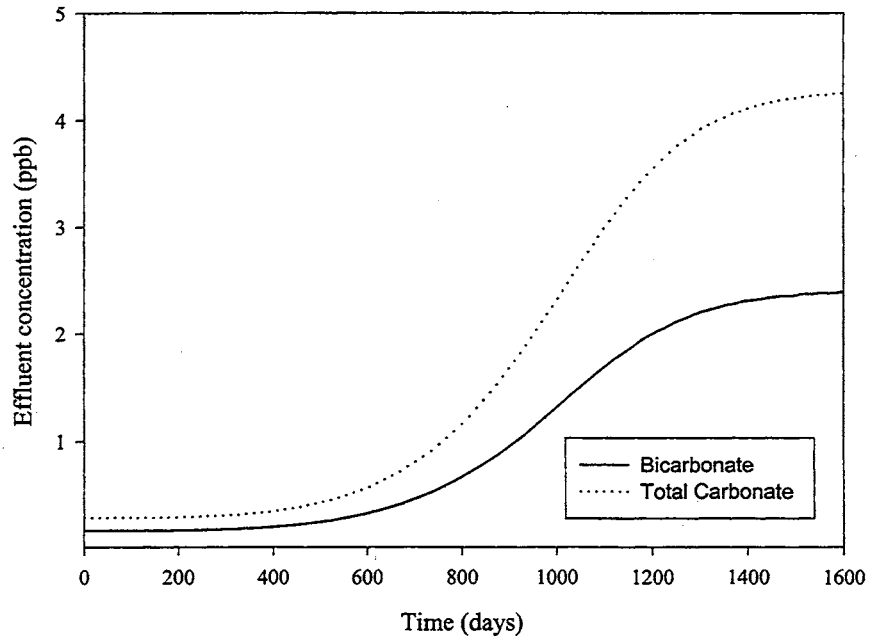


Figure IV-21 PP&L carbonate effluent history for a typical influent

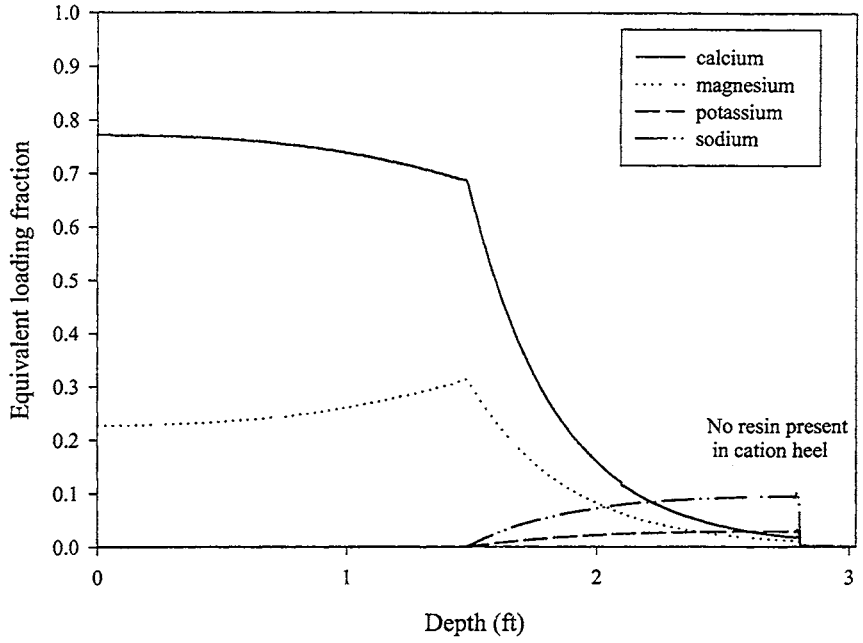


Figure IV-22 PP&L cation loading profile after 1600 days

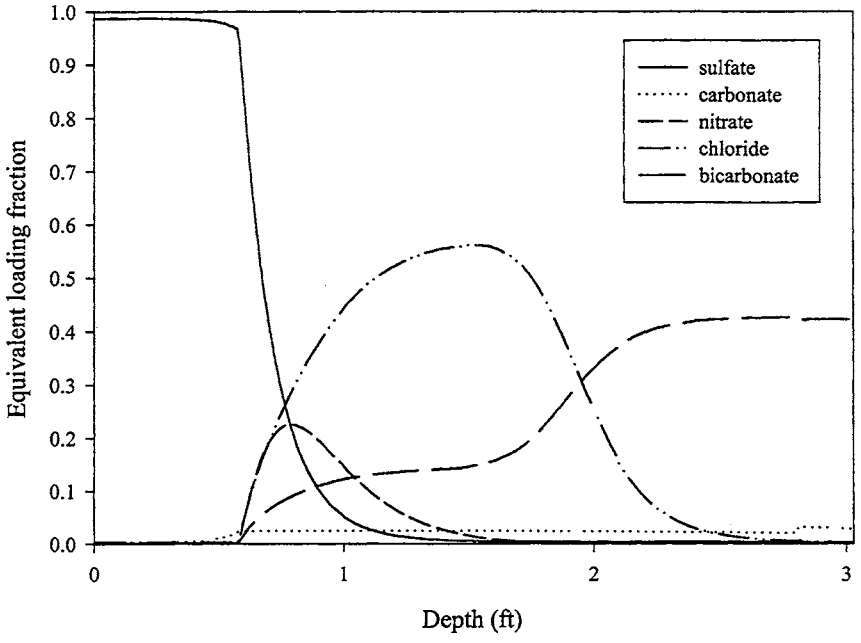


Figure IV-23 PP&L anion loading profile for normal run at 1600 days

Figure IV-22 shows the cation loading profile for the cation resin after 1600 days. The bed had been leaking significant sodium and potassium for quite some time. Note the sodium and potassium exchange zones are long, and do not use much of the exchange capacity. This is because of the low selectivity of sodium and potassium; at low concentrations the equilibrium loading does not approach the total capacity of the bed because hydrogen is present in equal (or greater) concentrations and reaches equilibrium with the resin.

Figure IV-23 is the anion loading profile at 1600 days for normal conditions. The anion exchange zones are much sharper because of the high selectivities and diffusivities. Sulfate is by far has the largest separation factor, it displaces all other anions before it. Divalent carbonate is barely present at a pH of ~7.0, but since the molecular form is carried through the length of the bed, the resin loads to almost 2.0%. Nitrate is present in small concentrations and is displaced by the carbonate. Chloride follows nitrate, steadily displacing carbonate and using much of the exchange capacity. Bicarbonate has a long exchange zone as a result of the molecular form being carried along the length of the bed. The bicarbonate is expected to break through long before chloride, which provides a comfort zone as the carbonate has a much lower corrosion potential than chloride.

Figure IV-24 is the effluent concentrations for several contaminants after almost one full day of upset challenge conditions. The upset begins at 622.5 days of operation, and continues for one full day. Chloride, sulfate and nitrate are not shown because they did not break 1.0 ppb during the upset period when sodium and carbonate break through at approximately 12 hours. These results are comforting, as the expected shut down time is less than 12 hours.

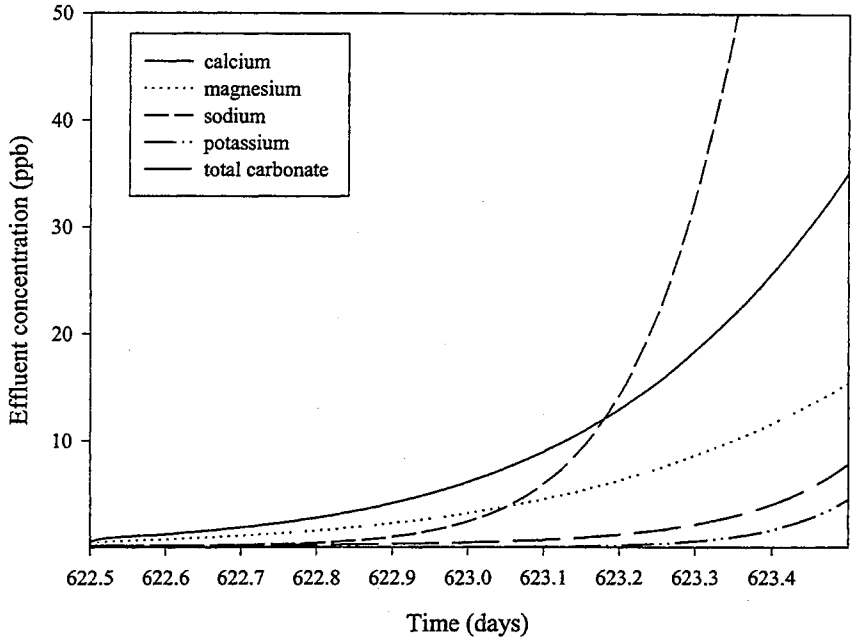


Figure IV-24 PP&L effluent concentration during upset challenge

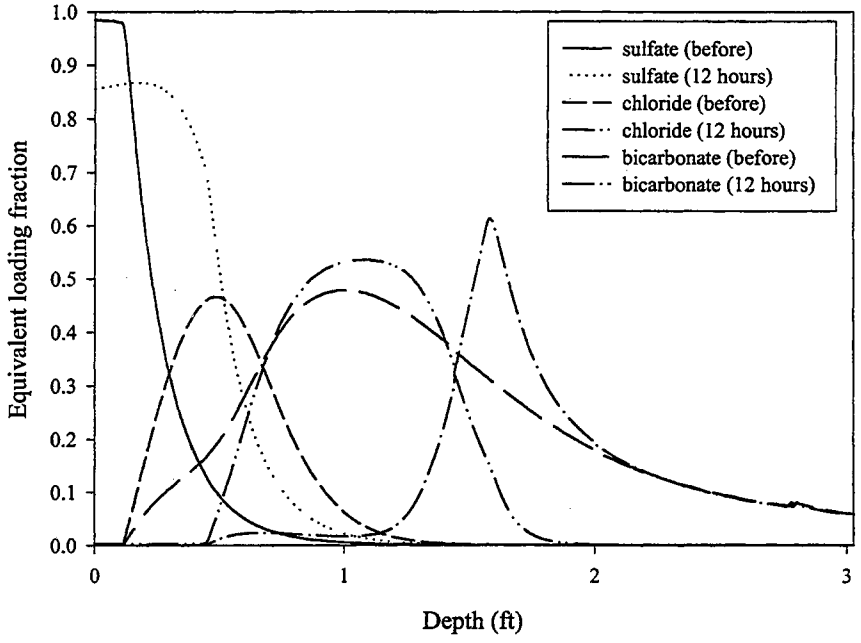


Figure IV-25 PP&L anion loading after 12 hour upset at 622.5 days of operation

Figure IV-25 is the loading profile comparison of bed before and after an upset challenge occurs for 12 hours. The nitrate and carbonate ions are not shown for clarity. The sulfate is still dominant, but it is partially displaced by the other ions to an equilibrium loading of 0.85. Chloride is rapidly loading in the bed, but it does not breakthrough until after one day of upset challenge conditions.

British Energy ammonia influent hydrogen cycle operation

British Energy has a gas-cooled nuclear reactor that uses a secondary loop with chemistry similar to that of a PWR, i.e. the cycle water is spiked with an amine after the condensate polisher to raise the pH and help prevent corrosion of the steam generator tubes. The ion exchange bed configuration is listed in Table IV-5.

The cation resin volume fraction is 0.66 and the anion resin volume fraction is 0.33, which gives approximately four times more cation capacity than anion capacity. This provides enough capacity to remove the amine from the cycle water. Some plants operate in the amine form of the resin, but this is often avoided because the preferential displacement of sodium by most amines will allow sodium to pass through the bed and corrode the steam generator. The influent contaminants for a typical service run are listed in Table IV-4.

Table IV-4 Typical service conditions for British Energy

| Contaminant | Conc. |
|---|---|
| Sodium (ppb) | 5 |
| Chloride (ppb) | 7.5 |
| Sulfate (ppb) | 0.3 |
| Ammonia (ppb) | 1000 |

Table IV-5 British Energy service conditions

| *Parameter* | *Value* |
|---|---|
| Bed diameter (feet) | 10 |
| Bed depth (feet) | 3.68 |
| Volume fraction of cation resin | 0.66 |
| Volume fraction of anion resin | 0.34 |
| Void fraction | 0.35 |
| Flow rate (service, gpm) | 3170 |
| Temperature (°C) | 30 |
| Cation resin: | |
| Bead diameter (mm) | 0.65 |
| Capacity (meq/ml) | 2.0 |
| Form | Hydrogen |
| Anion resin: | |
| Bead diameter (mm) | 0.55 |
| Capacity (meq/ml) | 1.1 |
| Form | Hydroxyl |
| Desulfonation | Yes |
| Fouling | No |

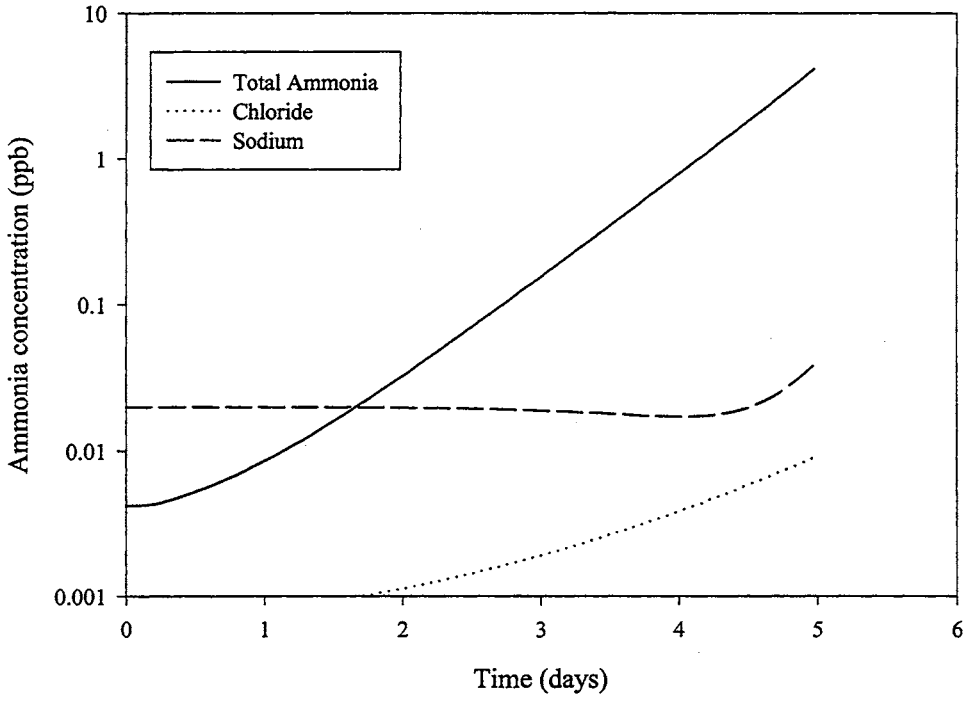


Figure IV-26 British Energy effluent concentrations at normal service conditions

The effluent concentration profiles are shown in Figure IV-26. Notice there is not a dissociative species initial bump that was present in previous versions of the model. The ammonia concentration reaches 100 ppt at approximately 2.7 days, and the effluent conductivity (not shown) increases 12 hours later. Sodium and chloride concentrations remained non-detectable until the ammonia breakthrough.

Metal oxide migration with changing influent concentrations

Many nuclear applications are interested in the ion exchange behavior of metal oxides because of the role metal oxides play as a transport medium for radioactivity, especially via the transport of $Co^{60}$ through the piping of the submarine. Metal oxide water chemistry is complex because of the possible formation of both cation and anion species from a single constituent, as well as the tendency of metal oxide complexes to form polynuclear aggregate species (Baes et al. 1976). The simulator is capable of modeling mononuclear cation hydrolysis products; however, the constituent (the species name is omitted) is assumed to be a divalent strong electrolyte for preliminary estimations. Table IV-6 shows the sequence of runs for the migration experiment, and Table IV-7 shows the bed parameters used for the service run.

Table IV-6 Sequential run parameters

| *Run* | *Days* | *Influent concentration (ppb)* | *Total days* |
|---|---|---|---|
| 1 | 303 | 11 | 303 |
| 2 | 365 | 0 | 669 |
| 3 | 265 | 1.9 | 934 |
| 4 | 265 | 0.9 | 1200 |

Table IV-7 Bed parameters for metal oxide elution

| *Parameter* | *Value* |
|---|---|
| Bed diameter (feet) | N/A |
| Bed depth (feet) | 3.36 |
| Volume fraction of cation resin | 0.4 |
| Volume fraction of anion resin | 0.6 |
| Void fraction | 0.35 |
| Flow rate (gpm/ft$^2$) | 12.9 |
| Temperature (°C) | 30 |
| Cation resin: | |
| Bead diameter (mm) | 0.65 |
| Capacity (meq/ml) | 2.0 |
| Form | Ammonia |
| Anion resin: | |
| Bead diameter (mm) | 0.55 |
| Capacity (meq/ml) | 1.1 |
| Form | Hydroxyl |
| Desulfonation | Yes |
| Fouling | No |

Figure IV-27 shows the effluent concentration history of the service run.

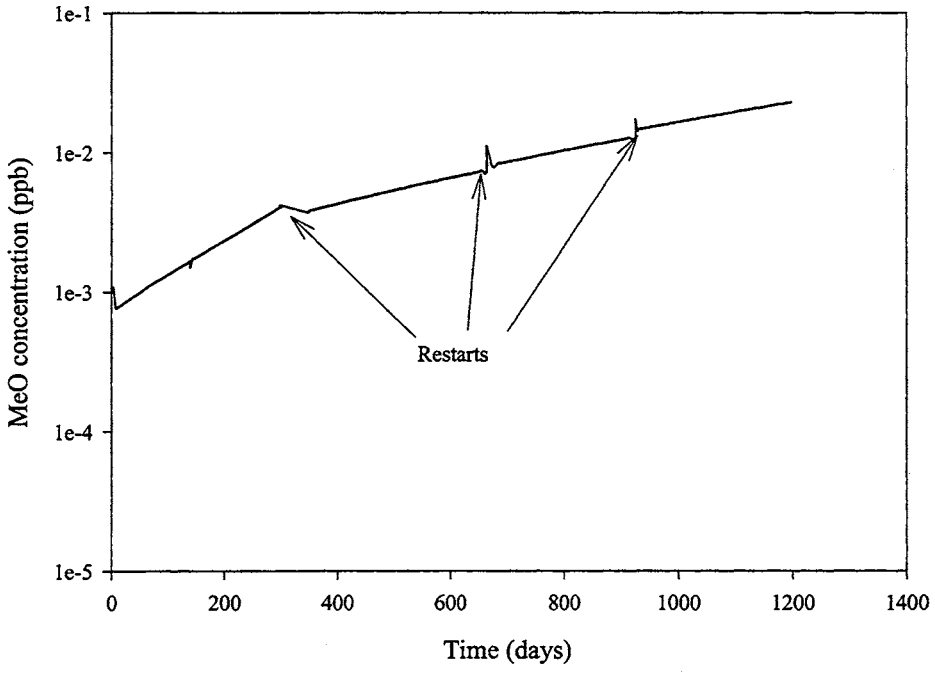


Figure IV-27 Metal oxide effluent concentration with influent concentration step changes

The restarts cause the discontinuities in the curve, but do not appear to affect the results significantly. The loading migration of the metal oxide throughout the service run is shown in Figure IV-28. It is interesting to note the pH of the influent and effluent was above 9.0 for the entire service run, yet the metal oxide did not migrate more quickly down the bed, as may be expected because the high concentration of ammonia may act as a regenerant.

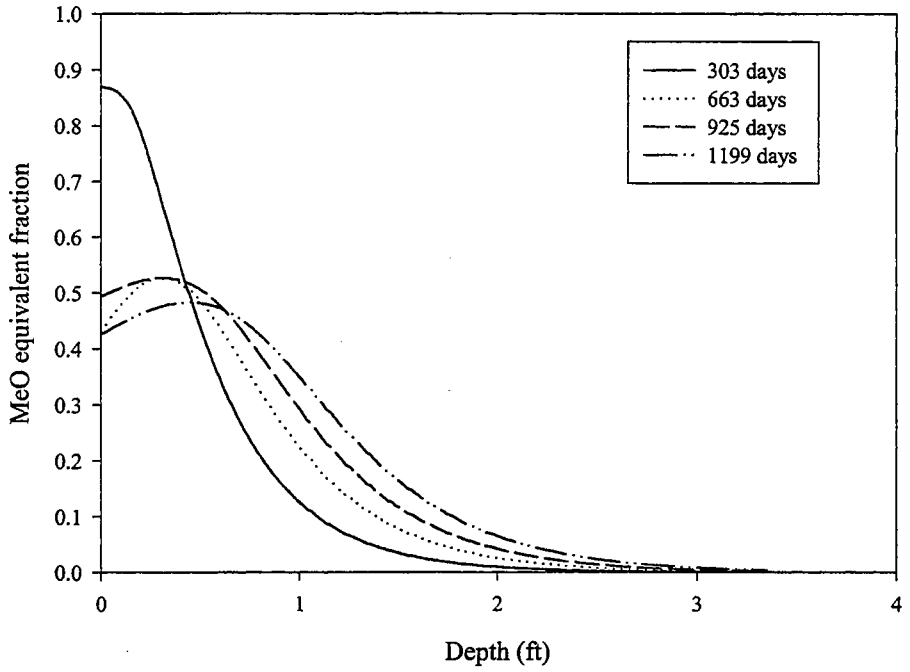


Figure IV-28 Loading profile variation of KAPL metal oxide with time

The elution of the metal oxide is a good example of the dynamic interaction of the solution concentration and resin loading. The first run has a high contaminant concentration, and the loading reaches almost 0.8. The second run has no contaminant in the solution, therefore the contaminant loading begins to elute through the bed chromatographically and leave the top of the bed. The third and fourth runs reach

equilibrium loadings at about 0.55 and 0.45, respectively, and the rest of the contaminant distributes through the bed.

# CHAPTER V

# ESTIMATION OF RADIAL FLOW MASS TRANSFER COEFFICIENTS

## Introduction

The majority of mixed bed ion exchange columns are cylindrical with axial flow. However, in reactor water clean up (RWCU) systems with high concentrations of suspended solids, a cylindrical column may quickly build-up suspended solids at the top of the bed, causing an increased pressure drop during operation. Because of large pressure drop, the mixed bed often must be replaced before the available exchange capacity has been exhausted (Fejes, et al., 1989).

A radial flow mixed bed may be used to alleviate the pressure drop problem by increasing the flow area and decreasing the flow path. These advantages of radial flow mixed beds has been shown in the RWCU in some ABB Atom power plants (Fejes et al., 1989)

Figure V-1 shows the basic schematic of an inward flow radial column. The water enters the outer perimeter and flows through with increasing velocity to the center of the vessel where it leaves through the bottom.

The variable flow velocity complicates mathematically modeling the radial flow mixed bed. Lou (1993) developed a numerical model based upon the principles

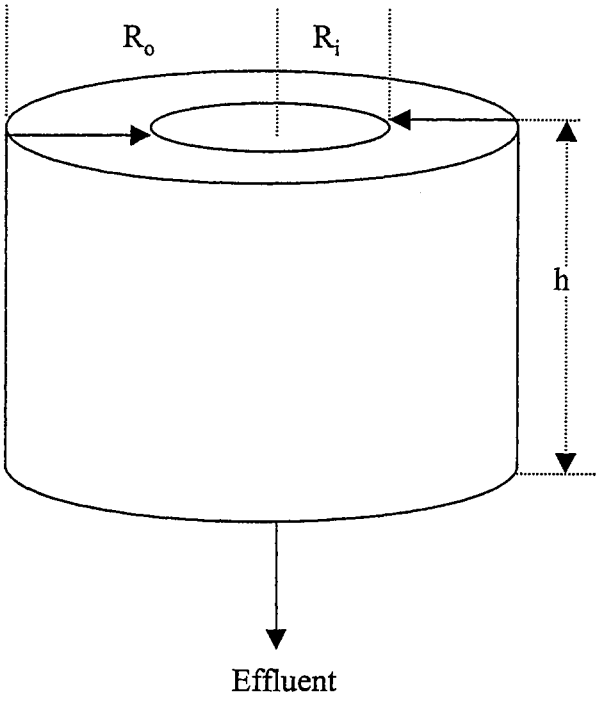


Figure V-1 Inward flow radial flow mixed bed

used in this work for a sodium chloride influent. The model was a coupled, high-order system of differential equations; it included radial dispersion and used Patankar's control volume method for the solution of the terms. The model produced apparently reasonable results that were useful to rate the performance of a radial flow bed; however, it was never implemented as readily usable software.

Harries and Ray (1984) developed a simplified film mass transfer coefficient model to rate the performance of a cylindrical mixed bed. The model assumes zero interfacial concentrations and no interactions resulting from dissociation equilibrium; however, it characterizes the removal efficiency of an ionic species with respect to bed geometry and service parameters. The relationship is presented in a modified form without proof.

$$\ln\left(\frac{C_i^{eff}}{C_i^f}\right) = -\frac{6k_{f,i}(1-\varepsilon)(FR)}{d_{p,i}}\frac{\pi R^2 L}{F} \qquad (V.1)$$

where

F = the volumetric flow rate

$k_{f,i}$ = the average film mass transfer coefficient of ion 'i.'

L = the cylindrical bed depth

The model is useful for evaluating the kinetic performance of ion exchange resin, Lee (1993), Arunachalam (1996) and others have successfully shown the reduced mass transfer coefficients of fouled resin by using the influent and effluent concentrations of simple bench-scale column experiments.

This section proposes an analogous film mass transfer coefficient model for radial flow based upon the assumptions applied in the Harries model.

Model derivation

Equation (V.2) is the reduced continuity equation for a radial-flow packed bed assuming longitudinal and angular derivatives are equal to zero.

$$\frac{\partial C_i}{\partial t} + \frac{u_r}{\varepsilon}\frac{\partial C_i}{\partial r} - R_i = 0 \qquad (V.2)$$

$R_i$ is the reaction term and is equated to the change in resin phase concentration using a linear driving force model.

$$-R_i = \frac{1-\varepsilon}{\varepsilon}\frac{dq_i}{dt} = k_{f,i}a_s\left(C_i^* - C_i^b\right) \qquad (V.3)$$

Equation (V.3) is substituted in to Equation (V.2) to yield the following continuity equation.

$$\frac{\partial C_i}{\partial t}+\frac{u_r}{\varepsilon}\frac{\partial C_i}{\partial r}+(FR)\frac{(1-\varepsilon)}{\varepsilon}\frac{\partial q_i}{\partial t}=0 \qquad (V.4)$$

The equation as written is non-linear because the fluid velocity, u, is a function of the radius. However, the fluid velocity can be related to the rate with the following expression developed in Bird, et al., (1960).

$$ru_r = \phi \qquad (V.5)$$

where $\phi$ is a constant. For the radial-flow system,

$$\phi=\frac{F}{2\pi h} \qquad (V.6)$$

Substituting Equation (V.5) into Equation (V.4) yields,

$$\frac{\partial C_i}{\partial t}+\frac{\phi}{\varepsilon r}\frac{\partial C_i}{\partial r}+(FR)\frac{1-\varepsilon}{\varepsilon}\frac{\partial q_i}{\partial t} = 0 \qquad (V.7)$$

Defining the solution fraction and resin fraction dimensionless variables,

$$x_i=\frac{C_i}{C_i^f} \qquad (V.8)$$

$$y_i=\frac{q_i}{Q} \qquad (V.9)$$

and dividing Equation (V.7) by $\frac{C_i^f Q}{Q}$ gives the following continuity equation with dimensionless solution and resin fractions, and dimensional time and radius.

$$\frac{\partial x_i}{\partial t}+\frac{\phi}{\varepsilon r}\frac{\partial x_i}{\partial r}+(FR)\frac{1-\varepsilon}{\varepsilon}\frac{Q}{C_i^f}\frac{\partial y_i}{\partial t}=0 \qquad (V.10)$$

Equation (V.10) is a partial differential equation that has the solution fraction varying with time and the radius, and the resin fraction varying with time. The solution fraction shares a common boundary condition in time and space, the feed concentration

$C_i^f$. This implies the combination of variables may be applied; however, the 'r' term is still in the denominator of the radial variation of solution fraction.

The choice of dimensionless variables is critical. The dimensionless variables chosen for this work were found by substituting the velocity definition, Equation (V.5), into the dimensionless time and distance and used for cylindrical flow.

$$\tau = \frac{k_{f,i}C_i^f}{d_p Q}\left(t - \frac{r^2\varepsilon}{2\phi}\right) \tag{V.11}$$

$$\xi = \frac{k_i}{2\phi}\frac{(1-\varepsilon)r^2}{d_p} \tag{V.12}$$

The constant '2' is not in the velocity definition; however, it was needed to facilitate the reduction of the continuity equation to an ordinary differential equation.

The derivatives of the dimensionless variables are scale the dimensional time and distance to dimensionless time and distance.

$$\frac{\partial\tau}{\partial t} = \frac{k_i C_i^f}{d_p Q} \tag{V.13}$$

$$\frac{\partial\xi}{\partial t} = 0 \tag{V.14}$$

$$\frac{\partial\tau}{\partial r} = \frac{-k_i C_i^f \varepsilon r}{d_p Q\phi} \tag{V.15}$$

$$\frac{\partial\xi}{\partial r} = \frac{k_{f,i}}{\phi}\frac{(1-\varepsilon)r}{d_p} \tag{V.16}$$

Applying the chain rule to change the integration axes from dimensional time and distance to dimensionless time and distance.

$$\frac{\partial x_i}{\partial \xi} = \frac{\partial x_i}{\partial \xi}\frac{\partial \xi}{\partial t} + \frac{\partial x_i}{\partial \tau}\frac{\partial \tau}{\partial z} \tag{V.17}$$

$$\frac{\partial x_i}{\partial z} = \frac{\partial x_i}{\partial \xi}\frac{\partial \xi}{\partial z} + \frac{\partial x_i}{\partial \tau}\frac{\partial \tau}{\partial z} \tag{V.18}$$

$$\frac{\partial y_i}{\partial t} = \frac{\partial y_i}{\partial \xi}\frac{\partial \xi}{\partial t} + \frac{\partial y_i}{\partial \tau}\frac{\partial \tau}{dt} \tag{V.19}$$

Substituting the derivatives into Equation (V.10) and expanding yields;

$$\left[\frac{\partial x_i}{\partial \xi}(0) + \frac{\partial x_i}{\partial \tau}\left(\frac{k_{f,i}C_f}{d_pQ}\right)\right] + \frac{\phi}{\varepsilon r}\left[\frac{\partial x_i}{\partial \xi}\frac{k_i(1-\varepsilon)r}{\phi d_p} - \frac{\partial x_i}{\partial \tau}\frac{k_i C_f r\varepsilon}{d_pQ\phi}\right] + (FR)\frac{1-\varepsilon}{\varepsilon}\frac{Q}{C_i^f}\left[\frac{\partial y_i}{\partial \tau}(0) + \frac{\partial y_i}{\partial \tau}\frac{k_{f,i}C_i^f}{d_pQ}\right] = 0 \tag{V.20}$$

Equation (V.20) collapses to the following partial differential equation.

$$\frac{\partial x_i}{\partial \xi} = -(FR)\frac{\partial y_i}{\partial \tau} \tag{V.21}$$

Assuming the interfacial concentration is zero, the right hand side of Equation (V.21) can be related to the particle rate.

$$\frac{dy_i}{dt} = \frac{k_i a_s}{Q}C_i^f \tag{V.22}$$

Changing the integration axis to dimensionless time yields,

$$\frac{\partial y_i}{\partial \tau} = \frac{\partial y_i}{\partial t}\frac{\partial t}{\partial \tau} = \frac{k_i a_s C_i^f}{Q}\left(\frac{d_pQ}{k_{f,i}C_i^f}\right) \tag{V.23}$$

which reduces to the following function of $x_i$.

$$\frac{\partial y_i}{\partial \tau} = d_p a_s x_i \tag{V.24}$$

Equation (V.24) is substituted into Equation (V.21) to give an ordinary differential equation that can be integrated by the separation of variables.

$$\frac{\partial x_i}{\partial \xi} = -(FR) d_p a_s x_i \tag{V.25}$$

The boundary conditions are

$$C_i = C_i^f \; @ r = R_o$$
$$C_i = C_i^{eff} \; @ r = R_i$$

Separating the variables yields,

$$\frac{\partial x_i}{x_i} = -(FR) d_p a_s \partial \xi \tag{V.26}$$

Integrating,

$$\ln(x_i)\Big|_1^{x_{i,eff}} = -(FR) d_p a_s \Big|_{\xi_i}^{\xi_0} \tag{V.27}$$

$$\ln\left(\frac{C_{eff}}{C_f}\right) - \ln(1) = (FR) d_p a_s (\xi_0 - \xi_i) \tag{V.28}$$

Inserting the dimensionless definitions to transform Equation (V.28) back to dimensional distance,

$$\xi_0 = \frac{k_{f,i}(1-\varepsilon) R_o^2}{2\phi d_p} \tag{V.29}$$

$$\xi_1 = \frac{k_{f,i}(1-\varepsilon) R_i^2}{2\phi d_p} \tag{V.30}$$

and reducing yields the following equation.

$$\ln\left(\frac{C_{eff}}{C_f}\right) = (FR) \frac{k_{f,i}(1-\varepsilon) a_s}{2\phi} \left(R_o^2 - R_i^2\right) \tag{V.31}$$

Finally substituting the definition of the specific surface area, $a_s$, and $\phi$ yields the following expression in the final form

$$\ln\left(\frac{C_{eff}}{C_{inf}}\right)=(FR)\frac{-6k_{f,i}(1-\varepsilon)}{d_p}\frac{\pi\left(R_o^2-R_i^2\right)h}{F} \qquad (V.32)$$

Comparing Equations (V.32) and (V.1),

$$\ln\left(\frac{C_i^{eff}}{C_i^{f}}\right)=(FR)\frac{-6k_{f,i}(1-\varepsilon)}{d_p}\frac{\pi R^2 L}{F} \qquad (V.1)$$

it is easy to see the only difference is the volume of the container; $\pi R^2 L$ for the cylindrical flow bed, $\pi\left(R_o^2-R_i^2\right)h$ for the radial flow bed. Hence there are no differences between the equations besides the volume of the bed. The mass transfer coefficient values calculated from each expression are identical for equal volume and flow rate systems.

The terms in Equations (V.1) and (V.32) has physical significance; V/F is the superficial residence time of an element of fluid in the empty bed while the remainder of the right hand side represents the rate (with the units of inverse time) which ions are transferred into a specific volume of resin. It applies to both outward and inward flow radial beds.

Equation (V.32) is useful for evaluating the performance of a radial flow mixed bed, but the derivation has greater significance than the estimation of an experimental mass transfer coefficient. Equation (V.21) is exactly the same form as the cylindrical mixed bed equation; the only difference is the definition of the dimensionless time and distance variables.

The implementation of the cylindrical model to radial flow would be a relatively simple matter, notice an average mass transfer coefficient were calculated to account for the varying fluid velocity.

# CHAPTER VI

# CONCLUSIONS AND RECOMMENDATIONS

## Conclusions

A mixed bed ion exchange column simulator has been developed. The simulator was derived from fundamental continuity equations and uses correlations and constants to estimate system properties and parameters as a function of time and bed depth.

The simulator is a rate model that approximates the film diffusion controlled ion exchange behavior of several types of strong and weak electrolytes in a mixed bed column. The model is applicable from ultrapure water concentrations to 0.002N solutions. The analytical solution of the Nernst-Planck ionic flux expressions developed by Franzreb (1993) was successfully implemented to calculate the ion exchange rates. The model satisfies the charge balance at all times.

The model satisfies the following criteria established by the author:

- The column material balance is satisfied to within 1% error. The mass balance error is directly related to the distance step-size, but has shown no correlation to the time step-size.

- The ion exchange rates for monovalent species are rigorous within the thermodynamic and kinetic assumptions. However, an approximation based on the ionic selectivity coefficients and valences was required to estimate the resin-solution reaction equilibria for multivalent ions. The removal efficiency of a constituent is sensitive to influent concentration and flow rate.
- Ions elute chromatographically through the bed according to selectivity and diffusion principles. High selectivity ions displace low selectivity ions until reaction equilibrium is reached with the solution. High diffusivity ions have sharp exchange zones that quickly exchange to equilibrium loadings; low diffusivity ions have broader exchange zones that do not use all of the available capacity.
- The loading, rate and solution ratio surfaces are continuous without oscillation or discontinuity when the simulation has the correct distance step-size. If discontinuities in the surfaces occur, the likely remedy is the reduction of the distance step-size. If that does not work, the hard-coded separation factor limit of 5,000 may need to be reduced.
- Infinite run effluent concentrations gradually became equal to the influent concentrations, and the resin loadings reach equilibrium with the solution. Starting the exchange calculations further down the bed as the resin exhausts can reduce run-time. The criterion is sum of the absolute values of the ion exchange fluxes must be less than a specified tolerance.
- The effluent concentrations predicted by the model are within the limits of ultrapure water manufacture. Many ultrapure water plants produce water that is purer than the detection limits of modern instruments, and the model is stable reporting

concentrations below part per trillion levels. The effluent histories are also responsive to internal bed dynamics and external system changes.

Perhaps the most significant accomplishment of this work was the derivation of the continuity equation system. Each element of the partial differential equation system is defined in terms of the constituent solution and resin concentrations only. This removed the dependency of the continuity equations on common constants, and helped relieve the stiffness of the equation system. The author has not encountered the technique in the literature, and he expects the concept can be applied to several types of multicomponent adsorption modeling efforts.

The model can export the ionic loading profiles at any time during the simulation, and may be restarted at any flow rate and concentration. This technique allows sequential runs that may be used to model step changes, pulse changes, and eventually real-time data.

If a resin fraction loading constraint is violated, i.e. if the loading is negative or the sum of the loadings is greater than one, the only applicable alternative is the reduction of the time step-size, which also requires a restart of the simulation. Attempts to manipulate the exchange rate or the loading results in instabilities and the solution cannot be recovered.

The dynamics of the mixed bed column have been demonstrated using either animated two-dimensional figures, or by plotting the loading, rate and solution fractions as a three-dimensional surface that varies with time and distance. Profile analysis is a potentially useful tool to analyze and optimize bed performance.

The model simulates the effects of resin heels, desulfonation, and fouling. Anion resin heels are effective for removing sulfate shed from cation resin, and fouling reduces the removal efficiency of a constituent without affecting the equilibrium exchange capacity. However, fouling broadens the exchange zone and may reduce the cycle time of the bed.

Weak electrolyte exchange has been approximated with ionic fluxes and in general has reasonable results. However, as listed in the recommendations work, is required. Molecular adsorption followed by direct protonation/hydrolysis is known to occur and is not modeled. The model is also deficient in modeling molecular sorption without using exchange capacity.

## Recommendations

The following recommendations are intended to be action items that do not require a large budget, and should be completed as soon as possible.

Molecular mass transfer mechanism for weak electrolyte species—The current mass transfer rate is calculated using only ionic fluxes, but several authors have shown that molecular mass transfer is a valid mechanism and should be modeled. A reasonably accurate molecular interfacial concentration model must be derived or estimated to provide the concentration driving force.

Silica, borate and metal oxide chemistries—These species should be incorporated into the model as soon as possible, the additions primarily affect the dissociation equilibrium and the resin loading distribution.

Model error and sensitivity analysis—An error estimate of the model with respect to the many input parameters should be performed. The author recommends an

approximate probable error analysis that uses the numerical partial derivatives and expected variances to estimate the probable concentration errors for an influent.

Complete the implementation of FORTRAN 95 functionality—FORTRAN 90/95 has structures similar in form to C++ or Visual Basic. The type variables can define a generalized constituent that may have several ionic sub-species, or the constituent may even form polynuclear aggregate species. Type variables should simplify complex water chemistries such as metal oxide, borate and silica modeling, and would also facilitate multiple two-step and three step dissociative acids and bases. There will be several difficulties converting the existing dissociation equilibrium and ionic flux subroutines, and defining the proper constituent structures.

Thermodynamic reaction equilibrium—A more rigorous thermodynamic reaction equilibrium model is required. The current model is only approximate for multivalent species; the separation factors are not a function of the resin and solution phase concentrations, nor are they temperature dependent. The current model also assumes no ionic interactions. Equilibrium isotherm data taken at ultrapure water concentrations would be ideal for regressing separation factors, but an additional review of non-mass action equilibrium models may be useful.

Variable distance and time step-sizes—The node calculation has been optimized to the limits of this integration method without sacrificing model accuracy; hence the only way to significantly reduce run-time is to reduce the number of node calculations. Currently a constant step size is assumed for both integration axes, but at time and distance coordinates where the sum of the absolute value of the rates is below a predetermined tolerance, the step-size can be doubled or increased even more.

Additionally, if the loading constraint is exceeded, it should be relatively straightforward to use the previous loading profiles and restart the simulation at one-half the time step size.

Model benchmarking—The performance of the model needs to be compared to industrial data, preferably with ion specific ion effluent histories. Additionally, a comparison of the resin exhaustion as a function of time should be performed.

## Future work

The model will probably never be truly finished, and there are numerous future applications of the model. Some ideas for future projects include;

Regeneration modeling—Regeneration modeling has several additional complications from the ultrapure water model. Ionic activities are significant in the solution phase. Also a different rate model is required that accounts for diffusion of ions into the resin for ion exchange regeneration.

Multiple beds in parallel—A single mixed bed system has been modeled effectively; however, most systems have several mixed beds in parallel with different regeneration/replacement schedules. It is possible to combine the effluents of different runs by using interpolation methods with the effluent histories.

Multiple beds in series—Most ultrapure water plants have at least a cation exchange bed preceding the mixed bed, and often there is an anion exchange bed also. Naturally the influent concentrations are variable for downstream units, but the model is able to restart with new concentrations without great distortion of the loading profiles. Gramophadye (1996) made preliminary attempts to model ion exchange beds in series using a model similar to Bulusu's (1994) model.

Flow loop analysis—Most ultrapure water systems are configured in a loop with a holding tank that accepts make-up water as well as the recycle stream. The effects of make-up water addition on the ion exchange beds as well as the effects of dilution on the effluent concentrations as a function of time are desirable by several industries.

# REFERENCES


Alexander, G. B. H., and Iler, R. K. (1954). "The Solubility of Amorphous Silica in Water." J. Phys. Chem. **58**: 453-455.

Bates, J.C. (1999). Personal communication, British Energy, Glouchester, United Kingdom

Bulusu, R. (1994). Development of a Column Model to Predict Multicomponent Mixed Bed Ion Exchange Breakthrough. M.S. Thesis. Oklahoma State University, Stillwater

Caddel, J. R. (1954). "Mixed-bed Deionization at High Flow Rates." Chem. Eng. Progr. Sympo. Ser. **50**(14): 1-6.

Chowdiah, V. N. (1996). Liquid-Film Diffusion Controlled Ion-exchange Modeling: Study of Weak Electrolyte Mass Transport and Film Mass Transport and Film Mass-transfer Kinetics. Ph. D Dissertation. Oklahoma State University, Stillwater

Divekar, S. V., Foutch G. L., (1987). "Mixed-Bed Ion Exchange At Concentrations Approaching the Dissociation of Water. Temperature Effects." Industrial & Engineering Chemistry Research **26**(9): 1906-1909.

Dwivedi, P. N. and S. N. Upadhyay (1977). "Particle-Fluid Mass Transfer in Fixed and Fluidized Beds." Industrial & Engineering Chemistry, Process Design and Development **16**(2): 157-165.

Foutch, G. L. (1991). "Temperature Effects on Mixed-bed Ion Exchange Performance." Ultrapure Water Journal **8**(4): 56-58.

Franzreb, M., Holl, W. H. and Sontheimer, H. (1993). "Liquid-side Mass Transfer in Multicomponent Ion Exchange: I. System Without Chemical Reactions in the Film." Reactive Polymer **21**: 117-133.

Franzreb, M., (2000). Personal Communication, Oklahoma State University

Frisch, N. Kunin., R. (1960). "Kinetics of mixed-bed deionization: I." AIChE. J. **6**(4): 640-647.

Gear, C. W. (1971). Numerical Initial Value Problems in Ordinary Differential Equations. Englewood Cliffs, New Jersey, Prentice-Hall.

Gerald, C. F., Wheatley, P. O. (1989). Applied Numerical Analysis. Reading, Massachusetts, Addison-Wesley Publishing Company.

Glaski, F. A., J. S. Dranoff (1963). Ion Exchange Kinetics: A Comparison of Models, AIChE J., **9**, 426-431.

Gluekauf, E. (1947). "Theory of Chromatography, IV. The Influence of Incomplete Equilibrium on the Front Boundary of Chromatograms and on the Effectiveness of Separation." J. Chem. Soc.: 1315-1321.

Harries, R. R. (1987). "Ion Exchange Kinetics in Condensate Purification." Chemistry and Industry **4**: 104-109.

Harries, R. R. (1991). "Ion Exchange Kinetics in Ultra Pure Water Systems." J. Chem. Tech. Biotechnol. **51**: 437-447.

Haub, C. E. (1984). Model Development for Liquid Resistance-Controlled Reactive Ion Exchange at Low Solution Concentrations with Applications to Mixed-Bed Ion Exchange. M. S. Thesis, Oklahoma State University, Stillwater

Helfferich, F. G. (1962). Ion Exchange. New York, McGraw Hill.

Helfferich, F. G. (1965). "Ion Exchange Kinetics: V. Ion Exchange Accompanied by Reactions." J. Phys. Chem. **69**: 1178-1187.

Helfferich, F. G. (1984). "Weak Electrolytes, Polybasic Acids, and Buffers in Anion Exchange Columns I. Sodium Acetate and Sodium Carbonate systems." Reactive Polymers **3**: 51-66.

Helfferich, F. G. and Y.-L. Hwang (1985). "Kinetics of Acid Uptake By Weak-Base Anion Exchangers. Mechanism of Proton Transfer." AIChE Symposium Series(242): 17-27.

Helfferich, F. G. (1990). "Models and Physical Reality in Ion-Exchange Kinetics." Reactive Polymers **13**(1-2): 191-194.

Helfferich, F. G. (1990). "Ion-exchange Equilibria of Amino Acids on Strong-acid Rresins: Theory." Reactive Polymers **12**(1): 95-100.

Hussey, D. F. (1996). Devolpment of Generalized Multicomponent Ion Exchange Reaction Equlibrium Model. M. S. Thesis, Oklahoma State University, Stillwater

Jansen, M. L., G. W. Hofland, et al. (1996). "Effect of pH and Concentration on Column Dynamics of Weak Electrolyte Ion Exchange." AIChE Journal **42**(7): 1925-1937.

Jansen, M. L., J. J. Straathof, et al. (1996). "Rigorous Model for Ion Exchange Equilibria of Strong and Weak Electrolytes." AIChE Journal **42**(7): 1911-1924.

Jansen, M. L., J. Houwers, et al. (1997). "Effect of Dissociation Equilibria on Ion-exchange Processes of Weak Electrolytes." AIChE Journal **43**(1): 73-82.

Kataoka, T., Sato, M. and Ueyama, K. (1968). "Effective Liquid Phase Diffusivity in Ion exchange." J. Chem. Eng. Jpn. **1**: 38-42.

Kataoka, T. M. S., and K. Ueyama (1971). "Influence of a noncounterion valence on liquid phase diffusion in ion exchange." Kogyo Kagaku Zasshi **74**: 1052-1058.

Kataoka, T., Yoshida, H. and Ueyama, K. (1972). "Mass Transfer in Laminar Region Between Liquid and Packing Material Surface in the Packed Bed." J. Chem. Eng. Jpn. **5**(2): 132-136.

Kataoka, T. Y., H. and Yamada, T. (1973). "Liquid Phase Mass Transfer in Ion Exchange Based on the Hydraulic Radius Model." J. Chem. Eng. Jpn. **6**(2): 172-177.

Kataoka, T. a. Y. H. (1976). "Liquid Phase Diffusion Controlling in Irreversible Ion Exchnage." J. Chem. Eng. Jpn. **6**: 326-329.

Kataoka, T., H. Yoshida, et al. (1976). "Liquid Phase Mass Transfer in Ion Exchange Accompanied By Chemical Reaction." Journal of Chemical Engineering of Japan **9**(2): 130-135.

Kataoka, T., H. Yoshida, et al. (1987). "Liquid-Side Ion Exchange Mass Transfer in a Ternary System." AIChE Journal **33**(2): 202-210.

Koon, J. H. and W. J. Kaufman (1975). "Ammonia Removal From Municipal Wastewaters By Ion Exchange." Journal Water Pollution Control Federation **47**(3 pt 1): 448-465.

Kunin, R. (1950). Ion Exchange Resins. New York, John Wiley & Sons.

Kunin, R. (1960). Elements of Ion Exchange. New York, Reinhold Publishing Co.

Lou, J. (1997). Modeling of Boron Sorption Equlibrium and Kinetic Studies of Ion Exchange with Boron Solution. M. S. Thesis, Oklahoma State University, Stillwater

McNulty, J. T., Eumann, M., Bevan, C. A. and Tan, V.C.T. (1986). Anion Exchange Resin Kinetic Testing and Indispensable Diagnostic Tool for Condensate Polisher

Troubleshooting. 47th Annual Meeting International Water Conference, Pittsburgh, Pennsylvania.

McNulty, J. T., Bevan, C.A. and Carlin, W.H. (1992). Condensate Polishing and Blowdown Demineralization in Morpholine/Boric Acid Matrices. IEX'92, Churchill College, Cambridge.

Noh, B. I. (1992). Effects of Step Change in Feed Concentration and Incomplete Mixing of Anion and Cation Resin on the Performance of Mixed-bed Ion Exchange. Ph. D dissertation, Oklahoma State University, Stillwater

Pate, K. T. (1991). "Control of Dissolved Silica in High-Purity Systems." Ultrapure Water Journal **8**(4): 35-43.

Pondugula, S. K. (1994). Mixed Bed Ion Exchange Modeling for Divalent Ions in a Ternary system. M. S. Thesis, Oklahoma State University, Stillwater

Press, W. H., Teukolsky, Saul A., Vetterling, William T., Flannery, Brian P. (1992). Numerical Recipes in Fortran. Cambridge, Cambridge University Press.

Rahman, K. (1979). "Film Diffusion Controlled Kinetics in Ternary Ion Exchange : Development of the Basic Equations." Chem. Eng. Res. Bull. **3**: 27-30.

Rahman, K. (1981). "Mass Transfer in Liquid Fluidized Beds of Ion Exchange Particles." Chem. Eng. Sci. **36**(2): 293-300.

Reid, R. C., Parusnitz, J. M. and Sherwook, T. K. (1987). The Properties of Gases and Liquids. New York, McGraw-Hill.

Robinson, R. A. (1955). Electrolyte Solutions. New York, Academic Press Inc.

Sadler, M. A. (1993). Developments in the Production and Control of Ultrapure Water. Cambridge, U.K., The Royal Society of Chemistry.

Samuelson, O. (1963). Ion Exchange Separations in Analytical Chemistry, John Wiley And Sons, New York

Schlogl, R. (1954). "Elektrodiffusion in Freier Losung und Geladenen Membranen." Z. Phys. Chem. **1**: 305-339.

Schlogl, R., Helfferich, F., (1957). "Comment on the Significance of Diffusion Potentials in Ion Exchange Kinetics." J. Chem. Phys. **26**: 5-7.

Smith, T. G. and J. S. Dranoff (1964). Film-Diffusion Controlled Kinetics of Binary Ion Exchange. Ind. Eng. Chem. Fundam., 3, 195-200

Stokes, R. H. (1965). "Tracer Diffusion in Binary Solutions Subject to a Dimerization Equilibrium." J. Phys. Chem. **69**(11): 4012-4016.

Streat, M. (1995). "'Waters Were Made Sweet'. Advances in Ion Exchange Technology." Industrial & Engineering Chemistry Research **34**(8): 2841.

Sunkavalli, S. K. V. (1996). Development of Generalized Equilibrium and Rate Models to Predict Ion Exchange Column Performance. M. S. Thesis, Oklahoma State University, Stillwater

Thompson, R. H. (1991). "Morphine Advances as a Method for Reducing Iron Transport in Feedwater." Power(February): 26-32.

Turner, J. C. R., and Snowdon, C. B. (1968). Liquid-side Mass Transfer in Ion Exchange: An Examination of the Nernst-Planck Model, Chem. Eng. Sci., **23**, 221-230

Wagner, J. D. Dranoff, J. S., (1967). "The Kinetics of Ion Exchange Accompanied by Irreversible Reaction. III. Film Diffusion Controlled Neutralized of a Strong Acid Exchanger by a Weak Base." J. Phys. Chem. **71**(13): 4551-4553.

Wilson, E. J. a. G., C.J. (1966). "Liquid Mass Transfer at Very Low Reynolds Numbers in Packed Beds." Ind. Eng. Chem. Fundam. **5**(1): 9-14.

Wong, Y. W. and J. L. Niedzwiecki (1982). "Simplified Model For Multicomponent Fixed Bed Adsorption." AIChE Symposium Series **78**(219): 120-127.

Yoon, T. K. (1990). The Effect of Cation to Anion Ratio on Mixed-bed Ion Exchange Performance at Ultra-low Concentrations. Ph. D Dissertation, Oklahoma State University, Stillwater

Yoshida, H. a. K., T. (1987). "Adsorption of Amines on H+-Form Ion Exchanger." Chem. Eng. Sci. **42**(7): 1805-1814.

Yoshida, H., K. Shimizu, et al. (1990). "Adsorption of Amine and Paints on H-form Resin from Electrodeposition Wastewater." AIChE Journal **36**(12): 1815-1821.

Yu, Q. a. W. N.-H. L. (1989). "Computer Simulations of Dynamics of Multicomponent Ion Exchange and Adsorption in Fixed Beds: Gradient-Directed Moving Finite Element Method." Computers Chem. Eng. **13**(8): 915-926.

Zecchini, E. J. Foutch., G. L. (1990). Solutions to Selected Problems in Multicomponent Mixed bed Ion Exchange Modeling. Ph. D. Dissertation, Oklahoma State University, Stillwater.

# APPENDIX A

## EQUILIBRIUM INTERFACIAL CONCENTRATIONS

### Interfacial concentrations for ions

Interfacial concentrations (solid-film interface) of ions are determined using ion exchange equilibria. Local equilibrium is assumed at the solid-film interface. The selectivity coefficient expression for a general case of ion B replacing ion A, can be written using mass action law, as

$$K_A^B = \left(\frac{q_B}{C_B^*}\right)^{z_A} \left(\frac{C_A^*}{q_A}\right)^{z_B} \qquad \text{(A.1)}$$

where q is the resin phase concentration and $C^*$ is the interfacial concentration.

For any ion 'i' we can express the resin phase concentration and the interfacial concentration as

$$q_i = Y_i Q \qquad \text{(A.2)}$$

$$C_i^* = X_i^* C_T^* \qquad \text{(A.3)}$$

Equation (A.1) can be written in terms of equivalent fractions, total resin capacity and total interfacial concentration as follows:

$$K_A^B = \left(\frac{Y_B}{X_B^*}\right)^{z_A} \left(\frac{X_A^*}{Y_A}\right)^{z_B} Q^{(z_A - z_B)} C_T^{*(z_B - z_A)} \tag{A.4}$$

Rearranging the above equation, the interfacial fractional concentration of ion B can be expressed as

$$X_B^* = Y_B \left(K_A^B\right)^{-1/z_A} \left(\frac{X_A^*}{Y_A}\right)^{z_B/z_A} \left(\frac{Q}{C_T^*}\right)^{1-z_B/z_A} \tag{A.5}$$

Generalizing the above expression, the interfacial fractional concentration of an ion 'i' exchanging for an ion 'A' can be written as

$$X_i^* = Y_i \left(K_A^i\right)^{-1/z_A} \left(\frac{X_A^*}{Y_A}\right)^{z_i/z_A} \left(\frac{Q}{C_T^*}\right)^{1-z_i/z_A} \tag{A.6}$$

If we have 'n-1' ions exchanging for ion A we can write 'n-1' such equations. But we have 'n+1' unknowns. One of the extra equations needed to completely specify the system is obtained from the loading constraints at the solid-film interface.

$$\sum_{i=1}^{n} X_i^* = 1.0 \tag{A.7}$$

Rewriting the interfacial fractional concentration (Equation (A.6)) as

$$X_i^* = \lambda_i \left(X_A^*\right)^{z_i/z_A} \tag{A.8}$$

where

$$\lambda_i = Y_i \left(K_A^i\right)^{-1/z_A} \left(Y_A\right)^{-z_i/z_A} \left(\frac{Q}{C_T^*}\right)^{1-z_i/z_A} \tag{A.9}$$

and substituting these in equation (A.7) we have

$$X_A^* + \sum_{i=1}^{n-1} \lambda_i \left(X_A^*\right)^{z_i/z_A} = 1.0 \qquad \text{(A.10)}$$

This is a polynomial independent in $X_A^*$ and could be solved using an iteration technique. Brent's method was used in this work.

If the reference ion concentration is zero, Equation (A.9) is undefined for all elements. Although theoretically not possible, it is numerically possible for the reference ion loading to equal zero. An alternative reference was chosen by Hussey (1996) by created a pseudo-ion with exchange properties found from the average of the ions loaded on the resin.

Noting the Gibbs energy of reaction is an additive quantity that can be averaged,

$$\sum_{i=1}^{n} y_i \frac{\Delta G^{rxn}}{RT} = \sum_{i=1}^{n} y_i \ln\left(K_A^i\right) \qquad \text{(A.11)}$$

Applying the property of logarithms allows the calculation of the pseudo-ion selectivity

$$K_H^{ref} = \prod_{i=1}^{n} K_H^{i\,y_i} \qquad \text{(A.12)}$$

and the mean ion valence is calculated from an algorithm similar to that developed by Franzreb (1993) for the mean coion valence.

$$z_{ref} = \frac{\sum_{i=1}^{n} z_i q_i}{\sum_{i=1}^{n} q_i} \qquad \text{(A.13)}$$

The reference ion for each species is switched to the pseudo-ion by changing the reference ion of the selectivity coefficient with the following expression.

$$K_{ref}^{i} = \frac{\left(K_H^i\right)^{z_{ref}}}{\left(K_H^{ref}\right)^{z_i}} \qquad (A.14)$$

In the above equations, the total interfacial concentration, $C_T^*$, is still unknown, its value depends if the resin is in equilibrium with the bulk solution or if exchange is occurring.

If the resin is in equilibrium with the solution, the only extra variable required to calculate the equilibrium concentrations is the r+eference ion concentration, hydrogen for cation resin, hydroxyl ions for the anion resin. The algorithm is described below:

1. Set $C_T^*$ equal to the reference ion concentration, $C_H$ for cations, $C_{OH}$ for anions.

2. Calculate each $X_i^*$ using the given loadings, $Y_i$ and Equations (A.7) through (A.10) for both cation and anion resins.

3. Calculate the ratios $C_H^{ratio} = \frac{C_H}{X_H^*}$ and $C_{OH}^{ratio} = \frac{C_{OH}}{X_{OH}^*}$.

4. Calculate the individual ion concentrations for each resin $C_i^* = X_i^* C_T^* C_{H/OH}^{ratio}$.

5. Sum the individual concentrations to form a new total interfacial concentration, $C_{T,new}^* = \sum_{i=1}^{n} C_i^*$ and return to step 1 until $C_{T,new}^* = C_{T,old}^*$

An analytical expression to calculate $C_T^*$ for systems with exchanging ions was developed by Franzreb (1993). The flux expression is complicated and is derived in Appendix C.

Interfacial concentrations for non-ionic species

Weak electrolytes mass transfer into or out of the resin requires the molecular interfacial concentration to complete the molecular flux expressions. This quantity is not straightforward to calculate; the interfacial concentrations of nonionic (molecular) forms need to be known to calculate the rate. In this work, the dissociation equilibrium relationship between the molecular species and the first dissociation product is used to determine interfacial concentrations of the nonionic forms,

$$[AH]^* = \frac{[A^-]^*[H^+]^*}{k_A} = \frac{k_w}{k_A}\frac{[A^-]^*}{[OH^-]^*} = \frac{k_w}{k_A}\frac{X_A^*}{X_{OH}^*} \qquad \text{(for acids)} \qquad \text{(A.15)}$$

$$[BOH]^* = \frac{[B^+]^*[OH^-]^*}{k_B} = \frac{k_w}{k_B}\frac{[B^+]^*}{[H^+]^*} = \frac{k_w}{k_B}\frac{X_B^*}{X_H^*} \qquad \text{(for bases)} \qquad \text{(A.16)}$$

where $k_A$ and $k_B$ are the dissociation constants for acid and base respectively; $[H^+]$ and $[OH^-]$ are the interfacial concentrations of hydrogen and hydroxyl respectively; $[A^-]^*$ and $[B^+]^*$ are the interfacial concentrations for ionic forms, which can be determined using the method mentioned above. Both concentrations are part of the total concentration, hence the total concentration drops out and the equivalent solution fractions remain.

# APPENDIX B

## DISSOCIATION EQUILIBRIUM RELATIONSHIPS

### Dissociation equilibrium for Type I dissociative species

Type I dissociative species has the characteristic of one-step dissociation equilibrium. Monovalent amines are a typical type I dissociative species. Chowdiah (1996) and Sunkavalli (1996) reviewed the dissociation equilibrium for monovalent amines. Based on their derivations, a generalized dissociation equilibrium for type I species can be generated. As we know, for monovalent amines,

$$RNH_2 + H_2O \xleftrightarrow{K_b} RNH_3^+ + OH^- \tag{B.1}$$

$$K_b = \frac{[RNH_3^+][OH^-]}{[RNH_2]} \tag{B.2}$$

and for monovalent organic acids,

$$RCOOH \xleftrightarrow{K_a} RCOO^- + H^+ \tag{B.3}$$

$$K_a = \frac{[RCOO^-][H^+]}{[RCOOH]} \tag{B.4}$$

Eq (B.2) and Eq (B.4) are the same form. Therefore, we can generalize the dissociation equilibrium for the type I species as

$$A^* \xleftrightarrow{K} A^{+-} + B^{-+} \tag{B.5}$$

$$K = \frac{[C_{D1}^{+-}][B^{-+}]}{[C_{D1}^{*}]} \tag{B.6}$$

where B could be $H^+$ or $OH^-$, depending the type I species is acid or base.

If the total concentration of type I species is defined as

$$C_{D1}^{T} = C_{D1}^{*} + C_{D1}^{+-} \tag{B.7}$$

then from Equations (B.6) and (B.7), we can derive the relationship between $C_{D1}^{+-}$ and $B^{-+}$, that is

$$C_{D1}^{+-} = \frac{K\, C_{D1}^{T}}{K + B^{-+}} \tag{B.8}$$

This relation is used to eliminate $C_{D1}^{+-}$ from the charge balance equation, so that the charge balance equation contains only one unknown $B^{-+}$ for solving.

Dissociation equilibrium for Type II dissociative species

Type II dissociative species has the characteristics of two-step dissociation. Carbonate is a typical type II dissociative species. Bulusu (1994) and Sunkavalli (1996) reviewed the water chemistry of carbonates, and the following dissociation equilibrium equations were presented:

$$CO_2 + H_2O \longleftrightarrow H_2CO_3 \tag{B.9}$$

$$H_2CO_3 \xleftarrow{K_1} H^+ + HCO_3^- \tag{B.10}$$

$$HCO_3^- \xleftarrow{K_2} H^+ + CO_3^{2-} \tag{B.11}$$

$$H_2O \xleftarrow{K_w} H^+ + OH^- \tag{B.12}$$

$$K_1 = \frac{[H^+][HCO_3^-]}{[H_2CO_3^*]} \tag{B.13}$$

$$K_2 = \frac{[H^+][CO_3^{2-}]}{[HCO_3^-]} \tag{B.14}$$

$$K_w = [H^+][OH^-] \tag{B.15}$$

where

$$[H_2CO_3^*] = [H_2CO_3] + [CO_2] \tag{B.16}$$

For the type II species, we can generalized its dissociation equilibrium as

$$C_{D2}^* \xleftrightarrow{K_1} C_{D2}^{+-} + B^{-+} \tag{B.17}$$

$$C_{D2,1}^{+-} \xleftrightarrow{K_2} C_{D2,2}^{2+-} + B^{-+} \tag{B.18}$$

$$K_1 = \frac{[C_{D2,1}^{+-}][B^{-+}]}{[C_{D2}^*]} \tag{B.19}$$

$$K_2 = \frac{[C_{D2,2}^{2+-}][B^{-+}]}{[C_{D2}^{+-}]} \tag{B.20}$$

where, $B^{-+}$ is a dummy ion, which could be $H^+$ or $OH^-$ depending the type II species is acid or base.

Given the total concentration $C_{D2}^T$ for the type II dissociative species, that is

$$C_{D2}^T = C_{D2}^* + C_{D2,1}^{+-} + C_{D2,2}^{2+-} \tag{B.21}$$

the concentrations for monovalent ions and divalent ions can be determined.

From Eq (B.20) and Eq (B.21), we have

$$C_{D2}^* = \frac{C_{D2,1}^{+-} B^{-+}}{K_1} \tag{B.22}$$

$$C_{D2,2}^{2+-} = \frac{K_2 C_{D2,1}^{+-}}{B^{-+}} \tag{B.23}$$

Substituting Eq (B.22) and Eq (B.23) into Eq (B.21) would lead to

$$C_{D2}^{T} = \frac{B^{-+} C_{D2,1}^{+-}}{K_1} + C_{D2,1}^{+-} + \frac{K_2 C_{D2,1}^{+-}}{B^{-+}} \tag{B.24}$$

Then the concentration of monovalent ion of typeII species can be written as:

$$C_{D2,1}^{+-} = \frac{C_{D2}^{T}}{X} \tag{B.25}$$

where

$$X = \frac{B^{-+}}{K_1} + \frac{K_2}{B^{-+}} + 1 \tag{B.26}$$

The expressions for the concentrations of other type II species can be written as:

$$C_{D2}^{*} = \frac{B^{-+} C_{D2}^{T}}{K_1 X} \tag{B.27}$$

$$C_{D2,2}^{2+-} = \frac{K_2 C_{D2}^{T}}{B^{-+} X} \tag{B.28}$$

The above relations Eq (B.25), (B.26) and (B.28) are used to express the concentrations of various forms of type II species in terms of the concentration of B ($H^+$ or $OH^-$) in the charge balance equation, so that only one unknown exists in the equation. Then the charge balance equation can be solved for this system.

Dissociation equilibrium for Type III dissociative species

Type III species has the characteristics of three-step dissociations. For instance, triprotic acid – phosphate is a typical type III dissociation species.

The dissociation equilibrium relationships for phosphate (Fast, 1984) are

$$H_3PO_4 \xleftrightarrow{K_1} H^+ + H_2PO_4^- \tag{B.29}$$

$$H_2PO_4^- \xleftrightarrow{K_2} H^+ + HPO_4^{2-} \tag{B.30}$$

$$HPO_4^{2-} \xleftrightarrow{K_3} H^+ + PO_4^{3-} \tag{B.31}$$

$$K_1 = \frac{[H^+][H_2PO_4^-]}{[H_3PO_4]} \tag{B.32}$$

$$K_2 = \frac{[H^+][HPO_4^{2-}]}{[H_2PO_4^-]} \tag{B.33}$$

$$K_3 = \frac{[H^+][PO_4^{3-}]}{[HPO_4^{2-}]} \tag{B.34}$$

Based on the above, we can generalize the dissociation equilibriums for type III species as

$$C_{D3}^* \xleftrightarrow{K_1} C_{D3}^{+-} + B^{-+} \tag{B.35}$$

$$C_{D3,1}^{+-} \xleftrightarrow{K_2} C_{D3,2}^{2+-} + B^{-+} \tag{B.36}$$

$$C_{D3,2}^{2+-} \xleftrightarrow{K_3} C_{D3,3}^{3+-} + B^{-+} \tag{B.37}$$

$$K_1 = \frac{[C_{D3,1}^{+-}][B^{-+}]}{[C_{D3}^*]} \tag{B.38}$$

$$K_2 = \frac{[C_{D3,2}^{2+-}][B^{-+}]}{[C_{D3,1}^{+-}]} \tag{B.39}$$

$$K_3 = \frac{[C_{D3,3}^{3+-}][B^{-+}]}{[C_{D3,2}^{2+-}]} \tag{B.40}$$

where, B is a dummy ion, which could be $H^+$ or $OH^-$ depending the type III species is acid or base.

If the total concentration of type III species is given, that is

$$C_{D3}^{T} = C_{D3}^{*} + C_{D3,1}^{+-} + C_{D3,2}^{2+-} + C_{D3,3}^{3+-} \tag{B.41}$$

then the concentration for each type III species can be determined.

From Eq, (B.38), (B.39) and(B.40), we have

$$C_{D3,1}^{+-} = \frac{K_1 C_{D3}^{*}}{B^{-+}} \tag{B.42}$$

$$C_{D3,2}^{2+-} = \frac{K_2 C_{D3,1}^{+-}}{B^{-+}} = \frac{K_1 K_2 C_{D3}^{*}}{\left(B^{-+}\right)^2} \tag{B.43}$$

$$C_{D3,3}^{3+-} = \frac{K_3 C_{D3,2}^{2+-}}{B^{-+}} = \frac{K_1 K_2 K_3 C_{D3}^{*}}{\left(B^{-+}\right)^3} \tag{B.44}$$

Substituting Eq (B.42), (B.43) and (B.44) into Eq (B.41) leads to

$$C_{D3}^{T} = C_{D3}^{*} + \frac{K_1 C_{D3}^{*}}{B^{-+}} + \frac{K_1 K_2 C_{D3}^{*}}{\left(B^{-+}\right)^2} + \frac{K_1 K_2 K_3 C_{D3}^{*}}{\left(B^{-+}\right)^3} \tag{B.45}$$

Solving for $C_{D3}^{*}$,

$$C_{D3}^{*} = \frac{C_{D3}^{T}}{X} \tag{B.46}$$

where

$$X = 1 + \frac{K_1}{B^{-+}} + \frac{K_1 K_2}{\left(B^{-+}\right)^2} + \frac{K_1 K_2 K_3}{\left(B^{-+}\right)^3} \tag{B.47}$$

Therefore, the expressions for other ionic forms of type III species are

$$C_{D3,1}^{+-} = \frac{K_1}{B^{-+}} \frac{C_{D3}^T}{X} \tag{B.48}$$

$$C_{D3,2}^{2+-} = \frac{K_1 K_2}{\left(B^{-+}\right)^2} \frac{C_{D3}^T}{X} \tag{B.49}$$

$$C_{D3,3}^{3+-} = \frac{K_1 K_2 K_3}{\left(B^{-+}\right)^3} \frac{C_{D3}^T}{X} \tag{B.50}$$

Equations(B.48), (B.49) and (B.50) are used to express various forms of type III species in terms of the concentration of B ion ($H^+$ or $OH^-$) in the charge balance equation, so that only one unknown exists in charge balance equation.

# APPENDIX C

## FLUX EXPRESSIONS AND PARTICLE RATE

Flux expressions for ions in multicomponent ion exchange are usually derived using Nernst-Planck model and basic principles of ion exchange. Haub and Foutch (1984), Zecchini and Foutch (1990) had successfully applied Nernst-Planck model to describe film diffusion-controlled mixed-bed ion exchange fluxes for monovlanet ions (binary or ternary systems). In addition, Pondugula (1994) further developed the flux expressions for divalent systems. But to handle multicomponent multivalent MBIE systems, generalized expression is required. In this work, the method proposed by Franzreb et al. (1993) is followed to derive the flux expressions for multicomponent, multivalent systems.

If neglecting the curvature of film, the Nernst-Planck equation can be expressed as

$$J_i = -D_i\left[\frac{\partial C_i}{\partial r} + \frac{C_i z_i F}{RT}\frac{\partial \phi}{\partial r}\right] \qquad (C.1)$$

where $\phi$ is the electric potential and $z_i$ is the ion valence. Assuming pseudo steady state allows us to replace the partial derivatives by ordinary derivatives. The flux expressions derived in this model are based on bulk-phase neutralization.

The conditions that must be satisfied within the film surrounding the resin are:

$$\sum z_i C_i = \sum z_j C_j \qquad \text{(Electroneutrality, charge balance)} \qquad \text{(C.2)}$$

where 'i' stands for counterions and 'j' represents coions.

$$z_j J_j = 0 \qquad \text{(No coion flux)} \qquad \text{(C.3)}$$

$$\sum z_i J_i = \sum z_j J_j \qquad \text{(No net current flow)} \qquad \text{(C.4)}$$

From Eq (C.3) and Eq (C.4)

$$\sum z_i J_i = 0 \qquad \text{(No net current flow)} \qquad \text{(C.5)}$$

The total equivalent ion concentration can be defined as:

$$C_T = \omega \sum_{i=1}^{n} z_i C_i = \omega_j \sum_{j=1}^{m} z_j C_j \qquad \text{(C.6)}$$

where, n is the number of counterions, m is the number of coions. And $\omega$ =+1 for cations and -1 for anions.

Using the no coion flux condition – Eq (C.3),

$$\frac{d\phi}{dr} = -\frac{RT}{F} \frac{z_j \frac{dC_j}{dr}}{z_j^2 C_j} \qquad \text{(C.7)}$$

From the no coion flux condition we have that the sum of the coion fluxes in the film is also zero. Now the electric potential term in the Nernst-Planck equation can be eliminated in terms of the total equivalent concentration as:

$$\frac{d\phi}{dr} = -\frac{RT}{F} \frac{\sum_{j=1}^{m} z_j \frac{dC_j}{dr}}{\sum_{j=1}^{m} z_j^2 C_j} \qquad \text{(C.8)}$$

Introducing a mean coion valence defined as

$$z_Y = \frac{\sum_{j=1}^{m} z_j^2 C_j}{\sum_{j=1}^{m} z_j C_j} \tag{C.9}$$

and combining with the definition for total concentration – Eq (C.6), the Eq (C.8) can be reduced to

$$\frac{d\phi}{dr} = \frac{-RT}{z_Y F} \frac{1}{C_T} \frac{dC_T}{dr} \tag{C.10}$$

Now the Nernst-Planck expression for counterions can be written as:

$$J_i = -D_i \left( \frac{dC_i}{dr} - \frac{C_i z_i}{C_T z_Y} \frac{dC_T}{dr} \right) \tag{C.11}$$

Applying the no net current flow condition - Eq (C.5) to Eq (C.11),

$$\sum_{i=1}^{n} z_i D_i \frac{dC_i}{dr} + \sum_{i=1}^{n} z_i D_i N_i \frac{C_i}{C_T} \frac{dC_T}{dr} = 0 \tag{C.12}$$

where, $N_i = -\frac{z_i}{z_Y}$. (C.13)

For monovalent system of ions or equal valence system of ions, the above equation could be easily integrated to obtain a relation between $C_i$ and $C_T$. This is not possible in the case of arbitrary valences. At this point the method proposed by Franzreb (1993) is used to proceed further. In this method, Eq (C.11) is differentiated to eliminate the unknown $J_i$. This leads to a homogeneous second order differential equation:

$$\frac{d^2 C_i}{dr^2} + \frac{N_i}{C_T} \frac{dC_i}{dr} \frac{dC_T}{dr} + N_i \frac{C_i}{C_T} \left( \frac{d^2 C_T}{dr^2} - \frac{1}{C_T} \left( \frac{dC_T}{dr} \right)^2 \right) = 0 \tag{C.14}$$

This method leads to an exact solution for the case of equal valences and only an approximation for the case of arbitrary valences. For counterions of equal valences, summation of Eq (C-14) for all the ions leads to

$$\sum_{i=1}^{n}\frac{d^2C_i}{dr^2}+\frac{1}{C_T}\frac{dC_T}{dr}\sum_{i=1}^{n}N_i\frac{dC_i}{dr}+\frac{1}{C_T}\frac{d^2C_T}{dr^2}\sum_{i=1}^{n}N_iC_i - \frac{1}{C_T^2}\left(\frac{dC_T}{dr}\right)^2\sum_{i=1}^{n}N_iC_i=0 \qquad (C.15)$$

Substituting Eq (C.6) and its derivatives in the above leads to

$$\frac{d^2C_T}{dr^2}=0 \qquad (C.16)$$

From the above equation it can be understood that for the case of counterions of equal valences, the profile of the total concentration in the film is linear. Zecchini and Foutch (1990) arrived at the same conclusion in their model for univalent ternary ions. The above equation combined with Eq (C-6) can be used to obtain relationships between the derivatives of $C_i$ and $C_T$. Substitution of all these derivatives in Eq (C.15) leads to

$$\frac{d^2C_i}{dC_T^2}+\frac{N_i}{C_T}\frac{dC_i}{dC_T}-\frac{N_iC_i}{C_T^2}=0 \qquad (C.17)$$

This is the Euler's differential equation the solution of which is

$$z_iC_i=A_iC_T+B_iC_T^{-P} \qquad (C.18)$$

For the case of equal valences, we have $P = N_i$. Using the boundary conditions

$$r=0, C_T=C_T^* \qquad (C.19)$$

$$r=\delta, C_T=C_T^o \qquad (C.20)$$

the values of the parameters $A_i$ and $B_i$ can be determined as follows:

$$A_i = \frac{1}{C_T^o}\left( z_i C_i^o - B_i \left( C_T^o \right)^{-P} \right) \tag{C.21}$$

and

$$B_i = \omega \frac{X_i^* - X_i^o}{\left(C_T^*\right)^{-P-1} - \left(C_T^o\right)^{-P-1}} \tag{C.22}$$

Eq (C.18) gives us a relation between the individual ion concentrations, $C_i$ and the total equivalent concentration, $C_T$. Substituting for $C_i$ and its derivative in the modified Nernst-Planck Equation (C.11), we get the following flux expression:

$$J_i = -\frac{D_i}{z_i}\frac{dC_T}{dr}\left[ \left( A_i - PB_i C_T^{-P-1} \right) + N_i \left( A_i + B_i C_T^{-P-1} \right) \right] \tag{C.23}$$

For the case of arbitrary valences, Eq (C-18) is only an approximation. In this case however, $N_i$ is not the same for all the counterions and hence, P cannot be equal to $N_i$. Combining the above equation with the condition of no net current flow (C.5) results in

$$\left( \sum_{i=1}^{n} D_i A_i + \sum_{i=1}^{n} N_i D_i A_i \right) + \left( \sum_{i=1}^{n} N_i D_i B_i - P \sum_{i=1}^{n} D_i B_i \right) C_T^{-P-1} = 0 \tag{C.24}$$

The only way the above equation can hold true is when both the terms are equal to zero. That leads to

$$\sum_{i=1}^{n} (1 + N_i) D_i A_i = 0 \tag{C.25}$$

Substitution of $A_i$ (Eq C-21) into the above and with some mathematical manipulations give the desired expression for total interfacial concentration, $C_T^*$:

$$C_T^* = \left( \frac{\sum_{i=1}^{n} (1+N_i) D_i X_i^o}{\sum_{i=1}^{n} (1+N_i) D_i X_i^*} \right)^{1/P+1} C_T^b \qquad \text{(C.26)}$$

Equating the second parentheses term to zero and substitution of $B_i$ would give us the expression for the exponent P as:

$$P = \frac{\sum_{i=1}^{n} N_i D_i \left( X_i^* - X_i^o \right)}{\sum_{i=1}^{n} D_i \left( X_i^* - X_i^o \right)} \qquad \text{(C.27)}$$

In an equal valance case, P is equal to Ni and in an arbitrary case, it would be in the neighborhood of Ni. The concentrations involved in this work are very low and lead to lot of numerical errors and instability. Because of numerical discrepancies, sometimes the value of P computed in the code is unusually high and leads to problems in further computations. Hence the expression for P (Eq C-27) is modified as follows:

$$P = \frac{\sum_{i=1}^{n} N_i D_i \left| X_i^* - X_i^o \right|}{\sum_{i=1}^{n} D_i \left| X_i^* - X_i^o \right|} \qquad \text{(C.28)}$$

Once again, substituting the above equations into Eq (C.11) and integrating between the boundary conditions given earlier, we would get the final desired form of the ionic flux expression:

$$J_i = \frac{D_i}{\delta} \left( (1 - \frac{N_i}{P})(C_i^* - C_i^b) + N_i A_i (1 + \frac{1}{P})(C_T^* - C_T^b) \right) \qquad \text{(C.29)}$$

Particle Rates

The rate of exchange is related to the flux of the species by

$$\frac{dq_i}{dt} = -J_i a_s \tag{C.30}$$

The resin phase concentration $q_i$ can be represented as:

$$q_i = y_i Q \tag{C.31}$$

Now Eq can be written as

$$\frac{dy_i}{dt} = \frac{-J_i a_s}{Q} \tag{C.32}$$

The rate of ion loadings in to the resin can be determined using the above equation once the individual ionic fluxes are known.

The effective diffusivity is defined as:

$$D_e = \frac{\sum_{i=1}^{n} |J_I \delta|}{\sum_{i=1}^{n} |C_i^* - C_i^o|} \tag{C.33}$$

The film thickness in Eq (C-28) is eliminated using the relation

$$\delta = D_e / K \tag{C.34}$$

where K is a mass transfer coefficient found from Dwivedi and Upadhyay's correlation (1979)

$$K = \frac{D_i}{d_p} Sc^{1/3} Re \left[ \frac{0.765}{(\varepsilon Re)^{0.82}} + \frac{0.365}{(\varepsilon Re)^{0.386}} \right] \tag{C.35}$$

In the above Equation, $D_i$ is the diffusivity of ion 'i', $d_p$ is the particle diameter, Re is Reynolds number, Sc is Schmidt number and $\varepsilon$ is void fraction.

Schmidt number (Sc) is defined using the effective diffusivity as

$$Sc = \frac{\mu}{\rho D_e} \tag{C.36}$$

Substituting Eq (C.32) in the flux expression Eq. (C.29), we get

$$\frac{J_i}{K} = \frac{D_i}{D_e}\left( (1 - \frac{N_i}{P})(C_i^* - C_i^b) + N_i A_i (1 + \frac{1}{P})(C_T^* - C_T^b) \right) \tag{C.37}$$

This $J_i/K$ is computed for each of the ions in the subroutines and returned to the main program in the computer code developed for this model.

Flux expressions for non-ionic species

The fluxes of nonionic (molecular) form species are usually described by Fick's second law, that is

$$J_i^m = -D_i^m \frac{dC_i^m}{dz} \tag{C.38}$$

Integrating Eq (C-37) yields

$$J_i^m = \frac{D_i^m}{\delta}(C_i^{mb} - C_i^{m*}) = k_i^m (C_i^{mb} - C_i^{m*}) \tag{C.39}$$

where, $k_{Mol,i} = \frac{D_{Mol,i}}{\delta}$ is molecular mass transfer coefficient. Frequently in a multicomponent system with dissociative species, the concentration of molecular form is much greater than that of ionic form, so that the effect of molecular concentration on the total mass transfer rate has to be taken into account (Jansen, 1996b). To account for this effect, an enhancement factor is introduced in this work to determine the flux for the nonionic form species, that is

$$\alpha = \mathrm{Log}\left(\frac{D_{Mol}C_{Mol}}{D_{Ion}C_{Ion}}\right) \tag{C.40}$$

where $D_{Mol}$ and $C_{Mol}$ are the diffusivity and concentration of the molecular form, and $D_{Ion}$ and $C_{Ion}$ are the diffusivity and concentration of the ionic form.

Therefore, the flux for the nonionic (molecular) form of weak electrolyte is

$$J_i^m = (1+\alpha)\frac{D_i^m}{\delta}(C_i^{mb} - C_i^{m*}) \tag{C.41}$$

As soon as the flux of nonionic form is determined by Eq (C.41), the mass transfer rate for the nonionic form can be calculated using Eq (C.30).

# APPENDIX D

## COLUMN MATERIAL BALANCE

Neglecting axial and radial dispersion, the overall column material balance for species 'i' in an ion exchange column can be expressed as

$$\frac{\partial C_i^T}{\partial t} + \frac{u}{\varepsilon}\frac{\partial C_i^T}{\partial z} + (FR)\frac{1-\varepsilon}{\varepsilon}\frac{\partial q_i^T}{\partial t} = 0 \qquad (D.1)$$

where $u_s$= superficial velocity, and $\varepsilon$ = void fraction. The total constituent capacity is equal to the sum of the equivalents (or moles) of all sub-species.

$$C_i^T = \sum_{k=1}^{n} C_{ik} + C_i^* \qquad (D.2)$$

where $C_{ik}$ is the concentration of the ionic species of a constituent molecule in mol/l (equivalents are used in most of the solution calculations), k is the index of the ionic sub-species, n is the total number of ionic species of a dissociative species type (e.g. for carbonic acid, n equals two for bicarbonate and carbonate), $C_i^*$ is the molecular species concentration, and $C_i^f$ is the total constituent feed concentration.

The resin phase total constituent concentration has a similar definition

$$q_i^T = \sum_{k=1}^{n} q_{ik} + q_i^* \tag{D.3}$$

It is desirable to normalize the initial and final concentrations to 1.0 in numerical calculations because in cases where one constituent concentration is much greater or less than another, the values of the numbers may be subject to round-off error. The following dimensionless variables are used to normalize the solution concentrations and resin concentrations to 1.0.

$$x_i = \frac{\sum_{k=1}^{n} C_{ik} + C_i^*}{C_i^f} = \frac{C_i^T}{C_i^f} \tag{D.4}$$

$$y_i = \frac{q_i^T}{q_i^e} = \frac{\sum_{k=1}^{n} q_{ik}}{q_i^e} \tag{D.5}$$

Dividing Equation (D.1) by $\frac{C_i^f q_i^e}{q_i^e}$ yields,

$$\frac{\partial x_i}{\partial t} + \frac{u}{\varepsilon}\frac{\partial x_i}{\partial z} + (FR)q_i^e \frac{1-\varepsilon}{\varepsilon}\frac{\partial y_i}{\partial t} = 0 \tag{D.6}$$

The method of characteristics is applied to reduce the order of the equations from third to second. The method combines the variation of one variable with two axes by selecting appropriate dimensionless variables and applying the chain rule. The dimensionless time and distance are defined as,

$$\tau_i = \frac{k_i C_i^f}{q_i^e \varepsilon}\left(t - \frac{z\varepsilon}{u}\right) \tag{D.7}$$

$$\xi_i = \frac{k_i (1-\varepsilon) z}{d_{p,i} u} \tag{D.8}$$

$k_i$ is the non-ionic mass transfer coefficient for species i, $d_{pi}$ is the particle diameter for the exchanging species resin type, $q_i^e$ is the resin capacity and $C_i^f$ is the total cationic feed concentration. The above expressions are differentiated with respect to time and distance respectively to yield:

$$\frac{\partial \xi_i}{\partial z} = \frac{k_i (1-\varepsilon)}{u_s d_{p,i}} \tag{D.9}$$

$$\frac{\partial \tau_i}{\partial z} = \frac{-k_i C_i^f \varepsilon}{d_{p,i} q_i^e u_s} \tag{D.10}$$

$$\frac{\partial \xi_i}{\partial t} = 0 \tag{D.11}$$

$$\frac{\partial \tau_i}{\partial t} = \frac{k_i C_i^f}{d_{p,i} q_i^e} \tag{D.12}$$

Applying the chain rule to each differential term of Equation (D.1) changes the integration axes.

$$\frac{\partial x_i}{\partial z} = \frac{\partial x_i}{\partial \xi_i}\frac{\partial \xi_i}{\partial z} + \frac{\partial x_i}{\partial \tau_i}\frac{\partial \tau_i}{\partial z} \tag{D.13}$$

$$\frac{\partial x_i}{\partial t} = \frac{\partial x_i}{\partial \xi_i}\frac{\partial \xi_i}{\partial t} + \frac{\partial x_i}{\partial \tau_i}\frac{\partial \tau_i}{\partial t} \tag{D.14}$$

$$\frac{\partial y_i}{\partial t} = \frac{\partial y_i}{\partial \xi_i}\frac{\partial \xi_i}{\partial t} + \frac{\partial y_i}{\partial \tau_i}\frac{\partial \tau_i}{\partial t} \tag{D.15}$$

Inserting Equations (D.9) to (D.12) into Equations (D.13) to (D.15)

$$\frac{\partial x_i}{\partial t} = \frac{\partial x_i}{\partial \xi}(0) + \frac{\partial x_i}{\partial \tau}\left(\frac{k_i C_i^f}{d_{p,i} q_i^e}\right) = \frac{k_i C_i^f}{d_{p,i} q_i^e}\frac{\partial x_i}{\partial \tau} \tag{D.16}$$

$$\frac{\partial x_i}{\partial z} = \frac{\partial x_i}{\partial \xi_i}\left(\frac{k_i(1-\varepsilon)}{u_s d_{p,i}}\right) + \frac{\partial x_i}{\partial \tau_i}\left(\frac{-k_i C_i^f \varepsilon}{d_{p,i} q_i^e u_s}\right) \tag{D.17}$$

$$\frac{\partial y_i}{\partial t} = \frac{\partial y}{\partial \xi_i}(0) + \frac{\partial y_i}{\partial \tau}\left(\frac{k_i C_i^f}{d_{p,i} q_i^e}\right) \tag{D.18}$$

Substituting Equations (D.16) to (D.18) into Equation (D.6),

$$\left[\frac{k_i C_i^f}{d_{p,i} q_i^e}\frac{\partial x}{\partial t}\right] + \frac{u_s}{\varepsilon}\left[\frac{\partial x_i}{\partial \xi_i}\left(\frac{k_i(1-\varepsilon)}{u_s d_{p,i}}\right) + \frac{\partial x_i}{\partial \tau_i}\left(\frac{-k_i C_i^f \varepsilon}{d_{p,i} q_i^e u_s}\right)\right] + (FR) q_i^e \frac{(1-\varepsilon)}{\varepsilon}\left[\frac{\partial y_i}{\partial \tau}\frac{k_i C_i^f}{d_{p,i} q_i^e}\right] = 0 \tag{D.19}$$

Equation (D.19) collapses to,

$$\frac{\partial x_i}{\partial \xi_i} + (FR)\frac{\partial y_i}{\partial \tau_i} = 0 \tag{D.20}$$

This expression is still a partial differential equation, but it is now only a second order equation. If the two terms are equated by subtracting the change in resin loading differential from both sides, the observation is made that at any given point in time and space the two differentials are equal to a constant that varies with time and space.

$$\frac{\partial x_i}{\partial \xi_i} = -(FR)\frac{\partial y_i}{\partial \tau_i} = R_i^T(\tau, \xi) \tag{D.21}$$

The constant is the constituent exchange rate. Analytical solutions exist when the exchange rate does not vary with time and space; however, in our system the only times the rates are constant is when they are at equilibrium with the resin, and the value is zero.

Each element of the differential equation system represents a constituent; and each constituent has its own dimensionless time and distance variable definitions. The elements of the differential equation system are changed to common reference axes by

choosing a reference constituent and applying the chain rule to each element of the equation system. The reference constituent is the constituent with the largest value of $\tau$, and the reference constituent is denoted with the subscript 'r.'

$$\frac{\partial x_i}{\partial \xi_r} = \frac{\partial x_i}{\partial \xi_i}\frac{\partial \xi_i}{\partial \xi_r} \tag{D.22}$$

$$\frac{\partial y_i}{\partial \tau_r} = \frac{\partial y_i}{\partial \tau_i}\frac{\partial \tau_i}{\partial \tau_r} \tag{D.23}$$

Inserting the chain rule definitions, Equations (D.9) through (D.12) into Equations (D.22) and (D.23)

$$\frac{\partial \xi_i}{\partial \xi_r} = \frac{\xi_i}{\xi_r} = \frac{\dfrac{k_i(1-\varepsilon)z}{u_s d_{p,i}}}{\dfrac{k_r(1-\varepsilon)z}{u_s d_{p,r}}} = \frac{k_i d_{p,r}}{k_r d_{p,i}} \tag{D.24}$$

$$\frac{\partial \tau_i}{\partial \tau_r} = \frac{\tau_i}{\tau_r} = \frac{\dfrac{k_i C_i^f}{d_{p,i} q_i^e}\left(t - \dfrac{z}{u_s}\varepsilon\right)}{\dfrac{k_r C_r^f}{d_{p,r} q_r^e}\left(t - \dfrac{z}{u_s}\varepsilon\right)} = \frac{k_i}{k_r}\frac{C_i^f}{C_r^f}\frac{d_{p,r}}{d_{p,i}}\frac{q_r^e}{q_i^e} \tag{D.25}$$

Inserting Equations (D.24) and (D.25) into Equation (D.21),

$$\frac{\partial x_i}{\partial \xi_r}\left(\frac{k_r}{k_i}\frac{d_{p,i}}{d_{p,r}}\right) + (FR)\frac{\partial y_i}{\partial \tau_r}\left(\frac{k_r}{k_i}\frac{C_r^f}{C_i^f}\frac{d_{p,i}}{d_{p,r}}\frac{q_i^e}{q_r^e}\right) = 0 \tag{D.26}$$

$$\frac{\partial x_i}{\partial \xi_r} + (FR)\frac{C_r^f}{C_i^f}\frac{q_i^e}{q_r^e}\frac{\partial y_i}{\partial \tau_r} = 0 \tag{D.27}$$

The constant $\dfrac{C_r^f}{C_i^f}\dfrac{q_i^e}{q_r^e}$ is encountered frequently, for brevity it is assigned to the constant array $\alpha_i$.

$$\alpha = \frac{C_r^f}{C_i^f}\frac{q_i^e}{q_r^e} \tag{D.28}$$

The column material balance is then written for an arbitrary constituent 'i,'

$$\frac{\partial x_i}{\partial \xi_r} = -(FR)\alpha\frac{\partial y_i}{\partial \tau_r} = R_i^T \tag{D.29}$$

The differential equation system has been defined, but an expression relating the ionic fluxes to $R_i^T$. From the base assumption that the mass flow rate per unit area of a constituent is equal to the sum of its ionic species fluxes plus the molecular flux, the constituent flux is defined below.

$$J_i^T = \sum_{k=1}^{m} J_{ik} + J_i^* \tag{D.30}$$

The constituent flux is incorporated into the column material balance by relating the change in constituent capacity with respect to time to the product of the constituent flux and the specific surface area.

$$\frac{dq_i^T}{dt} = -J_i^T a_s \tag{D.31}$$

The variable $a_s$ is the specific surface area per unit volume. For spherical particles in film diffusion, only the external surface area of the sphere is considered.

$$a_s d_{p,i} = \left(\frac{4\pi r^2}{\frac{4}{3}\pi r^3}\right)(2r) = 6 \tag{D.32}$$

The change in loading ratio with respect to time is found by dividing Equation (D.31) by $q_i^e$, and substituting Equation (D.32).

$$\frac{dy_i}{dt} = \frac{-6J_i^T}{q_i^e d_{p,i}} \tag{D.33}$$

In order to include the particle rate into the column material balance, the dt differential must be changed to a $\partial\tau_r$ differential by successive applications of the chain rule.

$$\frac{\partial y_i}{\partial \tau_r} = \frac{\partial y_i}{\partial t}\frac{\partial t}{\partial \tau_i}\frac{\partial \tau_i}{\partial \tau_r} \tag{D.34}$$

Substituting Equations (D.12) and (D.25) into Equation (D.34),

$$\frac{\partial y_i}{\partial \tau_r} = \left(\frac{-6J_i^T}{q_i^e d_{p,i}}\right)\left(\frac{d_{p,i} q_i^e}{k_i C_i^f}\right)\left(\frac{k_i}{k_r}\frac{C_i^f}{C_r^f}\frac{d_{p,r}}{d_{p,i}}\frac{q_r^e}{q_i^e}\right) \tag{D.35}$$

and reducing yields the change in the constituent loading ratio with respect to time.

$$\frac{\partial y_i}{\partial \tau_r} = -\frac{6J_i^T}{C_i^f k_i}\left(\frac{d_{pr}}{d_{pi}}\frac{q_r^e}{q_i^e}\frac{k_i}{k_r}\right) \tag{D.36}$$

The loading profiles are changed by relating the differential $\partial y_i/\partial\tau_r$ and $R_i^T$ to the loading profile $Y_i$. Note $y_i$ is the ratio of species 'i' capacity to its equilibrium capacity, while $Y_i$ is the fraction of the total capacity. These quantities are related according to Equation (D.37).

$$Y_i = y_i \frac{q_i^e}{Q_i} = y_i Y_i^e \tag{D.37}$$

Differentiating Equation (D.37) with respect to $y_i$ yields

$$\frac{dY_i}{dy_i} = Y_i^e \tag{D.38}$$

The differential is then used in the chain rule to relate the total rate to the change in resin equivalent fraction, as shown in Equation (D.39).

$$\frac{dY_i}{d\tau_r} = \frac{1}{\alpha}\frac{dy_i}{d\tau_r}\frac{dY_i}{dy_i} = Y_i^e \frac{C_i^f}{q_i^e}\frac{q_r^e}{C_r^f} R_i^T \qquad \text{(D.39)}$$

The author notes that in spite of the large number of equations used to derive these expressions, Equations (D.29) and (D.39) are the equations applied in the model for the change in solution ratio with respect to distance and the resin fraction with respect to time.

# APPENDIX E

## TEMPERATURE DEPENDENT PARAMETERS AND CORRELATIONS

Chemical and ionic properties are typically a function of temperature. Several researchers, notably Divekar (1987) and Liu (1999), have performed literature reviews to characterize the temperature dependence of diffusivities, dissociation constants, water properties, and cation resin desulfonation.

### Ionic diffusivities

Liu (1998) researched ionic diffusivity temperature dependence for a variety of species, and the results are below. If the ionic species is not listed in the species list, a general formula proposed by Reid et al., is applied to estimate temperature dependence.

$$D_T = D_{298}\frac{T}{334\mu} \qquad \text{(E.1)}$$

| | |
|---|---|
| Hydrogen[1] | $D_H = 8.931*10^{-10}(T+273.16)(221.71+5.52T-0.0144T^2)$ |
| Hydroxide[1] | $D_{OH} = 8.931*10^{-10}(T+273.16)(104.74+3.807T)$ |
| Sodium[1] | $D_{Na} = 8.931*10^{-10}(T+273.16)(23.005+1.0642T+0.003319T^2)$ |
| Potassium[5] | $D_K = 8.931*10^{-10}(T+273.16)(40.22+1.278T+0.00271T^2)$ |
| Silver[5] | $D_{Ag} = 8.931*10^{-10}(T+273.16)(33.12+1.065T+0.003538T^2)$ |
| Calcium[3] | $D_{Ca} = 8.931*10^{-10}(T+273.16)(23.27+1.575T)/2$ |
| Barium[5] | $D_{Ba} = 8.931*10^{-10}(T+273.16)(34.0+1.042T+0.00568T^2)$ |
| Magnesium[3] | $D_{Mg} = 8.931*10^{-10}(T+273.16)(28.81+0.819T+0.00542T^2)/2$ |
| Ammonia[2] | $D_{NH_4} = 8.931*10^{-10}(T+273.16)(39.1537+1.4055T)$ |

Chloride[1] $D_{Cl} = 8.931*10^{-10}(T+273.16)(39.649+1.392T+0.00332T^2)/2$

Sulfate[3] $D_{SO_4} = 8.931*10^{-10}(T+273.16)(35.76+2.079T)/2$

Bicarbonate[3] $D_{HCO_3} = 8.931*10^{-10}(T+273.16)\times 44.5$

Carbonate[3] $D_{CO_3} = 8.931*10^{-10}(T+273.16)(36.0+1.44T)/2$

Nitrate[5] $D_{NO_3} = 8.931*10^{-10}(T+273.16)(40.03+1.161T+0.003882T^2)$

Fluoride[5] $D_F = 8.931*10^{-10}(T+273.16)(107.7-6.61T+0.1804T^2)$

Bromide[5] $D_{Br} = 8.931*10^{-10}(T+273.16)(42.52+1.326T+0.004104T^2)$

Perchloride[5] $D_{ClO_4} = 8.931*10^{-10}(T+273.16)(36.96+1.136T+0.003443T^2)$

Acetate[5] $D_{CH_3COO} = 8.931*10^{-10}(T+273.16)(201+0.8169T+0.000603T^2)$

## Dissociation constants

Dissociation constants are also known functions of temperature. Correlations illustrating the temperature dependence of common weak electrolytes are below.

Water[1] $pK_w = -6.0875+0.0176T+\frac{4470.99}{T}$

Ammonia[2] $pK_{NH_3} = 4.8601+6.31\times 10^{-5}T-5.98\times 10^{-3}/T^2$

Morpholine[2] $pK_{Mor} = 5.7461+8.095\times 10^{-5}T-1.3881\times 10^{-2}/T^2$

Carbonates

1st. dissociation[3] $pK_1 = \frac{17052}{T}+215.21Log(T)-0.12675T-545.56$

2nd. Dissociation[3] $pK_2 = \frac{2902.39}{T}+0.02379T-6.498$

Phosphate:

1st dissociation[5] $pK_1 = \frac{799.31}{T}-4.5535+0.013486T$

2nd dissociation[5] $pK_2 = \frac{2073.0}{T}-5.9887+0.020912T$

3rd dissociation[5] $pK_3 = 12.1152-0.00908T+0.000127T^2$

where $T$ is temperature in °K.

## Solution properties

The viscosity and density of water also vary as a function of temperature. The following correlations are used to compensate for temperature.

Viscosity[1] (cp) $\mu = 1.5471 - 0.0317109T + 2.3345 \times 10^{-4} T^2$

Density[4] (g/cc)

$$\rho = \left[ \frac{1 + 0.134248 * SS2 - 3946263 * 10^{-3} * SS1}{3.1975 - 0.3151548 * SS2 - 1.203374 * 10^{-3} * SS1 + 7.48908 * 10^{-13} * SS1^4} \right]^{1/2}$$

where $SS1 = 374.11 - T$

$SS2 = SS1^{1/3}$

T is temperature in °C in the above correlations

---

Note* 1 – Divekar (1987); 2 – Zecchini (1990); 3 – Bulusu (1994); 4 – Sunkavalli (1996)
5 – Liu (1998)

VITA

Dennis Frank Hussey, M. S.

Candidate for the Degree of

Doctor of Philosophy

Thesis: DEVELOPMENT OF A MULTICOMPONENT FILM DIFFUSION CONTROLLED MIXED BED ION EXCHANGE COLUMN MODEL APPLICABLE TO VARIABLE INFLUENT SYSTEMS

Major Field: Chemical Engineering

Biographical:

Personal Data: Born in West Islip, New York, U. S. A., December 23, 1971

Education: Graduated Cleveland High School, Cleveland, Oklahoma May 1989. Received Bachelor of Science in Chemical Engineering at Oklahoma State University 1994. Received Masters of Science in Chemical Engineering at Oklahoma State University, 1997. Completed the requirements for the Doctor of Philosophy with a major in Chemical Engineering in May 2000

Experience: Teaching assistant for Unit Operations at Oklahoma State University in the spring of 2000, employed by Intel Corporation as an ultrapure water engineer at Portland, Oregon in the summer and fall of 1997, and also in Rio Rancho, New Mexico in the summer of 1996.

Professional memberships: Omega Chi Epsilon, Chemical Engineering Honor Society. American Institute of Chemical Engineering.